EUROPEAN ORGANIZATION FOR NUCLEAR RESEARCH (CERN)

CERN-EP-2024-335
2025/06/23

CMS-SUS-24-001

Search for bosons of an extended Higgs sector in b quark final states in proton-proton collisions at $\sqrt{s} = 13\,\text{TeV}$

The CMS Collaboration*

Abstract

A search for beyond-the-standard-model neutral Higgs bosons decaying to a pair of bottom quarks, and produced in association with at least one additional bottom quark, is performed with the CMS detector. The data were recorded in proton-proton collisions at a centre-of-mass energy of 13 TeV at the CERN LHC and correspond to an integrated luminosity of 36.7–126.9 fb^{-1}, depending on the probed mass range. No signal above the standard model background expectation is observed. Upper limits on the production cross section times branching fraction are set for Higgs bosons in the mass range of 125–1800 GeV. The results are interpreted in benchmark scenarios of the minimal supersymmetric standard model, as well as suitable classes of two-Higgs-doublet models.

Published in the Journal of High Energy Physics as doi:10.1007/JHEP06(2025)144.

*See Appendix A for the list of collaboration members

1 Introduction

The confirmation of the Higgs boson's existence by the ATLAS and CMS Collaborations [1–3] at the CERN LHC, with a mass of 125 GeV, reinforces the standard model (SM) as the most promising theory to date for understanding the fundamental constituents of matter and their mutual forces. The Higgs boson has been experimentally observed in its main production modes, namely gluon fusion and vector boson fusion, as well as production in association with vector bosons and top quark pairs [4, 5]. A recent CMS study has placed stringent constraints on its production in association with b quark pairs [6]. Also, the most prominent decay modes have been observed, including those to massive fermions of the third family [4, 5]. Measurements are being extended to include decays to the second family of fermions. Evidence for Higgs boson decays to muon pairs has been established [7], and upper limits on its branching fraction to charm quark pairs have been determined [8, 9]. The measurements of Higgs boson properties have so far been consistent with the SM expectations [4, 5, 10, 11].

Although the SM has been remarkably successful, it is nevertheless regarded as an incomplete theory. Various theories beyond the SM have been proposed that extend its Higgs sector [12]. The addition of a second complex Higgs doublet leads to two-Higgs-doublet models (2HDMs) [13]. The minimal supersymmetric extension MSSM [14] also features a Higgs sector with two complex Higgs doublets. Both cases result in five physical states of the Higgs bosons: two charged Higgs bosons $H^{\pm}$ and three neutral ones, jointly denoted as ϕ. Under the assumption of charge and parity (CP) conservation, the neutral Higgs bosons are one CP-odd (A) and two CP-even (h, H) states, where h denotes the lighter CP-even state, usually associated with the Higgs boson discovered at a mass of 125 GeV.

In the SM, the Higgs boson has large couplings to W and Z bosons. The Higgs boson mass of 125 GeV being below the threshold for W and Z pairs prevents those channels from dominating the decay width, resulting in $b\bar{b}$ being the most abundant decay mode. However, the situation changes for additional Higgs bosons. In a wide class of extended Higgs sector models, including those under consideration in this paper, a sum rule at lowest order implies that the squared couplings to gauge bosons of all neutral Higgs bosons sum up to the squared coupling of the SM Higgs boson to gauge bosons [15]. As the Higgs boson at 125 GeV is known to have gauge boson couplings within less than 10% from their SM values, the sum rule is close to saturated, and the gauge boson couplings of any additional scalar Higgs bosons must be significantly suppressed compared with those of an SM Higgs boson of the same mass. On the other hand, there is no such sum rule limitation for fermions. Even very heavy additional Higgs bosons may thus have large and dominant branching fractions to fermion pairs. For this reason, third-generation fermion pairs can be considered most promising channels in the search for heavy Higgs bosons.

In the most general case, 2HDMs allow for flavour-changing neutral currents and CP-violating terms at tree level. Since these effects have not been observed experimentally, it is common to suppress both by imposing a discrete $\mathbb{Z}_2$ symmetry. This leads to four types of models with natural flavour conservation: *Type-I*, *Type-II*, *Lepton-specific* (or *Type-X*), and *Flipped* (or *Type-Y*) models [13]. In the *Type-I* model, every charged fermion interacts with the same Higgs doublet. The *Type-II* model distinguishes between up-type quarks (u, c, t), which couple to one doublet, and down-type fermions (d, s, b, e, μ, τ), which couple to the other. This structure is also present in the MSSM. The *Lepton-specific* model assigns all charged leptons to interact with one doublet and all quarks with the other. In contrast, the *Flipped* model inverts this arrangement of the down-type fermions, with charged leptons and up-type quarks coupled to one doublet and down-type quarks to the other. While the *Type-I* and *Type-II* models have undergone extensive study, the *Flipped* model has not been explored as thoroughly by experiments. The decay process $\phi \to b\overline{b}$ is particularly well suited for investigating this model due to the potentially large branching fraction of the Higgs boson to b quark pairs, but experimentally very challenging because of overwhelming backgrounds.

The 2HDMs with CP conservation are characterised by seven free parameters. These parameters include the masses of the various Higgs bosons (m_{h}, m_{H}, m_{A}, $m_{\mathrm{H}^{\pm}}$), the mixing angle between the CP-even Higgs bosons (α), the ratio of the vacuum expectation values of the two Higgs doublets defined as $\tan\beta = v_2/v_1$, and the parameter m_{12}, which describes the potential mixing between the two Higgs doublets. In the limit $\cos(\beta - \alpha) \to 0$, referred to as the alignment limit, the lighter CP-even Higgs particle, h, manifests properties that are identical to those of the SM Higgs boson at the same mass across all four types of models.

In the case of the MSSM, the Higgs sector has the structure of a *Type-II* 2HDM. At tree level, the Higgs boson masses and α are constrained by the fermion-boson symmetry. Such constraints simplify the model to have only two free parameters at this level. These parameters are commonly chosen to be m_{A} and $\tan\beta$. Since the discovery of the Higgs boson at the LHC, the MSSM benchmark scenarios have been refined for better agreement with experimental observations [16, 17]. In this analysis, interpretations in the context of the M_{h}^{125} [18, 19], the $m_{\mathrm{h}}^{\mathrm{mod}}$ [16], and the hMSSM [20–22] scenarios are considered.

For $\tan\beta$ values larger than one, the couplings of the heavy neutral Higgs bosons to b quarks are enhanced both in the *Type-II* and *Flipped* models, and thus also in the MSSM. This increases the cross section for Higgs boson production in association with b quarks, which is thus a promising signature to study. In addition, there is an approximate mass degeneracy between the A and H bosons in the MSSM for the studied range of m_{A}. For the 2HDMs, we are considering scenarios in which the masses of these bosons are assumed to be equal [23]. These effects enhance the combined cross section for producing these Higgs bosons in association with b quarks by a factor of up to $2\tan^2\beta$ with respect to the SM. The decay $(\mathrm{A}, \mathrm{H}) \to b\overline{b}$ is expected to have a relatively high branching fraction, even at large values of the Higgs boson mass [24].

Searches for additional Higgs bosons in the $b\overline{b}$ decay mode have been performed previously at the CERN LEP [25] and by the CDF and D0 Collaborations at the Fermilab Tevatron [26]. At the LHC, the analyses in this decay mode with associated b jets have initially been performed by the CMS Collaboration using the 7 and 8 TeV data sets [27, 28]. Thereafter, the ATLAS and CMS Collaborations have published first results from data at 13 TeV [29, 30], with corresponding integrated luminosities of 27.8 fb^{-1} (recorded in 2015 and 2016) and 35.7 fb^{-1} (recorded in 2016), respectively. In the absence of a significant excess of events, upper limits on the $\mathrm{pp} \to b\phi(\to b\overline{b}) + X$ cross section have been provided by the ATLAS and CMS Collaborations in the 450–1400 and 300–1300 GeV mass ranges, respectively. The results were also interpreted within the 2HDMs and the MSSM benchmark scenarios.

In this paper we present a search for additional Higgs bosons with masses in the range 125–1800 GeV that decay into a $b\overline{b}$ pair and are produced in association with at least one additional b quark. The analysis focusses on a search for neutral Higgs bosons ϕ (h, H, and A) with mass m_{ϕ} that are produced in association with at least one b quark and decay to $b\overline{b}$, as shown by the diagrams in Fig. 1. The data were collected in proton-proton (pp) collisions by the CMS detector at the LHC with a centre-of-mass energy of $\sqrt{s} = 13$ TeV. The analysis is based on data taken in the years 2017–2018, and eventually combined with the previously published results based on the 2016 data [30], in total comprising an integrated luminosity of 36.7–126.9 fb^{-1} depending on the probed mass range. Compared to the previous CMS results in this final state [30], this analysis benefits from a larger data set, improved b jet identification using the DEEPJET algorithm [31], a more robust background estimation strategy based on transfer factors, and improved track reconstruction from the upgrade of the CMS pixel detector [32].

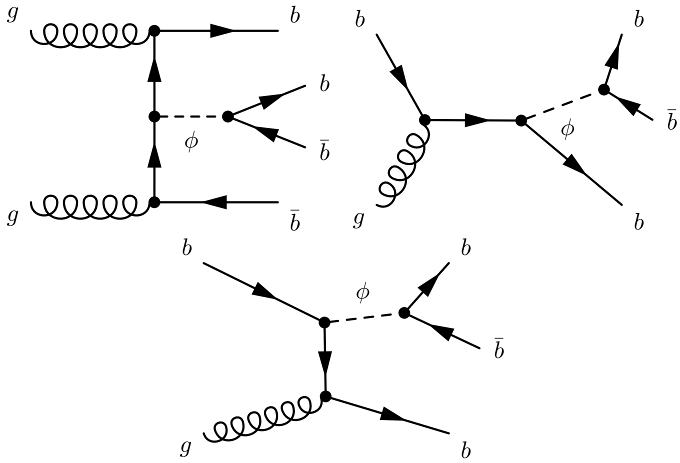

Figure 1: Example Feynman diagrams for the signal processes.

The paper is organised as follows. Section 2 gives an overview of the CMS detector. Section 3 describes the event reconstruction. Data and simulations used in this analysis are detailed in Section 4, while Section 5 summarises the analysis selection. Sections 6 and 7 describe signal and background models, respectively, with parametric approaches, and Section 8 the systematic uncertainties. Section 9 contains the results of the analysis and interpretations in the MSSM and general 2HDMs. Finally, a brief summary of the paper is provided in Section 10. Tabulated results are provided in the HEPData record for this analysis [33].

2 The CMS detector

The central feature of the CMS apparatus is a superconducting solenoid of 6 m internal diameter, providing a magnetic field of 3.8 T. Within the solenoid volume are a silicon pixel and strip tracker, a lead tungstate crystal electromagnetic calorimeter (ECAL), and a brass and scintillator hadron calorimeter (HCAL), each composed of a barrel and two endcap sections. Forward calorimeters extend the pseudorapidity coverage provided by the barrel and endcap detectors. Muons are measured in gas-ionisation detectors embedded in the steel flux-return yoke outside the solenoid. More detailed descriptions of the CMS detector, together with a definition of the coordinate system used and the relevant kinematic variables, can be found in Refs. [34, 35].

Events of interest are selected using a two-tiered trigger system. The first level (L1), composed of custom hardware processors, uses information from the calorimeters and muon detectors to select events at a rate of around 100 kHz within a fixed latency of about 4 μs [36]. The second level, known as the high-level trigger, consists of a farm of processors running a version of the full event reconstruction software optimised for fast processing, and reduces the event rate to around 1 kHz before data storage [37, 38].

3 Event reconstruction

The particle-flow event reconstruction [39] aims to reconstruct and identify each individual particle in an event, with an optimized combination of all subdetector information. In this process, the identification of the particle type (photon, electron, muon, charged hadron, neutral hadron) plays an important role in the determination of the particle direction and energy. Photons (including those coming from π^0 decays or from electron bremsstrahlung) are identified as ECAL energy clusters not linked to the extrapolation of any charged-particle trajectory to the ECAL. Electrons (including those coming from photon conversions in the tracker material or from b hadron semileptonic decays) are identified as a primary charged-particle track and potentially many ECAL energy clusters corresponding to the primary track extrapolation to the ECAL and to possible bremsstrahlung photons emitted while passing through the tracker material. Muons (including those from b hadron semileptonic decays) are identified as tracks in the central tracker consistent with either a track or several hits in the muon system, and associated with calorimeter deposits compatible with the muon hypothesis. Charged hadrons are identified as charged-particle tracks identified neither as electrons nor as muons. Finally, neutral hadrons are identified as HCAL energy clusters not linked to any charged-hadron trajectory, or as a combined ECAL and HCAL energy excess with respect to the expected charged-hadron energy deposit. The primary vertex is taken to be the vertex corresponding to the hardest scattering in the event, evaluated using tracking information alone, as described in Section 9.4.1 of Ref. [40].

For each event, jets are clustered from these reconstructed particles using the infrared- and collinear-safe anti-k_{T} algorithm [41, 42] with a distance parameter of 0.4. Jet momentum is determined as the vectorial sum of all particle momenta in the jet, and is found from simulation to be, on average, within 5 to 10% of the true momentum over the entire transverse momentum (p_{T}) spectrum and detector acceptance. Additional pp interactions within the same or nearby bunch crossings (pileup) can contribute additional tracks and calorimetric energy depositions to the jet momentum. To mitigate this effect, charged particles identified to originate from pileup vertices are discarded, and an offset correction is applied to correct for remaining contributions. Jet energy corrections are derived from simulation to bring the measured response of jets to that of particle level jets on average. In situ measurements of the momentum balance in dijet, photon + jet, Z + jet, and multijet events are used to account for any residual differences in the jet energy scale between data and simulation [43]. The jet energy resolution amounts typically to 15–20% at 30 GeV, 10% at 100 GeV, and 5% at 1 TeV [43]. Additional selection criteria are applied to each jet to remove jets potentially dominated by anomalous contributions from various subdetector components or reconstruction failures [44].

To identify jets resulting from the hadronisation of b quarks [45], the DEEPJET algorithm is used, as described in Ref. [31], and provides a unity-normalised score for different jet flavours. A specific value requirement for a jet on the score of the algorithm is referred to as b tagging, and positively identified jets are referred to as b-tagged jets or b jets. In this analysis, the medium working point of the DEEPJET algorithm is chosen. This working point corresponds to an expected b jet identification efficiency of ≈80% for an expected misidentification rate for jets originating from light-flavour quarks and gluons (c quarks) of 1 (15)% [46, 47].

Muons are measured in the pseudorapidity range $|\eta| < 2.4$, with detection planes made using three technologies: drift tubes, cathode strip chambers, and resistive-plate chambers. Matching muons offline to tracks measured in the silicon tracker results in a relative p_{T} resolution, for muons with p_{T} up to 100 GeV, of 1% in the barrel and 3% in the endcaps. The p_{T} resolution in the barrel is better than 7% for muons with p_{T} up to 1 TeV [48].

The missing transverse momentum vector $\vec{p}_{\mathrm{T}}^{\text{miss}}$ is computed as the negative vector sum of the transverse momenta of all the PF candidates in an event, and its magnitude is denoted as $p_{\mathrm{T}}^{\text{miss}}$ [49]. The $\vec{p}_{\mathrm{T}}^{\text{miss}}$ is modified to account for corrections to the energy scale of the reconstructed jets in the event.

Events with anomalous high-$p_{\mathrm{T}}^{\mathrm{miss}}$ can be due to a variety of reconstruction failures, detector malfunctions or noncollision backgrounds. Such events are rejected by event filters that are designed to identify more than 85–90% of the spurious high-$p_{\mathrm{T}}^{\mathrm{miss}}$ events with a mistagging rate less than 0.1% [49]. Although $\vec{p}_{\mathrm{T}}^{\mathrm{miss}}$ is not directly used in the event selection, such anomalous events can still introduce structures in the mass spectrum, potentially leading to a spurious excess.

4 Data and simulated samples

The data used for the analysis were collected with the CMS detector using LHC pp collisions at $\sqrt{s} = 13\,\mathrm{TeV}$. The copious rate of background from SM events composed uniquely of jets produced through the strong interaction, referred to as quantum chromodynamics (QCD) multijet events, at the LHC is one of the challenges for this analysis. A dedicated trigger scheme has been employed to address this challenge. These triggers require at least two jets with large p_{T}, in combination with b tagging requirements, and optionally a muon candidate compatible with a semileptonic b hadron decay. More details can be found in Section 5.

Simulated samples of signal and background processes are produced using different event generators. The signal samples are produced at next-to-leading order (NLO) in the strong coupling constant α_{S} using the POWHEG 2.0 implementation [50–53] in the four-flavour scheme (4FS) [54]. Multijet background events from QCD processes are generated at leading order with the MADGRAPH5_aMC@NLO event generator v2.6.5 [55–57] using the five-flavour scheme (5FS) and MLM jet merging [58]. These multijet samples are used for studying qualitative features of the background, but not for a quantitative background prediction. More details are described in Section 7.

The PDF4LHC15 [59] parton distribution functions (PDFs) are used for the generation of the signal process, while the NNPDF3.1 [60] PDFs are used for multijet background process. The description of the underlying event is parameterised according to the CP5 [61] tunes in both cases. For all generated samples, parton showering and hadronisation are modelled using the PYTHIA event generator [62], version 8.230. Pileup events are generated with PYTHIA and are added according to the expected pileup profile in the observed data. All generated events are passed through a GEANT4-based [63] simulation of the CMS detector and reconstructed using the same version of the CMS event reconstruction software used for the data.

5 Event selection

In the following, the jets are assumed to be sorted in the order of decreasing p_{T}. Only events with at least three jets are considered. The terms “leading jet”, “second leading jet” and “third leading jet” refer to the first, second and third item in this ordering. Similarly, the first two or three items may be collectively referred to as “the two” or “the three leading jets”.

The search for $\phi \to \mathrm{b}\overline{\mathrm{b}}$ decays is based on two different signatures. The fully hadronic (FH) selection requires at least the three leading jets to be b-tagged and is applied for the 2017–2018 data sets. Due to trigger rate limitations, this selection requires relatively high p_{T} thresholds for at least the two leading jets, which restricts the sensitivity of the analysis to Higgs boson masses of 300 GeV and above. The semileptonic (SL) selection equally requires at least the three leading jets to be b-tagged, but further requires one muon within the cone of any of the two leading jets in the event, compatible with the semileptonic decay of a b hadron. This results in further enrichment of the b jet signature and permits lower p_{T} thresholds. In absence of a suitable trigger for the 2018 data taking period, this selection is available only for the 2017 data set; it is only applied for Higgs boson masses up to 700 GeV, beyond which its sensitivity is negligible compared to the FH channel. Combining both selections allows probing neutral Higgs bosons in the mass range starting as low as 125 GeV and extending up to 1800 GeV. While the signal process may contain four b jets, the selection requires only at least three since one of these four b jets is frequently outside of the acceptance or does not pass the kinematic thresholds. The analysis aims to reconstruct ϕ candidates by searching for a peak in the invariant mass distribution, M_{12}, of the two leading jets, which are expected to originate from the Higgs boson decay in the majority of the signal events. For $m_{\phi} \geq 160$ GeV, the efficiency for correctly pairing the Higgs boson daughter jets exceeds 50% and reaches about 96% at the highest mass point, while it ranges down to 32% towards the lowest masses in the 2017 SL selection. The dominant background arises from the production of heavy-flavour multijet events containing either three b jets, or two b jets plus a third jet that is misidentified as a b jet and originates from either a charm quark, a light-flavour quark, or a gluon. Eventually, the results from the 2017–2018 data sets are combined with published results from the 2016 data set [30].

For the 2017 (2018) data set, FH events are selected at the trigger level by requiring at least two jets in the range of $|\eta| < 2.3$ with $p_{\mathrm{T}} > 100\,(112)$ GeV. An event is accepted only if the absolute value of the difference in pseudorapidity, $\Delta\eta$, between any two of these jets is less than or equal to 1.6, since this requirement further reduces the trigger rates while preserving a high trigger efficiency in the probed mass range of the Higgs bosons. At least two jets having $p_{\mathrm{T}} > 80$ GeV must be identified as b jets. This b jet identification uses the DeepCSVv2 algorithm [45] with slightly tighter requirements than for the offline analysis. For the SL events, the online selection is similar, but the p_{T} threshold for the leading jets is lowered to 40 GeV, at least two jets with $p_{\mathrm{T}} > 30$ GeV must be identified as b jets, and, in addition, at least one muon with $p_{\mathrm{T}} > 12$ GeV is required. The muon requirement considerably reduces the trigger rates and thus allows the reduction of the leading jet p_{T} thresholds. The resulting SL trigger rate is thus only about 80% larger than the rate of the FH trigger.

The efficiency of the jet p_{T} requirements in the trigger is estimated as a function of the jet p_{T} and η from data collected with a prescaled single-jet trigger with lower p_{T} threshold. This trigger is fully efficient in the kinematic range under consideration, and the fraction of such events fulfilling also the requirement of the nominal jet trigger measures its efficiency. The same procedure is applied to simulated events of multijet production. The ratio of these two efficiencies determines the scale factors that are used to correct all simulated samples in the analysis. The scale factor displays a sharp turn-on versus jet p_{T} just above the nominal threshold, and saturates quickly at unity.

The online b tagging efficiencies relative to the offline b tagging selection are obtained from data using prescaled dijet triggers with a single-b-tag requirement. A tag-and-probe method [64] is employed to determine the online b tagging efficiency as a function of jet p_{T}. The two leading jets are required to pass an offline kinematic selection and b tagging similar to the final analysis selection as described above. The second-leading jet must always pass the online b tagging requirement to ensure that it has passed the trigger requirement. It is then checked whether the first-leading jet also satisfies the online b tagging requirement; the fraction of such cases is a direct measure of the relative online b tagging efficiency. This procedure is applied in both data and simulation. The ratio of these efficiencies between the data and the simulation provides the online b tagging scale factor, displayed in Fig. 2, and it is found to range within 0.8–1.1 across the relevant jet p_{T} range.

Using a similar approach, the tag-and-probe method is applied to evaluate the muon trigger

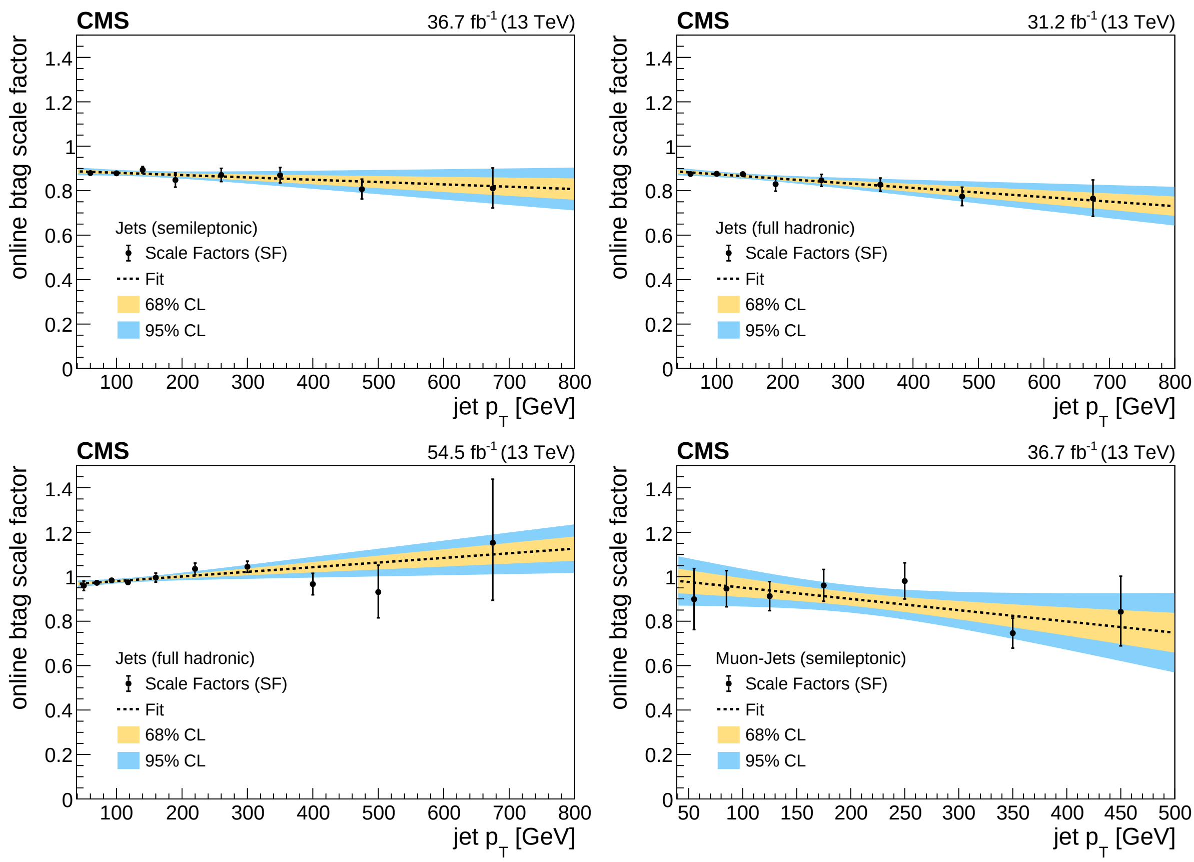

Figure 2: Online b tagging scale factors for b jets in the 2017 SL (upper left), 2017 FH (upper right) and 2018 FH (lower left) analyses, and for b jets with muons in the 2017 SL analysis (lower right). The results of linear fits are also shown, together with $\pm 1\sigma$ and $\pm 2\sigma$ uncertainty bands.

efficiency as a function of muon p_T using the $J/\psi \to \mu^+\mu^-$ resonance peak [48]. The data are collected with a prescaled single-muon trigger with lower p_T threshold in the double-muon data set and compared with simulations of multijet production. Events are selected in the J/ψ mass window to obtain a pure sample of muons with a soft p_T spectrum. As a result, the efficiency is estimated from the overall normalisation factor of the simultaneous invariant mass fit in the bins of muon p_T. The single-muon trigger efficiency exceeds 90% over the full η range, and the efficiency to reconstruct and identify muons is greater than 96%. Scale factors are obtained to correct all simulated samples, and fall within 0.90–1.05 across the p_T range of the probe muon.

In the FH channel, the offline selection requires at least three jets within $|\eta| < 2.2$, with the two leading jets having $p_T(j_1) > 110\,(130)$ GeV and $p_T(j_2) > 100\,(130)$ GeV in the 2017 (2018) data set, and the third-leading jet having $p_T(j_3) > 40$ GeV. The η selection is applied to benefit from optimal b tagging performance, and is safely within the η acceptance of the trigger. The three leading jets have to pass the DEEPJET b tagging requirement of the medium working point [45]. The $|\Delta\eta|$ between the two leading jets must be less than 1.5, and a pairwise separation of $\Delta R > 1$ between each two of the three leading jets is imposed to suppress background from $b\overline{b}$ pairs arising from gluon splitting, where $\Delta R = \sqrt{(\Delta\eta)^2 + (\Delta\phi)^2}$ with $\Delta\phi$ being the separation in the azimuthal angle.

In the SL channel, because of lower p_T requirements in the trigger path, events can be selected offline with lower p_T thresholds: $p_T(j_1) > 60$ GeV, $p_T(j_2) > 50$ GeV, and $p_T(j_3) > 30$ GeV for the three leading jets, respectively. As in the FH selection, the three leading jets have to pass the DEEPJET b tagging requirement of the medium working point. One nonisolated muon passing tight identification [48] is required with $p_T(\mu) > 13$ GeV and $|\eta| < 2.2$. This muon must lie within the cone of either of the two most energetic b jets in the event, satisfying $\Delta R(\mu, j) < 0.4$.

To avoid event duplications between the FH and SL selections, events containing at least one reconstructed muon fulfilling the criteria of the SL selection are vetoed from the FH channel in the 2017 data set. Apart from the kinematic requirements above, all objects selected offline are required to match the objects triggered online within an angular separation of $\Delta R < 0.3$. At least two among the selected three leading jets need to match online b jets in both FH and SL channels, while muon matching is required for the SL channel. In case both of the two leading jets contain a muon, the b jet with the largest muon p_T is required to match the muon requirement in the SL trigger.

Further corrections to improve the mass resolution are applied in the selection process. A b jet energy regression based on a deep neural network allows accounting for missing energy, for example because of neutrinos emitted in semileptonic decays of b hadrons [65]. Furthermore, a final state radiation (FSR) recovery technique is used to account for gluons emitted by b jets before hadronising. Jets not among the three leading jets in the event are treated as FSR candidates. If such a candidate lies within a distance $\Delta R < 0.8$ of one of the three leading jets, its four-momentum is added vectorially to that of the respective leading jet.

The selection detailed above defines the signal region (SR) of this analysis, and events passing this selection are referred to as the "triple b tag" sample in the following. To study the features of the multijet background, a control region (CR) is constructed in a similar way except for imposing a b tag veto on the third leading jet. This veto rejects jets that would satisfy a loose b tagging requirement. This requirement is defined by a 10% probability for light-flavour quark and gluon jets to be misidentified as b jets, and has a b jet identification efficiency of about 70%. The "b tag veto" CR has no overlaps with the triple b tag SR, while it preserves similar kinematic distributions for the three leading jets. In addition, the signal contamination in the

CR is negligible. A summary of the offline selection parameters is given in Table 1.

Table 1: Summary of the main parameters of the offline selection for the three data sets 2017 SL, 2017 FH, and 2018 FH, where j_1, j_2, j_3 indicate the first three leading jets. Entries denoted by "—" indicate that the selection is not applied. Signal region (SR) and control region (CR) only differ in the b tag selection, shown in the bottom rows, where ">M" ("< L") indicate that the respective jet should pass (fail) the requirement of the medium (loose) working point, respectively.

Variable	2017 SL		2017 FH		2018 FH	
$p_T(j_1)$ [GeV]	>60		>110		>130	
$p_T(j_2)$ [GeV]	>50		>100		>130	
$p_T(j_3)$ [GeV]	>30		>40		>40	
$\lvert\eta\rvert(j_1, j_2, j_3)$	<2.2		<2.2		<2.2	
$\lvert\Delta\eta\rvert(j_1, j_2)$	<1.5		<1.5		<1.5	
$\Delta R(j_1, j_2)$, $\Delta R(j_1, j_3)$, $\Delta R(j_2, j_3)$	>1		>1		>1	
$p_T(\mu)$ [GeV]	>13		>13		—	
$\lvert\eta\rvert(\mu)$	<2.2		<2.2		—	
$\min(\Delta R(\mu, j_1), \Delta R(\mu, j_2))$	<0.4		<0.4		—	
$N(\mu)$	≥1		=0		—	
	SR	CR	SR	CR	SR	CR
btag (j_1, j_2)	>M	>M	>M	>M	>M	>M
btag (j_3)	>M	< L	>M	< L	>M	< L

6 Signal model

The invariant mass of the two leading jets, M_{12}, represents the main analysis variable, and its distribution is used for the extraction of the signal. For each considered mass hypothesis of the Higgs boson, m_ϕ, the M_{12} distribution is obtained from the corresponding simulated signal sample, for nominal masses in the range of 125–1800 GeV.

Various scale factors are measured to correct the signal event simulation to match the data. These include the efficiencies of the trigger kinematic and online b tagging requirements, as described in Section 4, as well as jet energy scale and resolution [43]. Correction factors to account for the different offline b tagging efficiencies [46, 47], and muon identification efficiency [48] are also applied.

The signal efficiency after full selection for each value of m_ϕ is estimated from simulation and shown in Fig. 3. The total signal efficiency in the SR ranges between 0.3 (0.5) and 1.8 (3.6)% and peaks around 600 GeV in the 2017 (2018) FH channel. The main limiting factors are the kinematic selection, in particular the p_T thresholds, and the triple b tag requirement, which each reduce the efficiency by about one order of magnitude. A large part of this reduction already occurs in the online selection, whose efficiency ranges from 8 (6) to 16 (23)% in the 2017 (2018) FH channel, including a sizeable effect from online b tagging. Towards low values of m_ϕ, the effect of the p_T thresholds is strongest, while towards large masses, the degradation of the b tagging performance at very large jet p_T is most noticeable. The selection on $\Delta\eta$ of the two leading jets also plays a significant role. The signal efficiency in the 2018 FH data is generally higher compared to 2017 FH because of a less restrictive online b tagging selection. For the SL channel, the total signal efficiency increases gradually from 0.04 to 0.60% along the probed mass range of 125–700 GeV, its size compared to the FH channels reflecting the semileptonic branching fraction of b hadrons into final states with muons. In the CR, the signal efficiency is significantly lower than in the SR, typically by a factor of two or more. As the CR is far more populated by background than the SR, by about a factor of five, this results in an order of magnitude relative signal depletion of the CR.

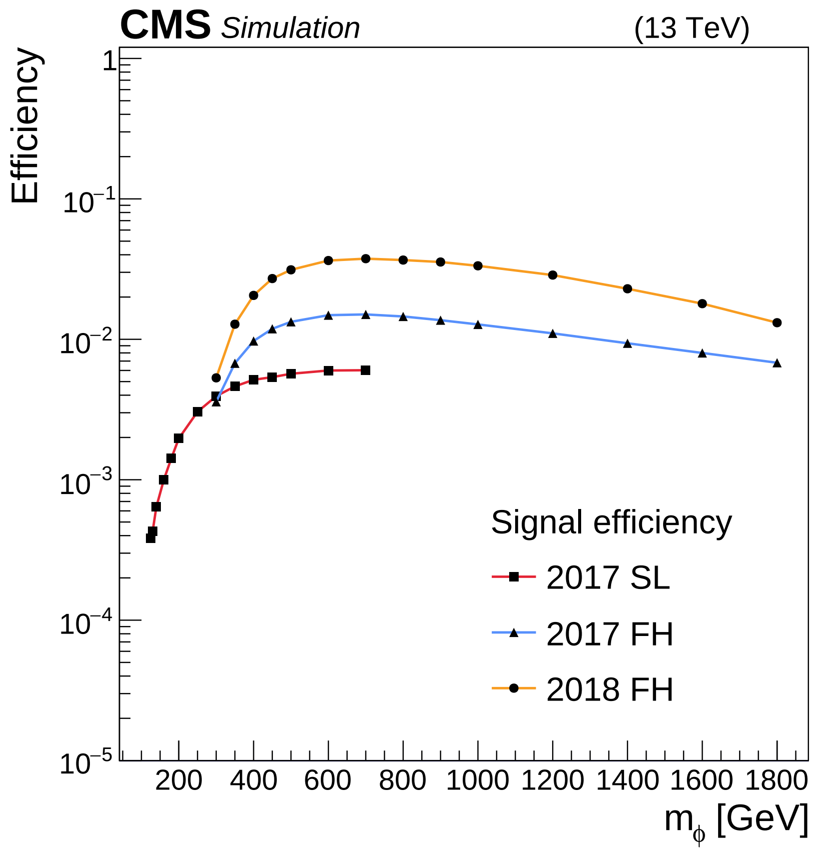

Figure 3: Signal efficiency as a function of the mass m_ϕ after triple b tag selection for 2017 SL (squares), 2017 FH (triangles), and 2018 FH (circles) channels.

In Fig. 4, the distributions of the reconstructed invariant mass of the two leading jets, M_{12}, obtained from simulation, are illustrated for the SL and FH channels in the 2017 and 2018 data sets for selected mass points. The natural width expected for an MSSM Higgs boson in the considered mass and $\tan\beta$ region is negligible compared to the detector resolution [30]. Therefore, the observed shape of the mass distribution is largely determined by the experimental resolution and the effects of wrong jet pairing, which occurs when the two leading jets used to compute M_{12} are not originating from the Higgs boson decay. Tails towards lower M_{12} values are attributed to incomplete reconstruction of the Higgs boson's decay products, particularly due to unaccounted momentum from neutrinos in semileptonic decays of b and c hadrons. Wrong jet pairing potentially gives rise to tails in both directions, but for the lower mass points the left-side tails are suppressed because of the effect of the jet p_T selection threshold. The resulting full width at half maximum is typically 20% (25–30%) of the nominal Higgs boson mass for the FH (SL) channels. To describe the M_{12} distribution as a smooth shape, each signal is parameterised by a double-sided Crystal Ball probability density function, which has a Gaussian core portion with smoothly-attached low- and high-end power law functions [66]. The results of the fits are also shown in Fig. 4.

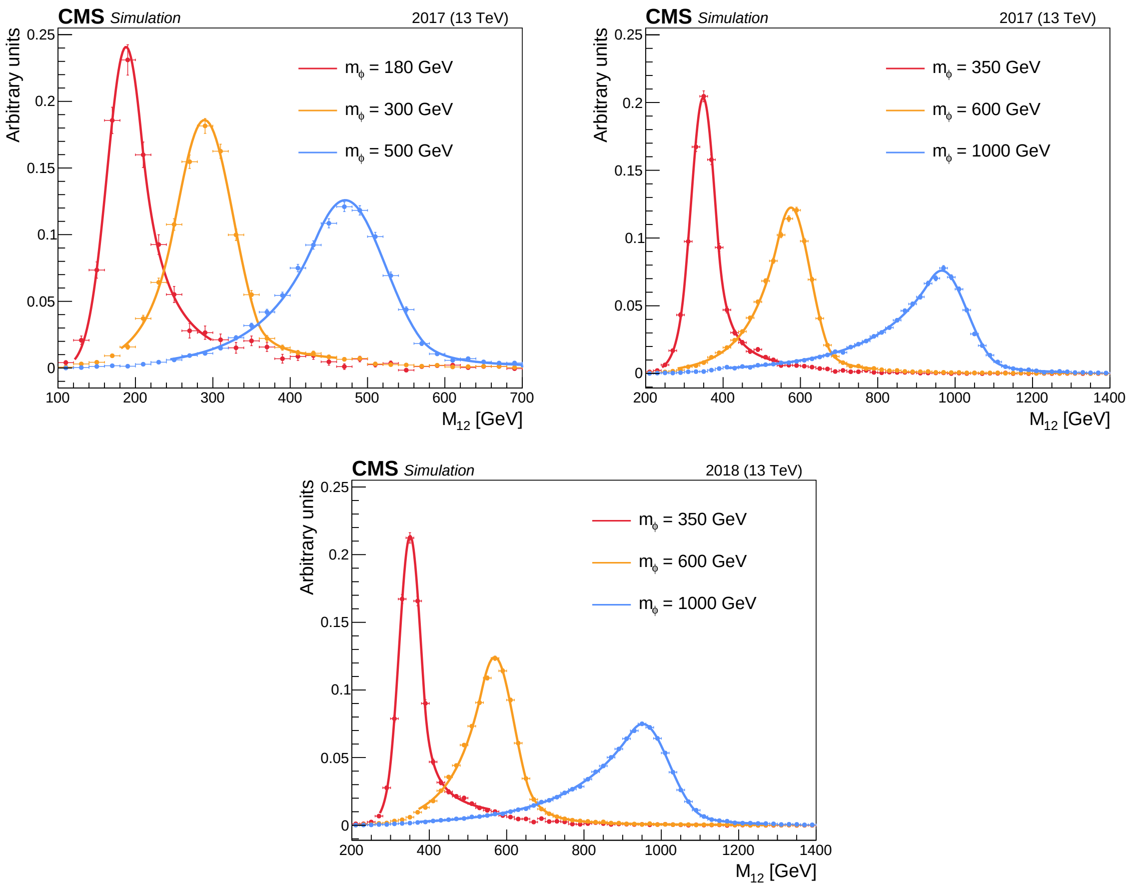

Figure 4: Simulated signal yields normalized to unit area for three representative values of the Higgs boson mass m_ϕ in the 2017 SL (upper left), 2017 FH (upper right), and 2018 FH (lower) channels. The solid curves show the signal parameterisations by double-sided Crystal Ball probability density functions.

7 Background model

The dominant background for this analysis originates from heavy-flavour multijet production yielding at least three energetic jets, of which at least two contain b hadrons. Top quark-antiquark production exhibits an M_{12} shape very similar to the multijet process. It is found to be at the level of only a few percent, and is implicitly included in the background model.

In multijet events, the distribution in M_{12} falls steeply at large values, while at low values it exhibits a marked turn-on behaviour mainly due to the kinematic selection at the trigger and offline levels. This effect shapes the distributions in the SR and the CR in the same way, since their selections only differ in a b tag requirement versus a b tag veto on the third leading jet. Simulation shows that the M_{12} distributions in the SR and CR are indeed very similar in shape [67, 68]. The background model is thus based on the shape of the M_{12} distribution in the CR, which is parameterised by a fitted analytic function and multiplied by a function referred to as "transfer factor", defined below, that accounts for mild shape differences between the SR and the CR.

For ease of parameterisation, the M_{12} range is divided into three (four) overlapping fit ranges for the SL (FH) data sets. These fit ranges are overlapping to ensure that the signal of each mass point, including tails, is sufficiently covered by one mass range. These fit ranges, their boundaries, and the associated Higgs boson mass points are listed in Table 2.

Table 2: Definition of fit ranges for the 2017 SL, 2017 FH, and 2018 FH channels in terms of M_{12} and the associated values of the nominal Higgs boson mass, m_ϕ, which are probed in this fit range.

Channel	Fit range	Mass range (M_{12}) [GeV]	Signal mass (m_ϕ) [GeV]
2017 SL	1	120–300	125, 130, 140, 160, 180, 200
	2	180–460	250, 300, 350
	3	240–800	400, 450, 500, 600, 700
2017 FH	1	240–560	300, 350, 400
	2	280–800	450, 500, 600
	3	400–1300	700, 800, 900
	4	600–2000	1000, 1200, 1400, 1600, 1800
2018 FH	1	270–560	300, 350
	2	320–800	400, 450, 500
	3	390–1270	600, 700, 800, 900
	4	500–2000	1000, 1200, 1400, 1600, 1800

Figures 5, 6, and 7 show the M_{12} distributions in the CR in each fit range for the 2017 SL, 2017 FH, and 2018 FH data sets, respectively, along with the parameterisations discussed in the following. The goodness-of-fit estimators indicate adequate descriptions of the distributions.

For the parameterisation of the mass distributions in the CR an extension of the Novosibirsk function is used. The Novosibirsk function was originally devised to describe a Compton spectrum [69]. Its extended form is defined as:

$$g(M_{12}) = p_2 \exp\left(-\frac{1}{2\sigma_0^2}\ln^2\left[1 - \frac{M_{12}-p_3}{p_4}p_5 - \frac{(M_{12}-p_3)^2}{p_4}p_5 p_6\right] - \frac{\sigma_0^2}{2}\right), \tag{1}$$

where p_2 is a normalisation parameter, p_3 the peak value of the distribution, p_4 and p_5 are the

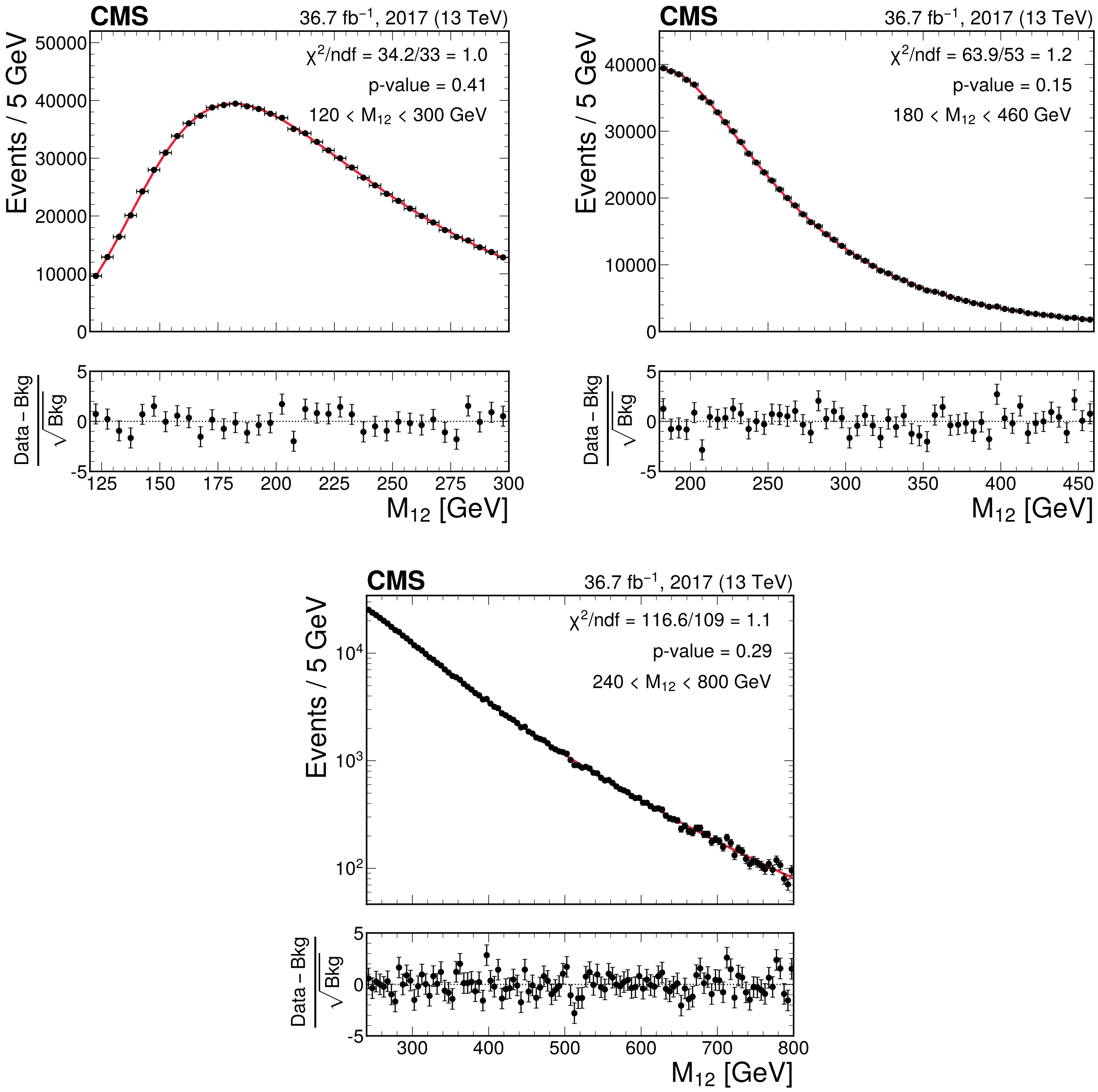

Figure 5: Invariant mass distributions of the three fit ranges in the b tag veto CR for the 2017 SL channel, overlaid with the fitted functions. The distributions are fitted in the M_{12} ranges of 120–300 GeV (upper left), 180–460 GeV (upper right), and 240–800 GeV (lower). The χ^2 and the corresponding p-value obtained from the goodness-of-fit test are displayed on each plot. The lower panels show the difference between the data and the fitted function, divided by the estimated statistical uncertainty for each bin. Good agreement between the fitted functions and the data is achieved.

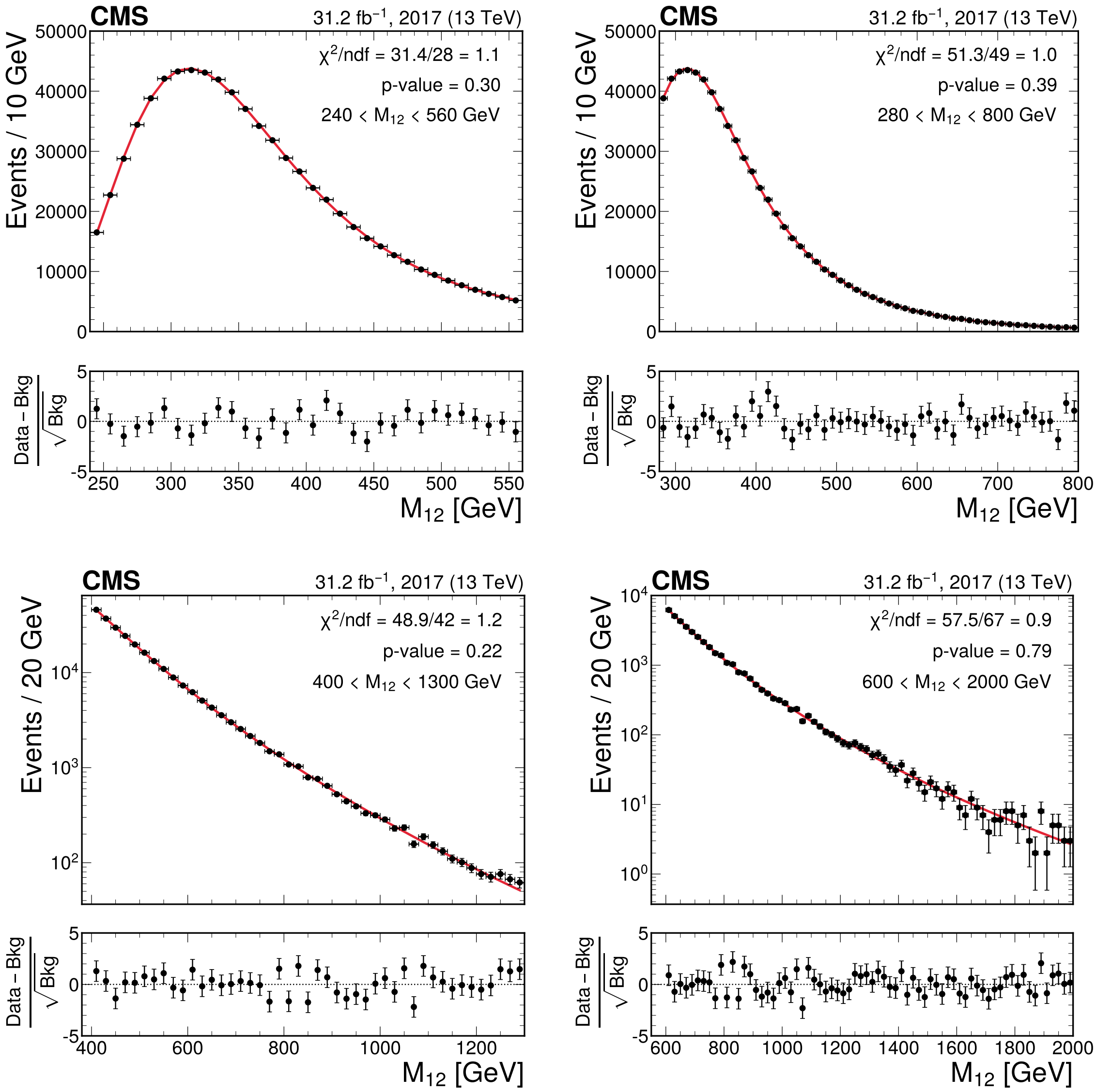

Figure 6: Invariant mass distributions of the four fit ranges in the b tag veto CR for the 2017 FH channel, overlaid with the fitted functions. The distributions are fitted in the M_{12} ranges of 240–560 GeV (upper left), 280–800 GeV (upper right), 400–1300 GeV (lower left), and 600–2000 GeV (lower right). The χ^2 goodness-of-fit test and corresponding p-value are indicated in each plot. The lower panels show the difference between the data and the fitted function, divided by the estimated statistical uncertainty for each bin. Good agreement between the fitted functions and the data is achieved.

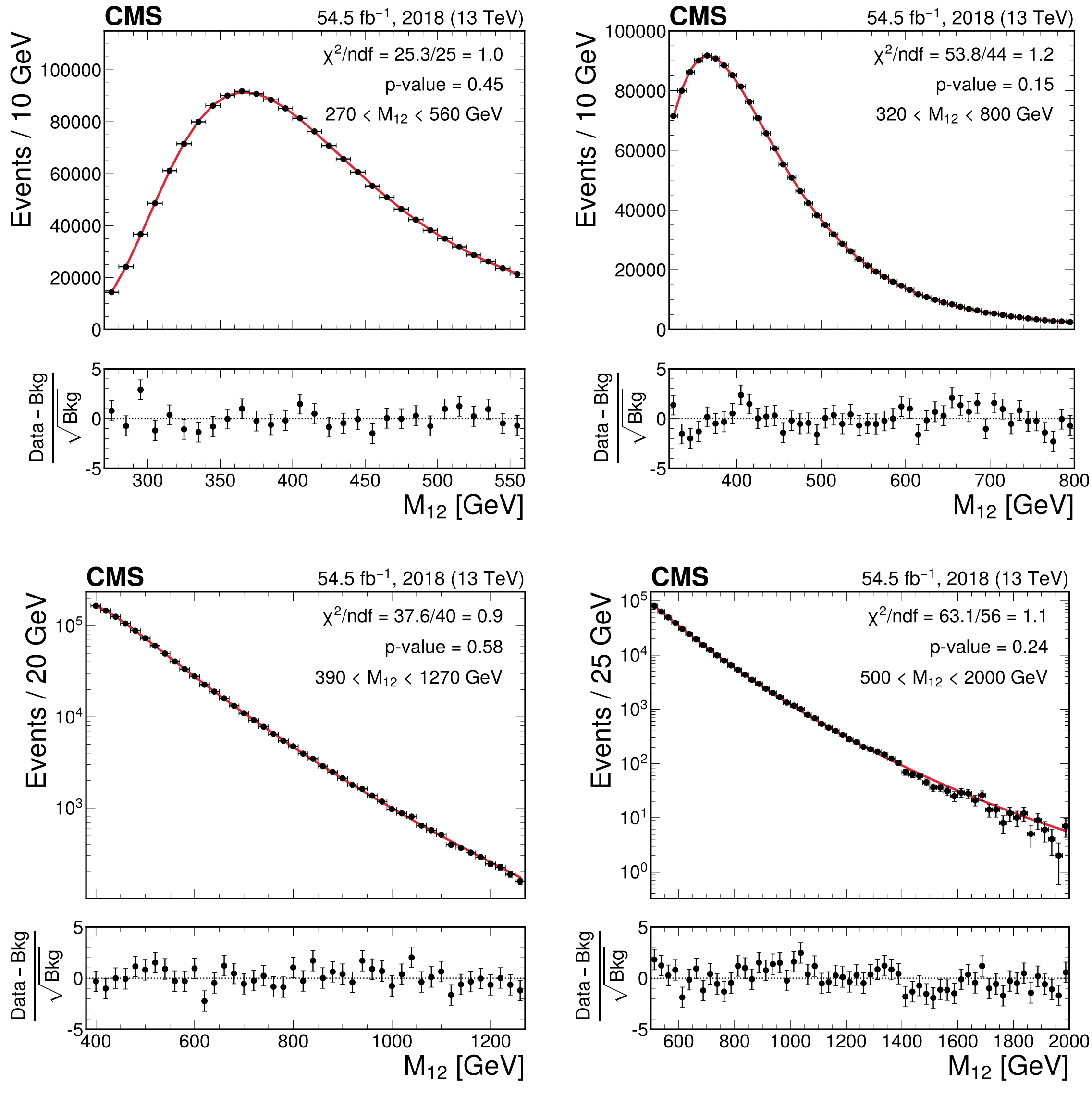

Figure 7: Invariant mass distributions of the four fit ranges in the b tag veto CR for the 2018 FH channel, overlaid with the fitted functions. The distributions are fitted in the M_{12} ranges of 270–560 GeV (upper left), 320–800 GeV (upper right), 390–1270 GeV (lower left), and 500–2000 GeV (lower right). The χ^2 goodness-of-fit test and corresponding p-value are indicated in each plot. The lower panels show the difference between the data and the fitted function, divided by the estimated statistical uncertainty for each bin. Good agreement between the fitted functions and the data is achieved.

parameters describing the asymmetry of the spectrum, and p_6 is the parameter of the extended term. The variable σ_0 is defined as:

$$\sigma_0 = \frac{2}{\xi} \sinh^{-1}(p_5\xi/2), \text{ where } \xi = 2\sqrt{\ln 4}. \tag{2}$$

In some fit ranges, the effect of the kinematic turn-on at the lower edge exhibits a more complex shape, which cannot be modelled by the extended Novosibirsk function alone. These include the first fit range of the SL channel and the second fit range of the FH channel in the 2017 data set. An additional turn-on factor, represented by a Gaussian error function, is introduced and multiplied by the extended Novosibirsk function. It has the following analytic form:

$$h(M_{12}) = 0.5\left[\mathrm{erf}(p_0[M_{12} - p_1]) + 1\right], \tag{3}$$

where

$$\mathrm{erf}(x) = \frac{2}{\sqrt{\pi}} \int_0^x \mathrm{e}^{-t^2} \mathrm{d}t, \tag{4}$$

and the parameters p_0 and p_1 describe the slope and centre of the turn-on flank, respectively.

The transfer factor is an analytic function that parameterises the ratio of the background mass distributions in SR and CR for each fit range and data set. This function is chosen to be a sum of Chebyshev polynomials up to the third degree following a study with multijet events in simulations. The coefficients of the Chebyshev polynomials are obtained in the final simultaneous fit to the data in the SR and CR, separately for each channel and data set. In addition, the choices of functional form may cause possible bias and give different results for the signal parameters, representing a systematic uncertainty associated with the choice of function. This uncertainty is accounted for with the discrete profiling method [70]. This method introduces an additional (discrete) nuisance parameter indicating the choice of the transfer factor in this analysis, which is profiled in an analogous way to continuous nuisance parameters.

The background model and the signal extraction method are validated by applying them in a signal-depleted validation region (VR). The selection in the VR proceeds in the same way as in the SR and CR, except that the b tagging score of the third leading jet must lie between the loose and the medium working points. By this definition, there is no overlap between VR, SR, and CR. The observed limits from these tests are found to be everywhere in agreement with the expected limits within uncertainties, indicating correct performance of the background model.

8 Signal extraction and systematic uncertainties

The signal extraction is performed with a simultaneous maximum likelihood fit to the M_{12} distributions in the SR and CR, at first separately for the 2017 SL, 2017 FH, and 2018 FH data sets. In this simultaneous fit, the CR data are modelled with the corresponding parameterization as discussed in Section 7 with floating parameters. The SR is modelled by a sum of the same parameterization with identical parameters multiplied by the respective transfer factor, and the signal shape multiplied by the signal strength parameter. The parameters of the transfer factor are also floating in the fit. The simultaneous fit ensures that the uncertainties in the CR background function are taken into account with all correlations also in the SR.

Apart from the statistical uncertainties in each data set, systematic uncertainties originating from both theoretical and experimental sources are considered. In the signal extraction fit, all uncertainties are implemented as penalty terms, i.e. "nuisance parameters" [71], to the likelihood function. The following systematic uncertainties are taken into account in the expected signal and background estimation, as well as for the interpretations within the MSSM and generic 2HDMs:

Integrated luminosity The integrated luminosities for the 2017 and 2018 data-taking years have 2.3 and 2.5% individual uncertainties, respectively [72, 73], while the overall uncertainty for the 2016–2018 period is 1.6%.

Pileup The systematic uncertainty introduced by the total inelastic pp cross section that is used in the simulation of pileup events is quantified by varying the effective total inelastic cross section of 69.2 mb within its $\pm$4.6% uncertainty [74].

Prefiring correction In the 2017 data-taking period, an increase in the offset of the ECAL timing pulse caused the ECAL L1 trigger to accept the event during the previous bunch crossing (referred to as "prefiring", producing dead time) [75]. This results in a relative reduction of the signal efficiency by 0.3–2%. The uncertainty in the efficiency correction is taken into account.

Online kinematic efficiency The efficiency of the jet selection at the trigger level is determined from the data using single-jet control triggers. The uncertainty is very small, at most at the percent level, and only relevant for the lowest mass points that are closest to the kinematic thresholds. The uncertainty in the muon identification efficiency at trigger level is determined using the J/ψ signal and amounts to about 5%.

Online b tagging efficiency The online b tagging efficiency is determined from the data with dedicated control triggers using a tag-and-probe method as described in Section 4. The systematic uncertainty in the online b tagging efficiency increases with increasing jet p_T from about 1 to 5% per jet over the considered p_T range. For b jets containing muons, the uncertainty varies between 3 and 10% over the p_T range.

Jet energy scale and resolution Uncertainties in the jet energy scale and resolution affect solely the signal efficiency and the shape of its mass distribution. They are evaluated by varying the energy and resolution corrections for all jets in the signal model within one standard deviation [43].

Offline b tagging efficiency The uncertainty in the offline b tagging efficiency depends on the jet p_T and ranges from 2–15% per jet. The combined uncertainty in the b tagging of three jets per selected signal event, together with the additional uncertainty in the online b tagging of two jets, constitutes the total systematic uncertainty in b jet identification [46, 47].

Muon identification The uncertainty in the offline muon identification efficiency ranges from 1–3% [48].

Uncertainty in the choice of background parameterisation Different forms of transfer factors are considered, described by Chebyshev polynomials up to the third order. They are integrated in the signal extraction procedure by means of the discrete profiling method, as described in Section 7.

Theory-related uncertainties The theoretical uncertainty in the QCD factorisation and renormalisation scales (μ_F and μ_R), and uncertainties in the choice of the PDFs and α_S are addressed following the recommendations of the LHC Higgs Working Group [76]. The uncertainties arising from the parton shower modelling are found to have negligible impact on the analysis.

Only the uncertainties in jet energy scale and resolution are found to affect the shape of the signal mass distributions, while the choice of background parameterisation impacts the shape of the background distributions. Other systematic uncertainties only concern the signal yield. The dominant systematic uncertainty lies in the background estimation over most of the mass range, followed by uncertainties in the b tagging efficiency uncertainties. At very large masses, the b tagging efficiency contributes the dominant uncertainty.

9 Results

As mentioned in Section 8, a binned maximum likelihood fit of the signal plus background parameterisations to the data M_{12} distribution is performed to extract the number of potential signal events. The test statistic chosen to determine the signal yield is based on the maximum likelihood ratio profiled as a function of the signal strength, i.e., the ratio of the signal yield to the one predicted by the signal model as defined by Eq. (25) in [71]. The fit is performed simultaneously to the triple b tag SR and the b tag veto CR, first separately for the 2017 SL, 2017 FH, and 2018 FH data sets, and then a combined fit over all three data sets is performed for the final results. The results have been determined using the CMS statistical analysis tool, COMBINE [71].

9.1 Cross section results

The invariant mass distributions in the SR from the three different data sets are shown in Figs. 8–10, including the result of the simultaneous CR and SR fit under the background-only hypothesis. In general, the fits show good agreement with the background-only hypothesis.

No significant excess of signal events is observed over the SM background estimation. For each signal mass hypothesis, the results are used to set 95% confidence level (CL) upper limits on the production cross section times branching fraction $\sigma(\mathrm{pp} \to \mathrm{b}\phi + \mathrm{X})\mathcal{B}(\phi \to \mathrm{b\bar{b}})$ using the modified frequentist $\mathrm{CL_s}$ criterion [77, 78], and making use of the asymptotic approximation [79]. Systematic uncertainties are treated as nuisance parameters and profiled in the statistical inference using log-normal priors for uncertainties in the signal yield, and Gaussian priors for shape uncertainties.

Upper limits on the cross section times branching fraction for the three different data sets are shown in Figs. 11, 12, and 13. The observed limits are generally within or near ± 2 standard deviations (σ) of the expected limit. The largest excesses are observed in the 2017 SL analysis with local (global) significances of 3.2 (2.4) σ at $m_\phi = 250\,\mathrm{GeV}$, and 2.7 (1.9) σ at $m_\phi = 300\,\mathrm{GeV}$, where the global significance accounts for the look-elsewhere effect [80] within the 2017 SL, 2017 FH, and 2018 FH analyses.

The results from the three data sets 2017 SL, 2017 FH, and 2018 FH are combined with each other and with the previously published results from the 2016 data [30]. The resulting combined upper limits for cross section times branching fraction are shown in Fig. 14, and compared to the results from the individual data sets.

The best limits are obtained with the 2018 FH analysis, resulting from the larger integrated luminosity and the less restrictive trigger conditions. All 2017–2018 results benefit from the upgrade of the CMS pixel detector [32], which generally improves the reconstruction of tracks near the interaction point. These analyses further benefit from the improved b jet identification performance due to the DEEPJET algorithm [31], the more flexible matching of online and offline b tag selections and the use of the transfer factor method for background modelling. All these improvements are reflected in the comparison with the result from the 2016 data. For

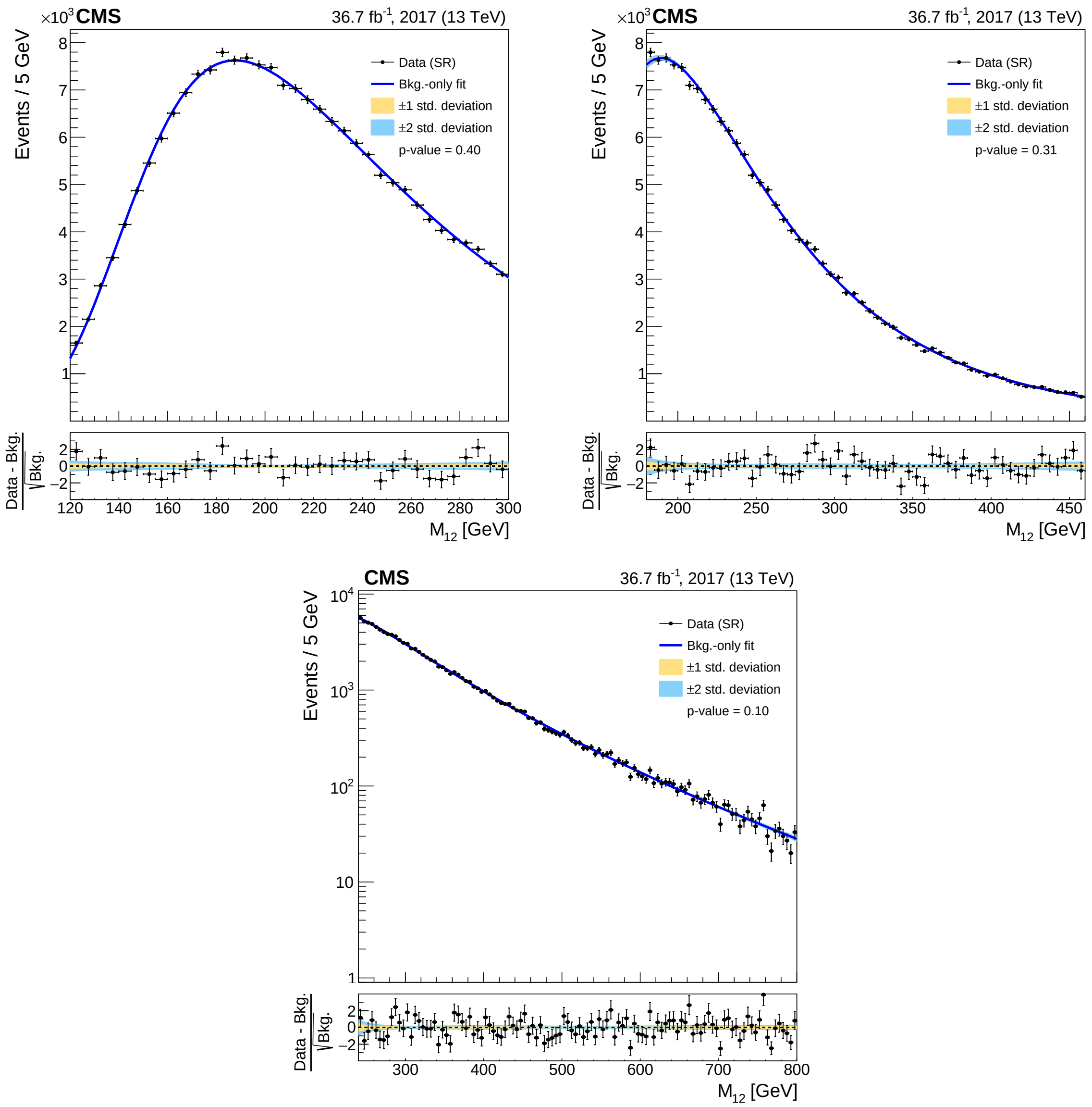

Figure 8: Background-only fits to the M_{12} distribution in each fit range of the 2017 analysis in the SL category, shown together with $\pm 1\sigma$ and $\pm 2\sigma$ uncertainty bands extracted from the fit in the upper panels. The lower panels show the difference between data and fitted background, divided by the statistical uncertainty of the latter. The distributions are fitted in the M_{12} ranges of 120–300 GeV (upper left), 180–460 GeV (upper right), and 240–800 GeV (lower).

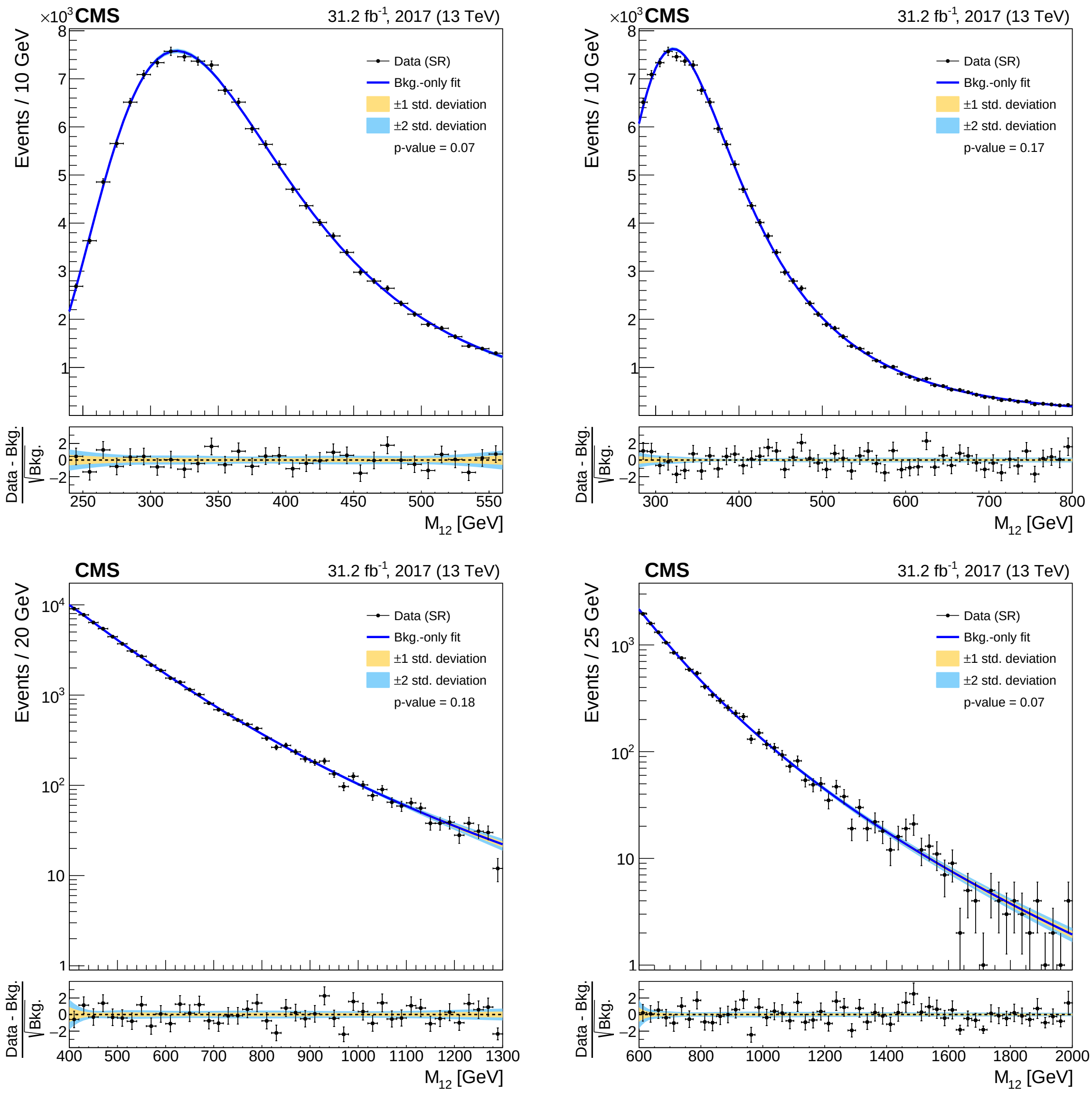

Figure 9: Background-only fits to the M_{12} distribution in each fit range of the 2017 analysis in the FH category, shown together with $\pm1\sigma$ and $\pm2\sigma$ uncertainty bands extracted from the fit in the upper panels. The lower panels show the difference between data and fitted background, divided by the statistical uncertainty of the latter. The distributions are fitted in the M_{12} ranges of 240–560 GeV (upper left), 280–800 GeV (upper right), 400–1300 GeV (lower left), and 600–2000 GeV (lower right).

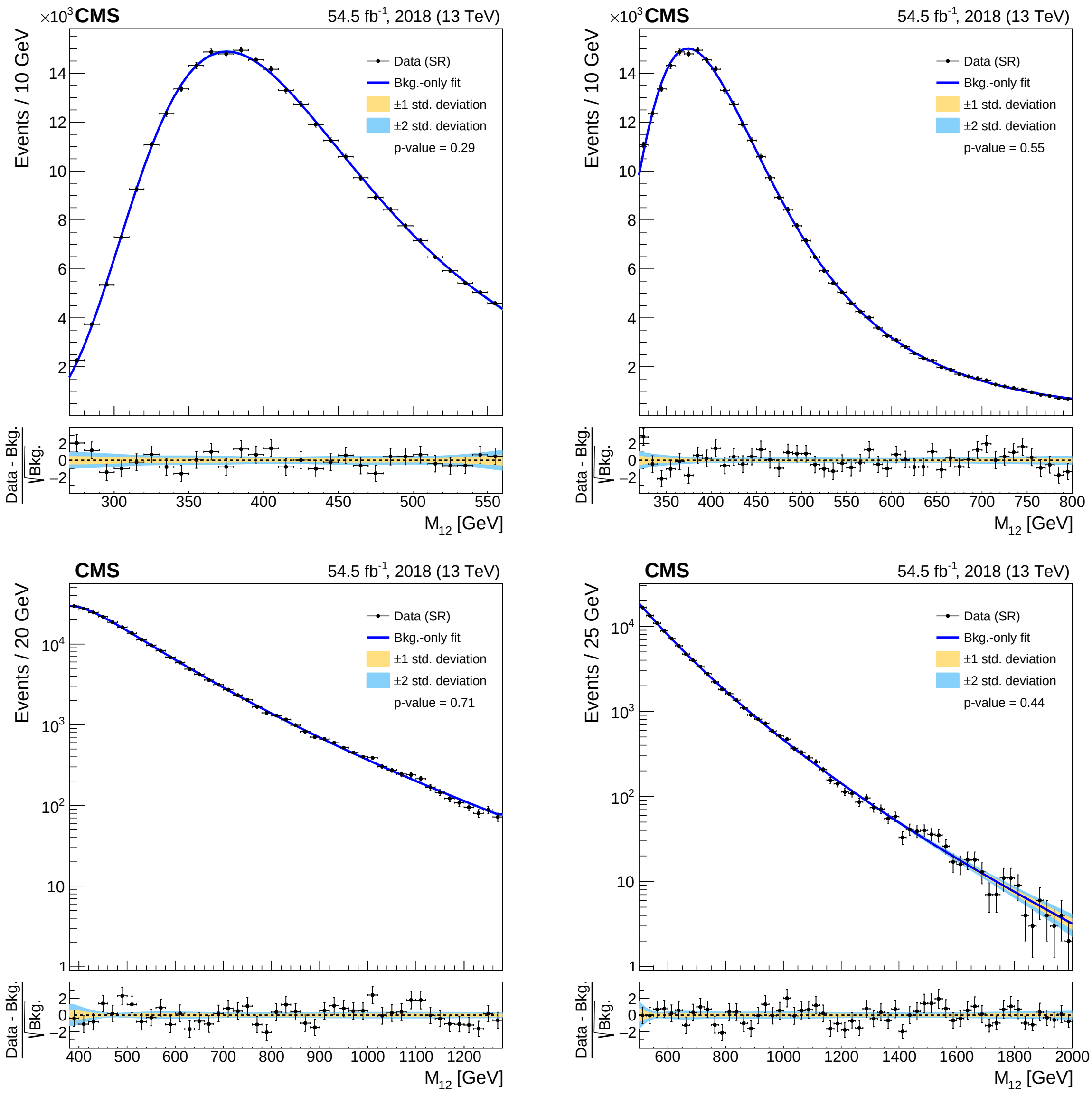

Figure 10: Background-only fits to the M_{12} distribution in each fit range of the 2018 analysis in the FH category, shown together with $\pm 1\sigma$ and $\pm 2\sigma$ uncertainty bands extracted from the fit in the upper panels. The lower panels show the difference between data and fitted background, divided by the statistical uncertainty of the latter. The distributions are fitted in the M_{12} ranges of 270–560 GeV (upper left), 320–800 GeV (upper right), 390–1270 GeV (lower left), and 500–2000 GeV (lower right).

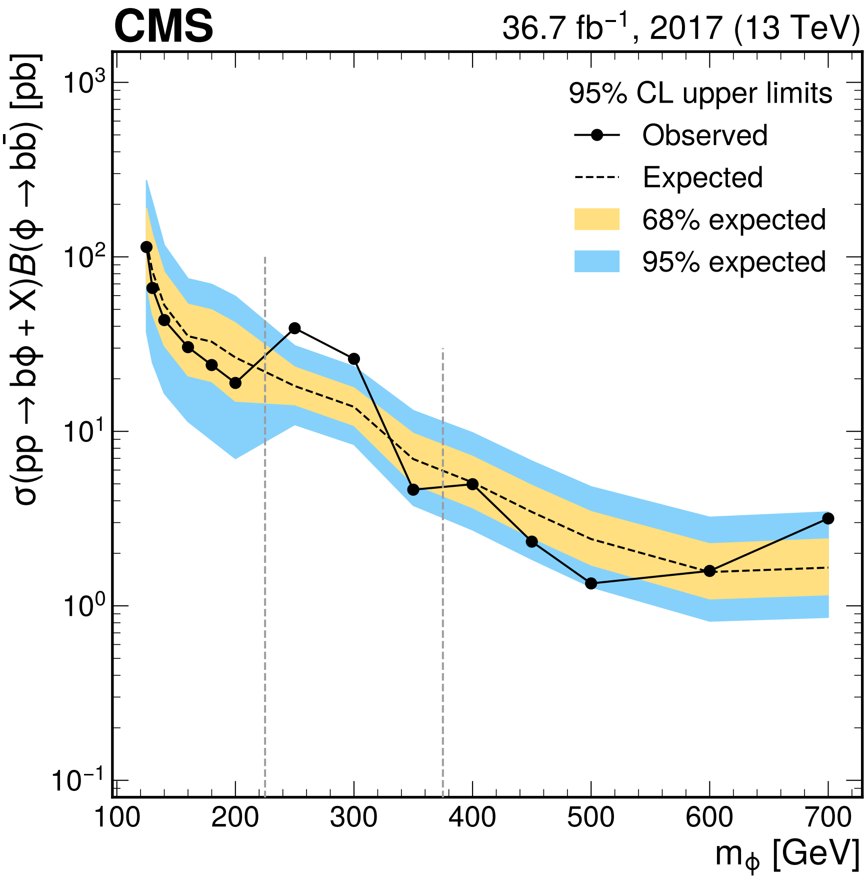

Figure 11: Expected and observed upper limits for the b-quark-associated Higgs boson production cross section times branching fraction of the decay into a b quark pair at 95% CL as functions of m_ϕ for the 2017 SL category. The vertical dashed lines indicate the boundaries of usage of the different fit ranges, as reflected in the rightmost column of Table 2.

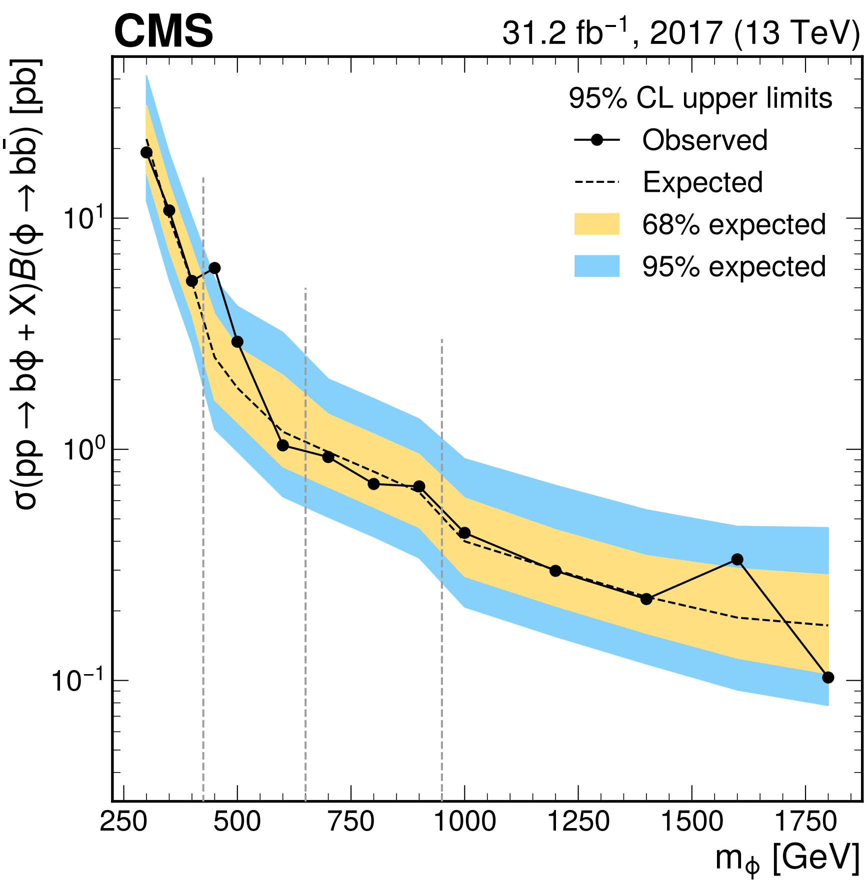

Figure 12: Expected and observed upper limits for the b-quark-associated Higgs boson production cross section times branching fraction of the decay into a b quark pair at 95% CL as functions of m_ϕ for the 2017 FH category. The vertical dashed lines indicate the boundaries of usage of the different fit ranges, as reflected in the rightmost column of Table 2.

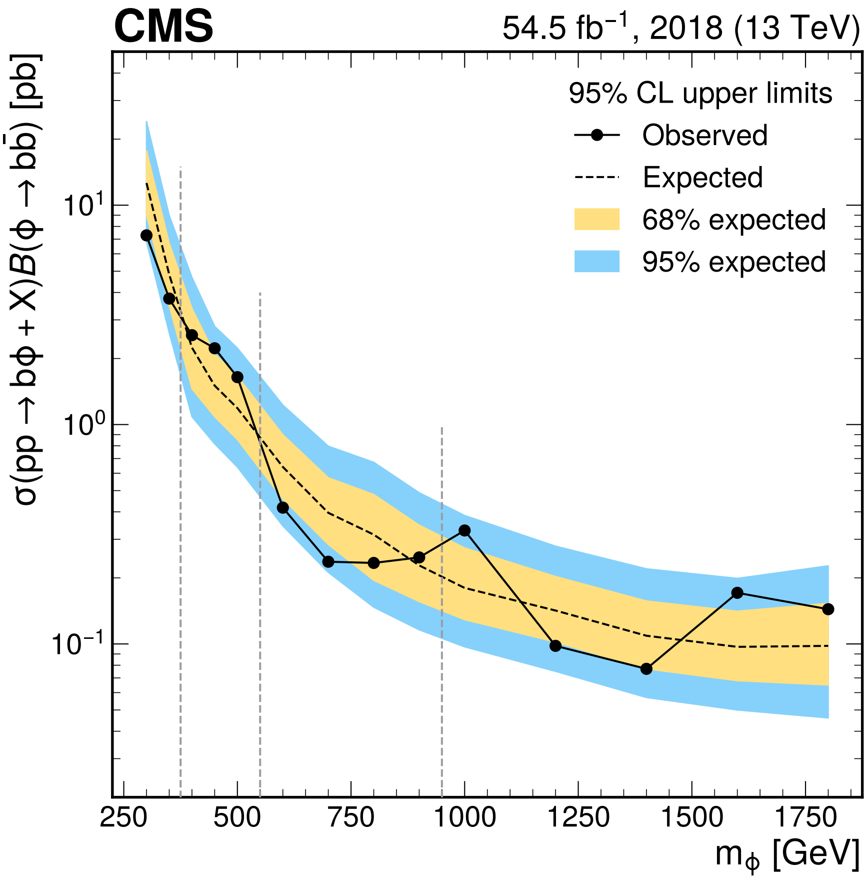

Figure 13: Expected and observed upper limits for the b-quark-associated Higgs boson production cross section times branching fraction of the decay into a b quark pair at 95% CL as functions of m_ϕ for the 2018 FH category. The vertical dashed lines indicate the boundaries of usage of the different fit ranges, as reflected in the rightmost column of Table 2.

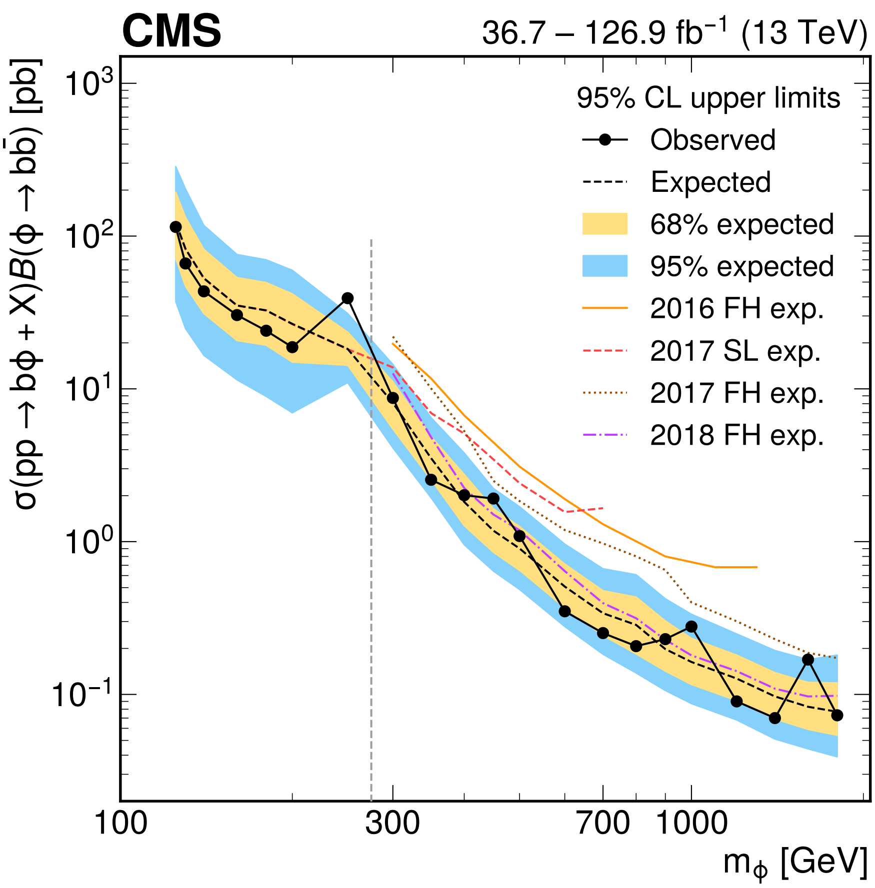

Figure 14: Expected and observed upper limits for the b-quark-associated Higgs boson production cross section times branching fraction of the decay into a b quark pair at 95% CL as functions of m_ϕ, corresponding to the combination with the 2016 data. The vertical dashed line separates the mass range where only the 2017 SL category contributes on its left, from the region where also the 2017 FH and 2018 FH categories contribute on its right. The expected limits from the 2017 SL, 2017 FH, and 2018 FH data sets as well as from the previously published result based on the 2016 data set are also shown as colored lines.

$m_\phi = 1400\,\text{GeV}$, the combined observed limits range down to about 0.07 pb. The 2017 SL analysis gives unique results for m_ϕ in the range of 125–250 GeV, and, at $m_\phi = 300\,\text{GeV}$, its sensitivity is on a par with the 2017 FH analysis.

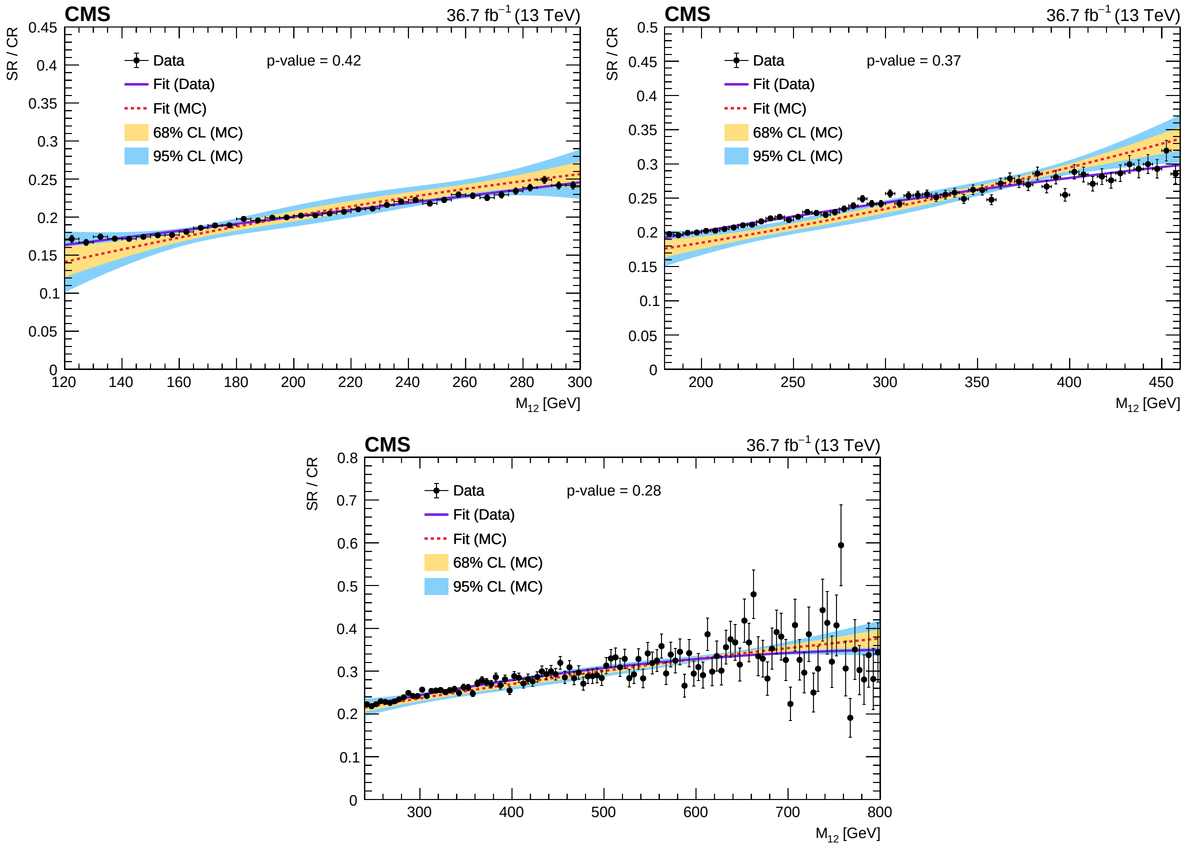

Figure 15: Ratio of M_{12} distributions in SR and CR of the 2017 analysis in the SL category, for data (filled circles), fitted with a sum of Chebyshev polynomials up to the second degree (solid line). The ratio is shown in the M_{12} ranges of 120–300 GeV (upper left), 180–460 GeV (upper right), and 240–800 GeV (lower). The p value resulting from each fit is also quoted. The result of a similar fit based on QCD multijet simulation is superimposed (dashed line) with $\pm 1\sigma$ and $\pm 2\sigma$ bands of statistical uncertainty extracted from the fit.

The unblinding of the SR allows a direct verification of the assumptions underlying the background model. The 2017 SL data set is shown as a representative example. Figure 15 shows the ratio of the M_{12} distributions in the SR and the CR, taken from Figs. 8 and 5, respectively, for each of the three fit ranges. As expected, the ratio is found to be only slowly varying as a function of M_{12}, and it is well modelled by a sum of Chebyshev polynomials as they are used for the transfer factor as described in Section 7. The results of the corresponding fits with simulated QCD multijet events are superimposed. There is qualitative agreement in the sense that data and simulation can be described with similar parameterisations. While the analysis does not rely in any way on a quantitative description of the data by the QCD simulation, the observed level of agreement is worth noting.

9.2 Interpretation in the MSSM

The results from the combination with the 2016 data are interpreted within various scenarios of the MSSM. For each benchmark scenario, the cross sections computed centrally by the LHC Higgs Working Group [76] for b-associated Higgs boson production are used. They are

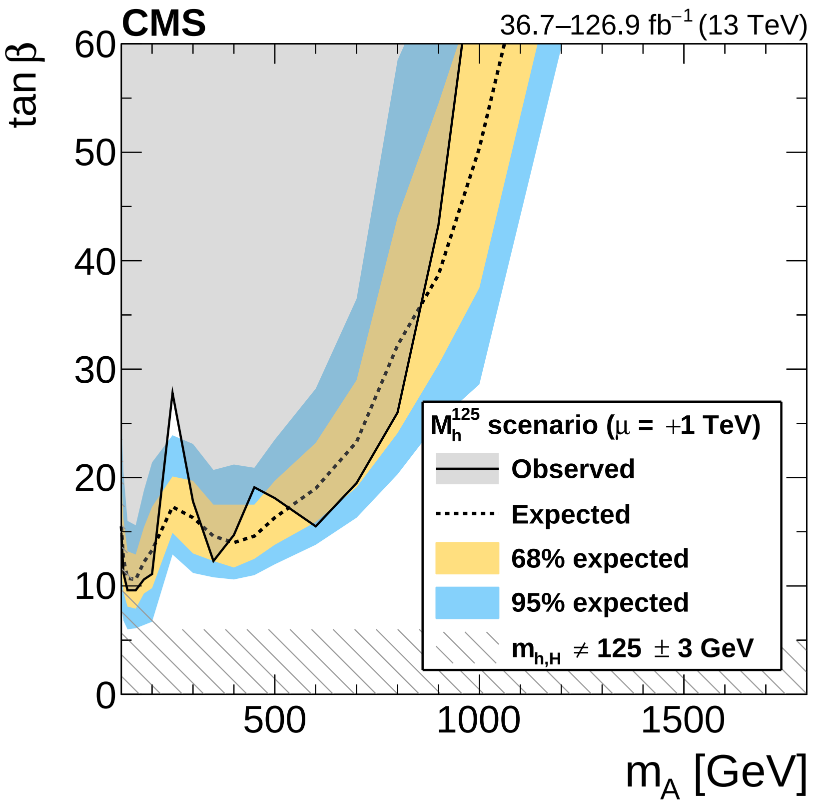

Figure 16: Interpretation in the M_{h}^{125} scenario of the MSSM: observed and expected upper limits at 95% CL on the parameter $\tan\beta$ as functions of the mass m_{A} of the CP-odd Higgs boson. The higgsino mass parameter has been set to $\mu = +1\,\mathrm{TeV}$. The hashed area indicates the parameter region in which the mass of the lightest MSSM Higgs boson does not coincide with 125 GeV within a margin of 3 GeV.

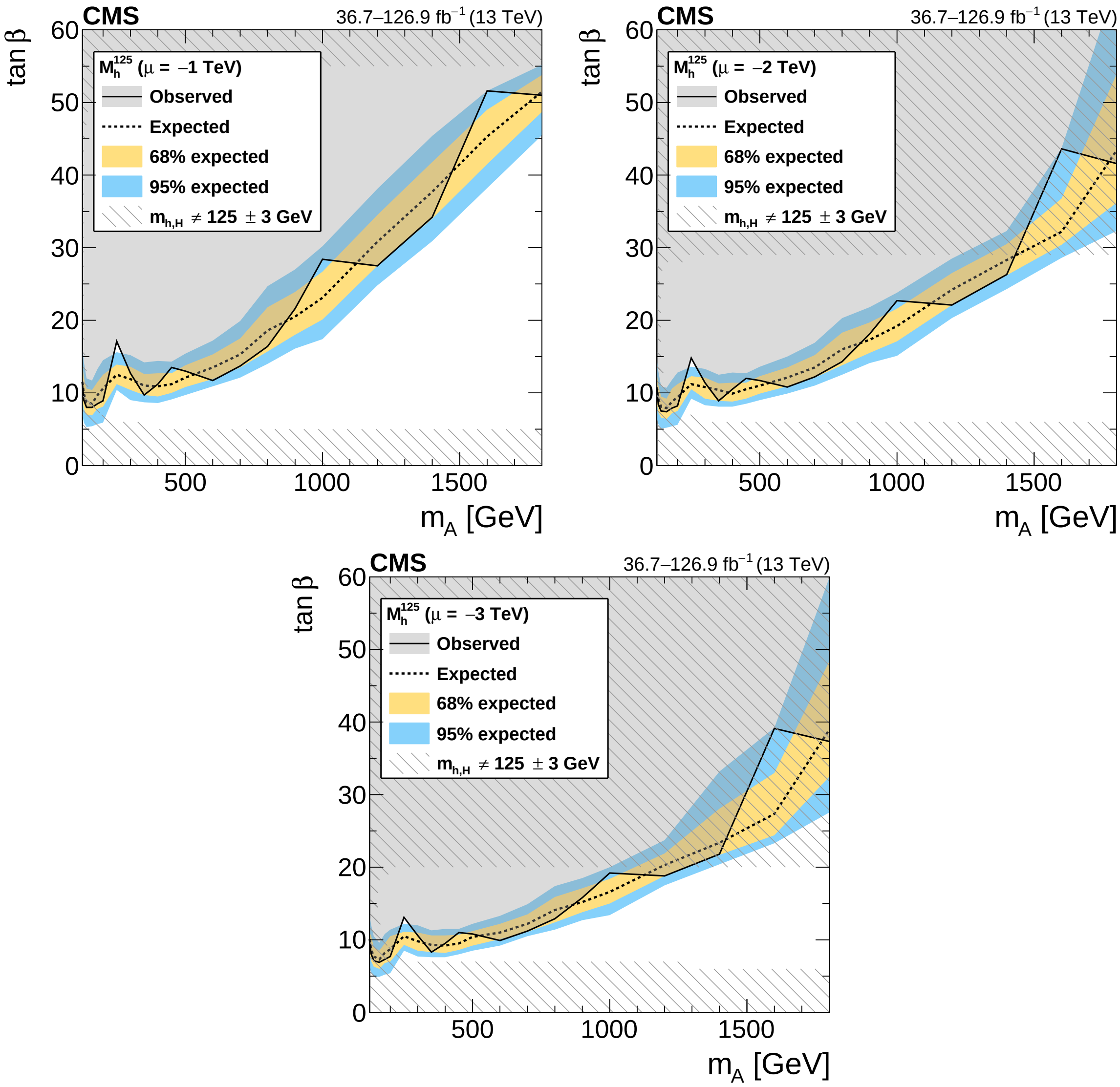

Figure 17: Interpretation in the M_{h}^{125} scenario of the MSSM: observed and expected upper limits at 95% CL on the parameter $\tan\beta$ as functions of the mass m_{A} of the CP-odd Higgs boson. The higgsino mass parameter has been set to $\mu = -1\,\mathrm{TeV}$ (upper left), $\mu = -2\,\mathrm{TeV}$ (upper right), and $\mu = -3\,\mathrm{TeV}$ (lower). The hashed area indicates the parameter region in which the mass of the lightest MSSM Higgs boson does not coincide with 125 GeV within a margin of 3 GeV.

computed according to the four- and five-flavour schemes at NLO [81, 82] and NNLO [83], respectively. The predictions of both schemes are harmonized in the total cross section with Santander matching [84] for the hMSSM and $m_{\mathrm{h}}^{\mathrm{mod+}}$ scenarios, and with FONLL [85, 86] in case of the M_{h}^{125} scenario. Branching fractions to the $\mathrm{b\overline{b}}$ final state are based on the FEYNHIGGS [87–93] framework for all scenarios except for the hMSSM where HDECAY [94, 95] was used.

Figure 16 shows the interpretation within the M_{h}^{125} scenario, with the default setting of the higgsino mass parameter of $\mu = +1\,\mathrm{TeV}$. The most stringent upper limits on the parameter $\tan\beta$ of about 9 are reached in the mass region of 130–150 GeV. The structure of the expected limit reflects the maximum of the background distribution near a reconstructed invariant mass of 180 GeV and the onset of the fully hadronic channel above 300 GeV. They represent the most stringent limits on $\tan\beta$ obtained from the $\mathrm{b\overline{b}}$ channel to date.

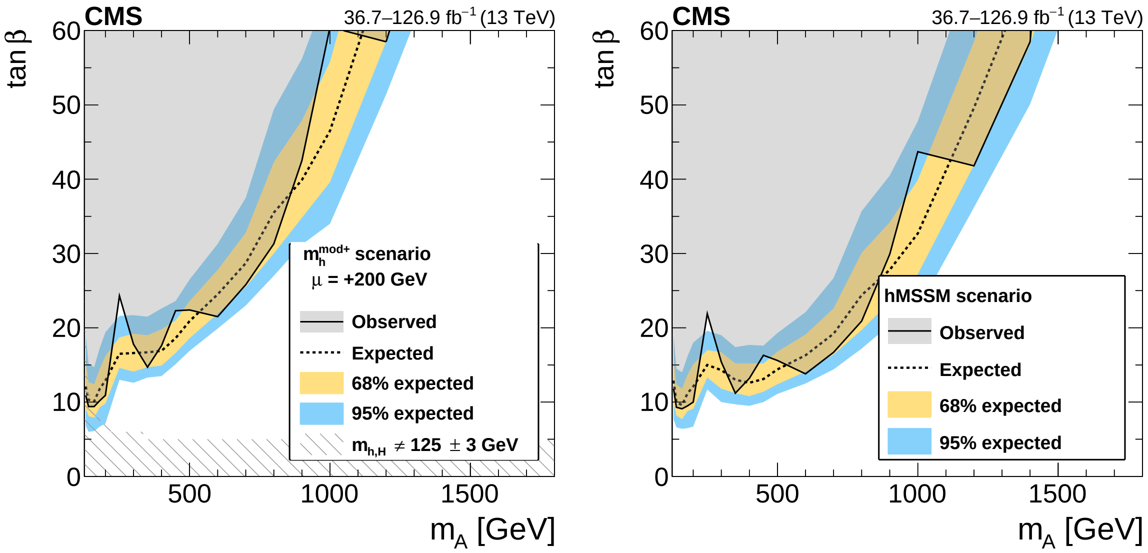

Figure 18: Interpretation in the m_h^{mod+} (left) and hMSSM (right) scenarios of the MSSM: observed and expected upper limits at 95% CL on the parameter $\tan\beta$ as functions of the mass m_A of the CP-odd Higgs boson. In the left plot, the hashed area indicates the parameter region in which the mass of the lightest MSSM Higgs boson does not coincide with 125 GeV within a margin of 3 GeV.

The $(A, H) \to b\overline{b}$ decay channel is uniquely sensitive to negative values of the higgsino mass parameter μ, as the bottom Yukawa coupling correction Δ_b [17, 68] is directly proportional to μ. Since the product of cross section and branching fraction of this process is proportional to $1/(1+\Delta_b)^4$, negative values of μ enhance the total production rate. Interpretations in M_h^{125} scenarios considering negative higgsino mass parameters of $\mu = -1$, -2, and -3 TeV [19] are shown in Fig. 17. The limits on $\tan\beta$ extend approximately down to 8 at 160 GeV and up to 51 at 1800 GeV in the $\mu = -1$ TeV case. The hashed region, indicating the parameter space incompatible with the observed Higgs boson mass of 125 ± 3 GeV due to theoretical constraints, grows with the absolute value of μ in these scenarios. In the $\mu = -2\,(-3)$ TeV scenario, $\tan\beta$ values of above 7.5 (7) are excluded at 160 (180) GeV, ranging up to nearly 30 (20) in the allowed parameter space at about 1500 (1300) GeV. To facilitate comparisons with other studies, Fig. 18 also shows interpretations in the m_h^{mod+} and hMSSM scenarios.

9.3 Interpretation in 2HDMs

The results are interpreted in 2HDM scenarios as functions of their parameters. The b-associated production cross sections and the branching fractions at NNLO precision are computed using the SusHi [96, 97], 2HDMC [98] and LHAPDF [99] programs. Generally, 2HDMs feature a large number of free parameters, which can be reduced down to three parameters according to scenario G defined in Ref. [23], namely m_A, $\tan\beta$, and $\cos(\beta-\alpha)$. The interpretations are performed for the benchmark scenarios where the coupling of the Higgs boson to b quarks is enhanced for $\tan\beta > 1$, i.e. the *Type-II* and *Flipped* benchmark scenarios. In each interpretation, one parameter is fixed and limits are provided in the space of the remaining two parameters.

The left panels in Fig. 19 show the limits in the *Type-II* and *Flipped* models in the $\tan\beta$ and m_A parameter space for $\cos(\beta-\alpha) = 0.1$. The limits in both benchmark scenarios are rather similar, and values of $\tan\beta$ can be excluded down to about 8 at 140 GeV, 12 at 400 GeV, 17 at 600 GeV, 30 at 900 GeV, and 50 at 1200 GeV. In the *Flipped* model, the sensitivity of the $b\overline{b}$ channel is unique since no other difermion mode is sensitive in this area of the parameter space.

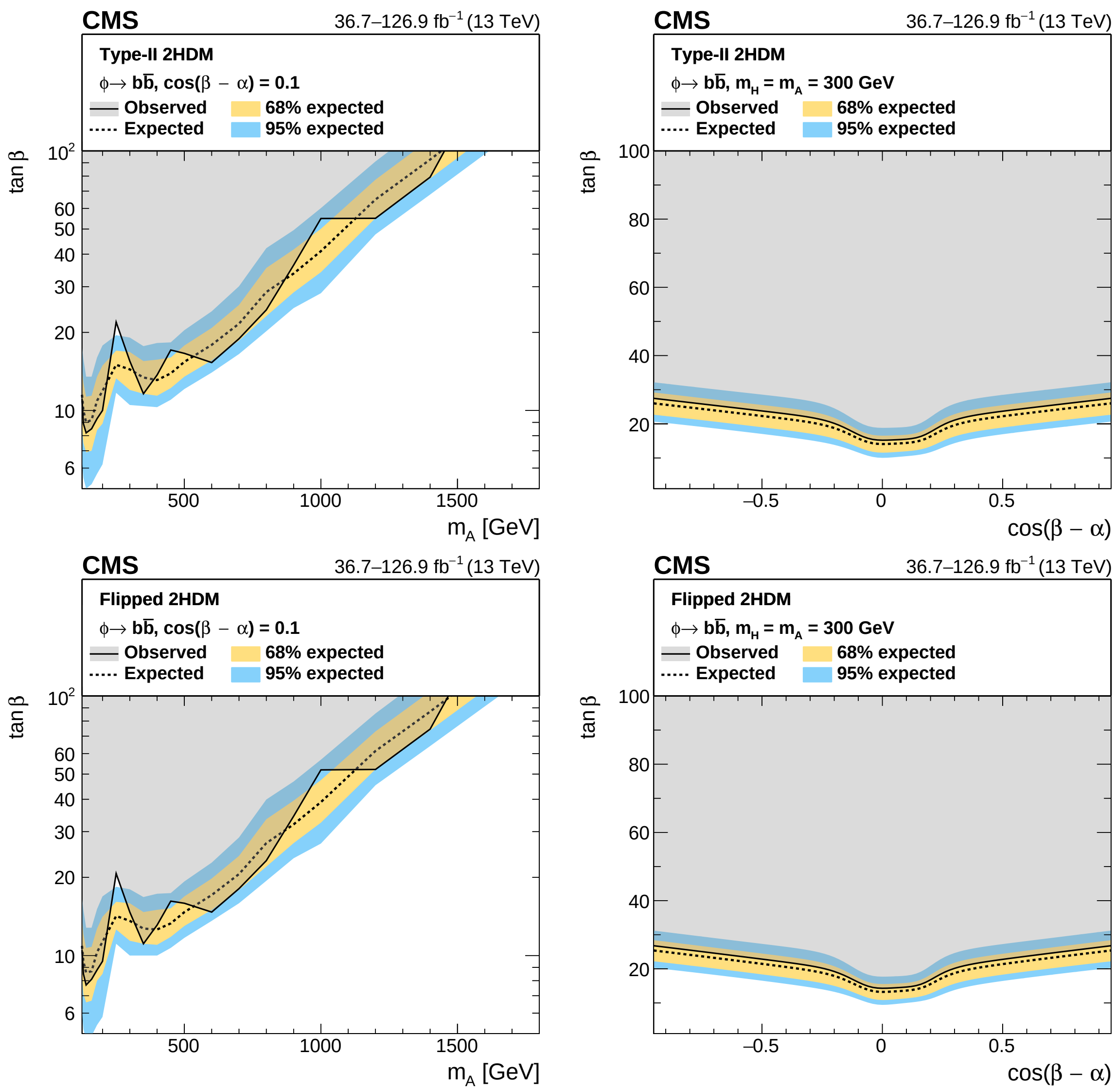

Figure 19: Interpretation in 2HDM scenarios: observed and expected upper limits at 95% CL on the parameter $\tan\beta$ as a function of $m_{\mathrm{A,H}}$ for $\cos(\beta-\alpha) = 0.1$ (left), and as functions of $\cos(\beta-\alpha)$ for masses of $m_{\mathrm{A}} = m_{\mathrm{H}} = 300\,\mathrm{GeV}$ (right), for the 2HDM *Type-II* scenario (upper), and the 2HDM *Flipped* scenario (lower).

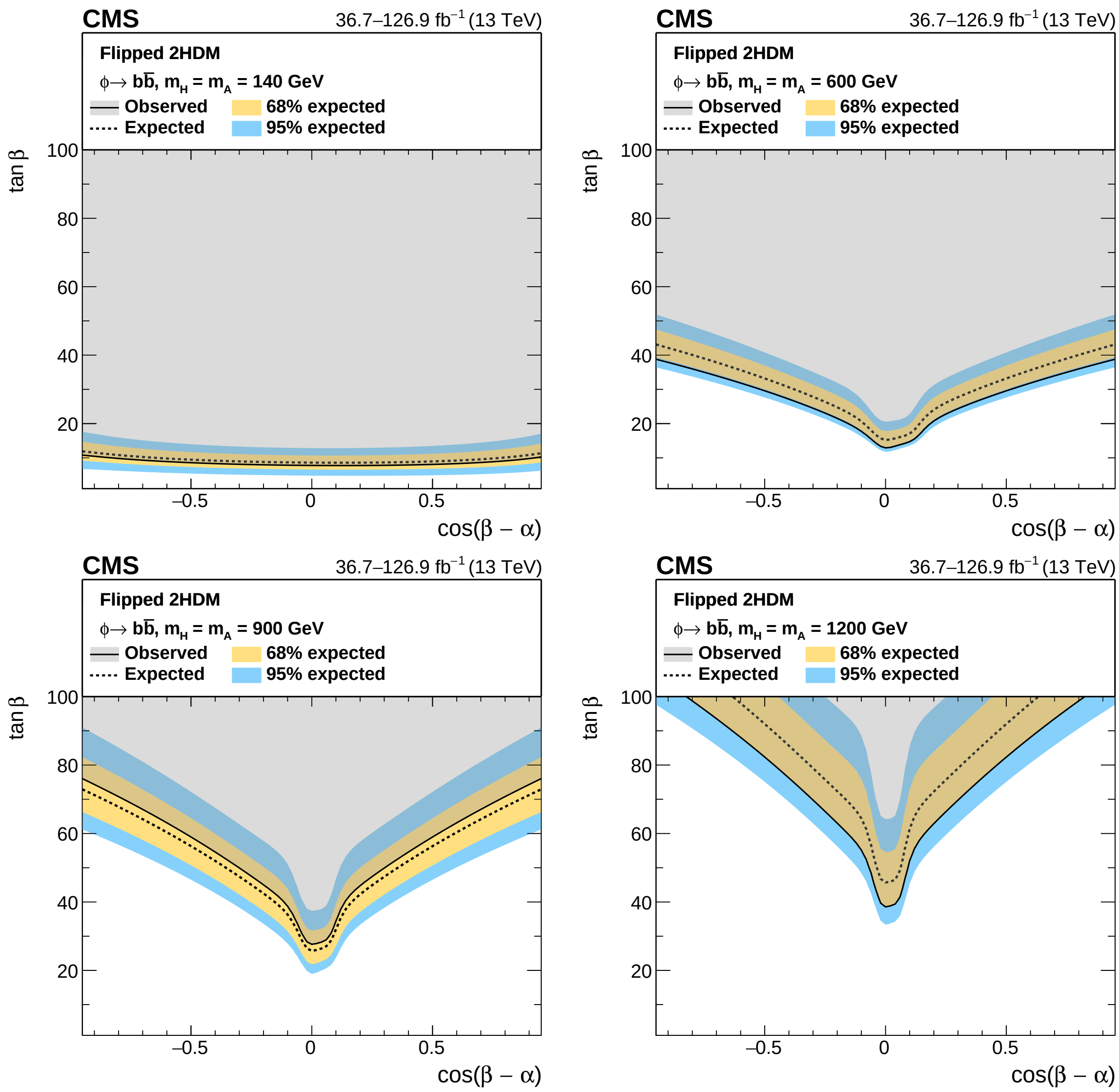

Figure 20: Interpretation in the 2HDM flipped scenario: observed and expected upper limits at 95% CL on the parameter $\tan\beta$ as functions of $\cos(\beta-\alpha)$ for masses of $m_{\mathrm{A}} = m_{\mathrm{H}} = 140$, 600, 900, and 1200 GeV.

Values of $\cos(\beta-\alpha)$ further away from the alignment limit display a visible deterioration in the $\tan\beta$ limits that grows with increasing mass, as can be seen in the right panels of Fig. 19 for $m_{\mathrm{A}} = m_{\mathrm{H}} = 300\,\mathrm{GeV}$ in the *Type-II* and *Flipped* models, and in Fig. 20 for four other mass points in the *Flipped* model, which are very similar to those from the *Type-II* model. This effect can be largely attributed to the branching fractions of these Higgs bosons. For the H boson, the most important decay mode competing with $\mathrm{H} \to \mathrm{b\bar{b}}$ is $\mathrm{H} \to \mathrm{hh}$ if the H mass is above its kinematic threshold. Outside of the alignment limit, this channel tends to saturate the total decay width quickly. The dips in the $\tan\beta$ exclusions near $\cos(\beta-\alpha) = 0$ indicate the region where the H boson contribution to the combined sensitivity is still sizable. This dip does not exist for $m_{\mathrm{A}} = m_{\mathrm{H}} = 140\,\mathrm{GeV}$, which is below the $\mathrm{H} \to \mathrm{hh}$ threshold. For the A boson, on the other hand, the most important competing decay mode is $\mathrm{A} \to \mathrm{Zh}$. The increase of the AZh coupling, at the expense of the $\mathrm{A} \to \mathrm{b\bar{b}}$ branching fraction, is reflected in the steady increase of the $\tan\beta$ limits for larger $|\cos(\beta-\alpha)|$.

10 Summary

A search for beyond-the-standard-model neutral Higgs bosons, ϕ, produced in association with b quarks and decaying into a pair of b quarks is presented using a CMS data set of 13 TeV proton-proton collisions, based on an integrated luminosity of 36.7–126.9 fb^{-1}. The multi b quark final state is selected with requirements targeting both fully hadronic and semileptonic b quark decays, allowing for a sensitivity in the mass range extending from 125 to 1800 GeV. No significant excess of events above the expected SM background is observed. Exclusion limits at 95% confidence level on the production cross section times branching fraction are obtained. The results are also interpreted as constraints in the parameter space of MSSM and 2HDM scenarios to which this search is sensitive. These results represent the most stringent limits to date in the high-mass regime with this final state.

Acknowledgments

We congratulate our colleagues in the CERN accelerator departments for the excellent performance of the LHC and thank the technical and administrative staffs at CERN and at other CMS institutes for their contributions to the success of the CMS effort. In addition, we gratefully acknowledge the computing centres and personnel of the Worldwide LHC Computing Grid and other centres for delivering so effectively the computing infrastructure essential to our analyses. Finally, we acknowledge the enduring support for the construction and operation of the LHC, the CMS detector, and the supporting computing infrastructure provided by the following funding agencies: SC (Armenia), BMBWF and FWF (Austria); FNRS and FWO (Belgium); CNPq, CAPES, FAPERJ, FAPERGS, and FAPESP (Brazil); MES and BNSF (Bulgaria); CERN; CAS, MoST, and NSFC (China); MINCIENCIAS (Colombia); MSES and CSF (Croatia); RIF (Cyprus); SENESCYT (Ecuador); ERC PRG, RVTT3 and MoER TK202 (Estonia); Academy of Finland, MEC, and HIP (Finland); CEA and CNRS/IN2P3 (France); SRNSF (Georgia); BMBF, DFG, and HGF (Germany); GSRI (Greece); NKFIH (Hungary); DAE and DST (India); IPM (Iran); SFI (Ireland); INFN (Italy); MSIP and NRF (Republic of Korea); MES (Latvia); LMTLT (Lithuania); MOE and UM (Malaysia); BUAP, CINVESTAV, CONACYT, LNS, SEP, and UASLP-FAI (Mexico); MOS (Montenegro); MBIE (New Zealand); PAEC (Pakistan); MES and NSC (Poland); FCT (Portugal); MESTD (Serbia); MICIU/AEI and PCTI (Spain); MOSTR (Sri Lanka); Swiss Funding Agencies (Switzerland); MST (Taipei); MHESI and NSTDA (Thailand); TUBITAK and TENMAK (Turkey); NASU (Ukraine); STFC (United Kingdom); DOE and NSF (USA).

Individuals have received support from the Marie-Curie programme and the European Research Council and Horizon 2020 Grant, contract Nos. 675440, 724704, 752730, 758316, 765710, 824093, 101115353, 101002207, and COST Action CA16108 (European Union); the Leventis Foundation; the Alfred P. Sloan Foundation; the Alexander von Humboldt Foundation; the Science Committee, project no. 22rl-037 (Armenia); the Fonds pour la Formation à la Recherche dans l'Industrie et dans l'Agriculture (FRIA-Belgium); the Beijing Municipal Science & Technology Commission, No. Z191100007219010 and Fundamental Research Funds for the Central Universities (China); the Ministry of Education, Youth and Sports (MEYS) of the Czech Republic; the Shota Rustaveli National Science Foundation, grant FR-22-985 (Georgia); the Deutsche Forschungsgemeinschaft (DFG), among others, under Germany's Excellence Strategy – EXC 2121 "Quantum Universe" – 390833306, and under project number 400140256 - GRK2497; the Hellenic Foundation for Research and Innovation (HFRI), Project Number 2288 (Greece); the Hungarian Academy of Sciences, the New National Excellence Program - ÚNKP, the NKFIH research grants K 131991, K 133046, K 138136, K 143460, K 143477, K 146913, K 146914, K 147048, 2020-2.2.1-ED-2021-00181, TKP2021-NKTA-64, and 2021-4.1.2-NEMZ_KI-2024-00036 (Hungary); the Council of Science and Industrial Research, India; ICSC – National Research Centre for High Performance Computing, Big Data and Quantum Computing and FAIR – Future Artificial Intelligence Research, funded by the NextGenerationEU program (Italy); the Latvian Council of Science; the Ministry of Education and Science, project no. 2022/WK/14, and the National Science Center, contracts Opus 2021/41/B/ST2/01369 and 2021/43/B/ST2/01552 (Poland); the Fundação para a Ciência e a Tecnologia, grant CEECIND/01334/2018 (Portugal); the National Priorities Research Program by Qatar National Research Fund; MICIU/AEI/10.13039/501100011033, ERDF/EU, "European Union NextGenerationEU/PRTR", and Programa Severo Ochoa del Principado de Asturias (Spain); the Chulalongkorn Academic into Its 2nd Century Project Advancement Project, and the National Science, Research and Innovation Fund via the Program Management Unit for Human Resources & Institutional Development, Research and Innovation, grant B39G680009 (Thailand); the Kavli Foundation; the Nvidia Corporation; the SuperMicro Corporation; the Welch Foundation, contract C-1845; and the Weston Havens Foundation (USA).

References

[1] ATLAS Collaboration, "Observation of a new particle in the search for the standard model Higgs boson with the ATLAS detector at the LHC", *Phys. Lett. B* **716** (2012) 1, doi:10.1016/j.physletb.2012.08.020, arXiv:1207.7214.

[2] CMS Collaboration, "Observation of a new boson at a mass of 125 GeV with the CMS experiment at the LHC", *Phys. Lett. B* **716** (2012) 30, doi:10.1016/j.physletb.2012.08.021, arXiv:1207.7235.

[3] CMS Collaboration, "Observation of a new boson with mass near 125 GeV in pp collisions at $\sqrt{s}$ = 7 and 8 TeV", *JHEP* **06** (2013) 081, doi:10.1007/JHEP06(2013)081, arXiv:1303.4571.

[4] ATLAS Collaboration, "A detailed map of Higgs boson interactions by the ATLAS experiment ten years after the discovery", *Nature* **607** (2022) 52, doi:10.1038/s41586-022-04893-w, arXiv:2207.00092. [Erratum: doi:10.1038/s41586-022-05581-5].

[5] CMS Collaboration, "A portrait of the Higgs boson by the CMS experiment ten years after the discovery", *Nature* **607** (2022) 60, doi:10.1038/s41586-022-04892-x, arXiv:2207.00043.

[6] CMS Collaboration, "Search for bottom quark associated production of the standard model Higgs boson in final states with leptons in proton-proton collisions at $\sqrt{s} = 13$ TeV", *Phys. Lett. B* **860** (2025) 139173, doi:10.1016/j.physletb.2024.139173, arXiv:2408.01344.

[7] CMS Collaboration, "Evidence for Higgs boson decay to a pair of muons", *JHEP* **01** (2021) 148, doi:10.1007/JHEP01(2021)148, arXiv:2009.04363.

[8] ATLAS Collaboration, "Direct constraint on the Higgs-charm coupling from a search for Higgs boson decays into charm quarks with the ATLAS detector", *Eur. Phys. J. C* **82** (2022) 717, doi:10.1140/epjc/s10052-022-10588-3, arXiv:2201.11428.

[9] CMS Collaboration, "Search for Higgs boson decay to a charm quark-antiquark pair in proton-proton collisions at $\sqrt{s} = 13$ TeV", *Phys. Rev. Lett.* **131** (2023) 061801, doi:10.1103/PhysRevLett.131.061801, arXiv:2205.05550.

[10] ATLAS Collaboration, "Combined measurements of Higgs boson production and decay using up to 80 fb^{-1} of proton-proton collision data at $\sqrt{s} = 13$ TeV collected with the ATLAS experiment", *Phys. Rev. D* **101** (2020) 012002, doi:10.1103/PhysRevD.101.012002, arXiv:1909.02845.

[11] CMS Collaboration, "Combined measurements of Higgs boson couplings in proton-proton collisions at $\sqrt{s} = 13$ TeV", *Eur. Phys. J. C* **79** (2019) 421, doi:10.1140/epjc/s10052-019-6909-y, arXiv:1809.10733.

[12] J. Steggemann, "Extended scalar sectors", *Ann. Rev. Nucl. Part. Sci.* **70** (2020) 197, doi:10.1146/annurev-nucl-032620-043846.

[13] G. C. Branco et al., "Theory and phenomenology of two-higgs-doublet models", *Phys. Rep.* **516** (2012) 1, doi:10.1016/j.physrep.2012.02.002, arXiv:1106.0034.

[14] H. P. Nilles, "Supersymmetry, supergravity and particle physics", *Phys. Rep.* **110** (1984) 1, doi:10.1016/0370-1573(84)90008-5.

[15] P. Drechsel, G. Moortgat-Pick, and G. Weiglein, "Prospects for direct searches for light Higgs bosons at the ILC with 250 GeV", *Eur. Phys. J. C* **80** (2020) 922, doi:10.1140/epjc/s10052-020-08438-1, arXiv:1801.09662.

[16] M. Carena et al., "MSSM Higgs boson searches at the LHC: benchmark scenarios after the discovery of a Higgs-like particle", *Eur. Phys. J. C* **73** (2013) 2552, doi:10.1140/epjc/s10052-013-2552-1, arXiv:1302.7033.

[17] M. S. Carena, S. Heinemeyer, C. E. M. Wagner, and G. Weiglein, "MSSM Higgs boson searches at the Tevatron and the LHC: Impact of different benchmark scenarios", *Eur. Phys. J. C* **45** (2006) 797, doi:10.1140/epjc/s2005-02470-y, arXiv:hep-ph/0511023.

[18] E. Bagnaschi et al., "MSSM Higgs boson searches at the LHC: benchmark scenarios for Run 2 and beyond", *Eur. Phys. J. C* **79** (2019) 617, doi:10.1140/epjc/s10052-019-7114-8, arXiv:1808.07542.

[19] H. Bahl et al., "HL-LHC and ILC sensitivities in the hunt for heavy Higgs bosons", *Eur. Phys. J. C* **80** (2020) 916, doi:10.1140/epjc/s10052-020-08472-z, arXiv:2005.14536.

[20] L. Maiani, A. D. Polosa, and V. Riquer, "Bounds to the Higgs sector masses in minimal supersymmetry from LHC data", *Phys. Lett. B* **724** (2013) 274, doi:10.1016/j.physletb.2013.06.026, arXiv:1305.2172.

[21] A. Djouadi et al., "The post-Higgs MSSM scenario: Habemus MSSM?", *Eur. Phys. J. C* **73** (2013) 2650, doi:10.1140/epjc/s10052-013-2650-0, arXiv:1307.5205.

[22] A. Djouadi et al., "Fully covering the MSSM Higgs sector at the LHC", *JHEP* **06** (2015) 168, doi:10.1007/JHEP06(2015)168, arXiv:1502.05653.

[23] H. E. Haber and O. Stål, "New LHC benchmarks for the $\mathcal{CP}$ -conserving two-higgs-doublet model", *Eur. Phys. J. C* **75** (2015) 491, doi:10.1140/epjc/s10052-015-3697-x, arXiv:1507.04281. [Erratum: doi:10.1140/epjc/s10052-016-4151-4].

[24] LHC Higgs Cross Section Working Group, "Handbook of LHC Higgs cross sections: 3. Higgs properties", *CERN* (2013) doi:10.5170/CERN-2013-004, arXiv:1307.1347.

[25] ALEPH, DELPHI, L3, and OPAL Collaborations, LEP Working Group for Higgs Boson Searches, "Search for neutral MSSM Higgs bosons at LEP", *Eur. Phys. J. C* **47** (2006) 547, doi:10.1140/epjc/s2006-02569-7, arXiv:hep-ex/0602042.

[26] CDF and D0 Collaborations, "Search for neutral Higgs bosons in events with multiple bottom quarks at the Tevatron", *Phys. Rev. D* **86** (2012) 091101, doi:10.1103/PhysRevD.86.091101, arXiv:1207.2757.

[27] CMS Collaboration, "Search for a Higgs boson decaying into a b-quark pair and produced in association with b quarks in proton-proton collisions at 7 TeV", *Phys. Lett. B* **722** (2013) 207, doi:10.1016/j.physletb.2013.04.017, arXiv:1302.2892.

[28] CMS Collaboration, "Search for neutral MSSM Higgs bosons decaying into a pair of bottom quarks", *JHEP* **11** (2015) 071, doi:10.1007/JHEP11(2015)071, arXiv:1506.08329.

[29] ATLAS Collaboration, "Search for heavy neutral Higgs bosons produced in association with b-quarks and decaying into b-quarks at $\sqrt{s} = 13$ TeV with the ATLAS detector", *Phys. Rev. D* **102** (2020) 032004, doi:10.1103/PhysRevD.102.032004, arXiv:1907.02749.

[30] CMS Collaboration, "Search for beyond the standard model Higgs bosons decaying into a $b\bar{b}$ pair in pp collisions at $\sqrt{s} = 13$ TeV", *JHEP* **08** (2018) 113, doi:10.1007/JHEP08(2018)113, arXiv:1805.12191.

[31] E. Bols et al., "Jet flavour classification using DeepJet", *JINST* **15** (2020) P12012, doi:10.1088/1748-0221/15/12/P12012, arXiv:2008.10519.

[32] CMS Tracker Group Collaboration, "The CMS phase-1 pixel detector upgrade", *JINST* **16** (2021) P02027, doi:10.1088/1748-0221/16/02/P02027, arXiv:2012.14304.

[33] HEPData record for this analysis, 2024. doi:10.17182/hepdata.155471.

[34] CMS Collaboration, "The CMS experiment at the CERN LHC", *JINST* **3** (2008) S08004, doi:10.1088/1748-0221/3/08/S08004.

[35] CMS Collaboration, "Development of the CMS detector for the CERN LHC Run 3", *JINST* **19** (2024) P05064, doi:10.1088/1748-0221/19/05/P05064, arXiv:2309.05466.

[36] CMS Collaboration, "Performance of the CMS level-1 trigger in proton-proton collisions at $\sqrt{s} = 13$ TeV", *JINST* **15** (2020) P10017, doi:10.1088/1748-0221/15/10/P10017, arXiv:2006.10165.

[37] CMS Collaboration, "The CMS trigger system", *JINST* **12** (2017) P01020, doi:10.1088/1748-0221/12/01/P01020, arXiv:1609.02366.

[38] CMS Collaboration, "Performance of the CMS high-level trigger during LHC Run 2", *JINST* **19** (2024) P11021, doi:10.1088/1748-0221/19/11/p11021, arXiv:2410.17038.

[39] CMS Collaboration, "Particle-flow reconstruction and global event description with the CMS detector", *JINST* **12** (2017) P10003, doi:10.1088/1748-0221/12/10/P10003, arXiv:1706.04965.

[40] CMS Collaboration, "Technical proposal for the phase-II upgrade of the Compact Muon Solenoid", CMS Technical Proposal CERN-LHCC-2015-010, CMS-TDR-15-02, 2015.

[41] M. Cacciari, G. P. Salam, and G. Soyez, "The anti-k_T jet clustering algorithm", *JHEP* **04** (2008) 063, doi:10.1088/1126-6708/2008/04/063, arXiv:0802.1189.

[42] M. Cacciari, G. P. Salam, and G. Soyez, "Fastjet user manual", *Eur. Phys. J. C* **72** (2012) 1896, doi:10.1140/epjc/s10052-012-1896-2, arXiv:1111.6097.

[43] CMS Collaboration, "Jet energy scale and resolution in the CMS experiment in pp collisions at 8 TeV", *JINST* **12** (2017) P02014, doi:10.1088/1748-0221/12/02/P02014, arXiv:1607.03663.

[44] CMS Collaboration, "Pileup mitigation at CMS in 13 TeV data", *JINST* **15** (2020) P09018, doi:10.1088/1748-0221/15/09/P09018, arXiv:2003.00503.

[45] CMS Collaboration, "Identification of heavy-flavour jets with the CMS detector in pp collisions at 13 TeV", *JINST* **13** (2018) P05011, doi:10.1088/1748-0221/13/05/P05011, arXiv:1712.07158.

[46] CMS Collaboration, "Performance of the DeepJet b tagging algorithm using 41.9 fb^{-1} of data from proton-proton collisions at 13 TeV with phase 1 CMS detector", CMS Detector Performance Note CMS-DP-2018-058, 2018.

[47] CMS Collaboration, "B-tagging performance of the CMS legacy dataset 2018", CMS Detector Performance Note CMS-DP-2021-004, 2021.

[48] CMS Collaboration, "Performance of the CMS muon detector and muon reconstruction with proton-proton collisions at $\sqrt{s} = 13$ TeV", *JINST* **13** (2018) P06015, doi:10.1088/1748-0221/13/06/P06015, arXiv:1804.04528.

[49] CMS Collaboration, "Performance of missing transverse momentum reconstruction in proton-proton collisions at $\sqrt{s} = 13$ TeV using the CMS detector", *JINST* **14** (2019) P07004, doi:10.1088/1748-0221/14/07/P07004, arXiv:1903.06078.

[50] P. Nason, "A new method for combining NLO QCD with shower Monte Carlo algorithms", *JHEP* **11** (2004) 040, doi:10.1088/1126-6708/2004/11/040, arXiv:hep-ph/0409146.

[51] S. Frixione, P. Nason, and C. Oleari, "Matching NLO QCD computations with parton shower simulations: the POWHEG method", *JHEP* **11** (2007) 070, doi:10.1088/1126-6708/2007/11/070, arXiv:0709.2092.

[52] S. Alioli, P. Nason, C. Oleari, and E. Re, "A general framework for implementing NLO calculations in shower Monte Carlo programs: the POWHEG BOX", *JHEP* **06** (2010) 043, doi:10.1007/JHEP06(2010)043, arXiv:1002.2581.

[53] B. Jager, L. Reina, and D. Wackeroth, "Higgs boson production in association with b jets in the POWHEG BOX", *Phys. Rev. D* **93** (2016) 014030, doi:10.1103/PhysRevD.93.014030, arXiv:1509.05843.

[54] F. Maltoni, G. Ridolfi, and M. Ubiali, "b-initiated processes at the LHC: a reappraisal", *JHEP* **07** (2012) 022, doi:10.1007/jhep07(2012)022, arXiv:1203.6393. [Erratum: doi:10.1007/JHEP04(2013)095].

[55] J. Alwall et al., "MadGraph 5: Going beyond", *JHEP* **06** (2011) 128, doi:10.1007/JHEP06(2011)128, arXiv:1106.0522.

[56] J. Alwall et al., "The automated computation of tree-level and next-to-leading order differential cross sections, and their matching to parton shower simulations", *JHEP* **07** (2014) 079, doi:10.1007/JHEP07(2014)079, arXiv:1405.0301.

[57] S. Frixione and B. R. Webber, "Matching NLO QCD computations and parton shower simulations", *JHEP* **06** (2002) 029, doi:10.1088/1126-6708/2002/06/029, arXiv:hep-ph/0204244.

[58] J. Alwall et al., "Comparative study of various algorithms for the merging of parton showers and matrix elements in hadronic collisions", *Eur. Phys. J. C* **53** (2008) 473, doi:10.1140/epjc/s10052-007-0490-5, arXiv:0706.2569.

[59] J. Butterworth et al., "PDF4LHC recommendations for LHC Run II", *J. Phys. G* **43** (2016) 023001, doi:10.1088/0954-3899/43/2/023001, arXiv:1510.03865.

[60] NNPDF Collaboration, "Parton distributions from high-precision collider data", *Eur. Phys. J. C* **77** (2017) 663, doi:10.1140/epjc/s10052-017-5199-5, arXiv:1706.00428.

[61] CMS Collaboration, "Extraction and validation of a new set of CMS PYTHIA8 tunes from underlying-event measurements", *Eur. Phys. J. C* **80** (2020) 4, doi:10.1140/epjc/s10052-019-7499-4, arXiv:1903.12179.

[62] T. Sjöstrand et al., "An introduction to PYTHIA 8.2", *Comput. Phys. Commun.* **191** (2015) 159, doi:10.1016/j.cpc.2015.01.024, arXiv:1410.3012.

[63] GEANT4 Collaboration, "GEANT4—a simulation toolkit", *Nucl. Instrum. Meth. A* **506** (2003) 250, doi:10.1016/S0168-9002(03)01368-8.

[64] CMS Collaboration, "Measurement of inclusive W and Z boson production cross sections in pp collisions at $\sqrt{s} = 8$ TeV", *Phys. Rev. Lett.* **112** (2014) 191802, doi:10.1103/PhysRevLett.112.191802, arXiv:1402.0923.

[65] CMS Collaboration, "A deep neural network for simultaneous estimation of b jet energy and resolution", *Comput. Softw. Big Sci.* **4** (2020) 10, doi:10.1007/s41781-020-00041-z, arXiv:1912.06046.

[66] J. Gaiser et al., "Charmonium spectroscopy from inclusive ψ' and J/ψ radiative decays", *Phys. Rev. D* **34** (1986) 711, doi:10.1103/PhysRevD.34.711.

[67] A. Vagnerini, "Search for Higgs bosons in the final state with b-quarks in the semi-leptonic channel with the CMS 2017 data". PhD thesis, Hamburg U., Hamburg, 2020. doi:10.3204/PUBDB-2020-02277.

[68] P. Asmuss, "Search for high-mass bosons of an extended Higgs sector in b quark final states using the 2017 data set of the CMS experiment". PhD thesis, Hamburg U., Hamburg, 2021. doi:10.3204/PUBDB-2021-03020.

[69] Belle Collaboration, "A detailed test of the CsI(Tl) calorimeter for BELLE with photon beams of energy between 20 MeV and 5.4 GeV", *Nucl. Instrum. Meth. A* **441** (2000) 401, doi:10.1016/S0168-9002(99)00992-4.

[70] P. D. Dauncey, M. Kenzie, N. Wardle, and G. J. Davies, "Handling uncertainties in background shapes: the discrete profiling method", *JINST* **10** (2015) P04015, doi:10.1088/1748-0221/10/04/P04015, arXiv:1408.6865.

[71] CMS Collaboration, "The CMS statistical analysis and combination tool: COMBINE", *Comp. Softw. Big Sci.* **8** (2024) 19, doi:10.1007/s41781-024-00121-4, arXiv:2404.06614.

[72] CMS Collaboration, "CMS luminosity measurement for the 2017 data-taking period at $\sqrt{s}$ = 13 TeV", CMS Physics Analysis Summary CMS-PAS-LUM-17-004, 2018.

[73] CMS Collaboration, "CMS luminosity measurement for the 2018 data-taking period at $\sqrt{s}$ = 13 TeV", CMS Physics Analysis Summary CMS-PAS-LUM-18-002, 2019.

[74] CMS Collaboration, "Measurement of the inelastic proton-proton cross section at $\sqrt{s} = 13$ TeV", *JHEP* **07** (2018) 161, doi:10.1007/JHEP07(2018)161, arXiv:1802.02613.

[75] CMS Collaboration, "Performance of the CMS electromagnetic calorimeter in pp collisions at $\sqrt{s} = 13$ TeV", *JINST* **19** (2024) P09004, doi:10.1088/1748-0221/19/09/P09004, arXiv:2403.15518.

[76] LHC Higgs Cross Section Working Group Collaboration, "Handbook of LHC Higgs cross sections: 4. Deciphering the nature of the Higgs sector", *CERN Yellow Reports: Monographs* **2/2017** (10, 2016) doi:10.23731/CYRM-2017-002, arXiv:1610.07922.

[77] T. Junk, "Confidence level computation for combining searches with small statistics", *Nucl. Instrum. Meth. A* **434** (1999) 435, doi:10.1016/S0168-9002(99)00498-2, arXiv:hep-ex/9902006.

[78] A. L. Read, "Presentation of search results: The CL_s technique", *J. Phys. G* **28** (2002) 2693, doi:10.1088/0954-3899/28/10/313.

[79] G. Cowan, K. Cranmer, E. Gross, and O. Vitells, "Asymptotic formulae for likelihood-based tests of new physics", *Eur. Phys. J. C* **71** (2011) 1554, doi:10.1140/epjc/s10052-011-1554-0, arXiv:1007.1727. [Erratum: doi:10.1140/epjc/s10052-013-2501-z].

[80] E. Gross and O. Vitells, "Trial factors for the look elsewhere effect in high energy physics", *Eur. Phys. J. C* **70** (2010) 525, doi:10.1140/epjc/s10052-010-1470-8, arXiv:1005.1891.

[81] S. Dawson, C. B. Jackson, L. Reina, and D. Wackeroth, "Exclusive Higgs boson production with bottom quarks at hadron colliders", *Phys. Rev. D* **69** (2004) 074027, doi:10.1103/PhysRevD.69.074027, arXiv:hep-ph/0311067.

[82] S. Dittmaier, M. Krämer, and M. Spira, "Higgs radiation off bottom quarks at the Tevatron and the CERN LHC", *Phys. Rev. D* **70** (2004) 074010, doi:10.1103/PhysRevD.70.074010, arXiv:hep-ph/0309204.

[83] R. V. Harlander and W. B. Kilgore, "Higgs boson production in bottom quark fusion at next-to-next-to leading order", *Phys. Rev. D* **68** (2003) 013001, doi:10.1103/PhysRevD.68.013001, arXiv:hep-ph/0304035.

[84] R. Harlander, M. Kramer, and M. Schumacher, "Bottom-quark associated Higgs-boson production: reconciling the four- and five-flavour scheme approach", 12, 2011. arXiv:1112.3478.

[85] S. Forte, D. Napoletano, and M. Ubiali, "Higgs production in bottom-quark fusion in a matched scheme", *Phys. Lett. B* **751** (2015) 331, doi:10.1016/j.physletb.2015.10.051, arXiv:1508.01529.

[86] S. Forte, D. Napoletano, and M. Ubiali, "Higgs production in bottom-quark fusion: matching beyond leading order", *Phys. Lett. B* **763** (2016) 190, doi:10.1016/j.physletb.2016.10.040, arXiv:1607.00389.

[87] G. Degrassi et al., "Towards high precision predictions for the MSSM Higgs sector", *Eur. Phys. J. C* **28** (2003) 133, doi:10.1140/epjc/s2003-01152-2, arXiv:hep-ph/0212020.

[88] S. Heinemeyer, W. Hollik, and G. Weiglein, "FeynHiggs: A program for the calculation of the masses of the neutral CP even Higgs bosons in the MSSM", *Comput. Phys. Commun.* **124** (2000) 76, doi:10.1016/S0010-4655(99)00364-1, arXiv:hep-ph/9812320.

[89] M. Frank et al., "The Higgs boson masses and mixings of the complex MSSM in the Feynman-diagrammatic approach", *JHEP* **02** (2007) 047, doi:10.1088/1126-6708/2007/02/047, arXiv:hep-ph/0611326.

[90] T. Hahn et al., "High-precision predictions for the light CP-even Higgs boson mass of the minimal supersymmetric standard model", *Phys. Rev. Lett.* **112** (2014) 141801, doi:10.1103/PhysRevLett.112.141801, arXiv:1312.4937.

[91] H. Bahl and W. Hollik, "Precise prediction for the light MSSM Higgs boson mass combining effective field theory and fixed-order calculations", *Eur. Phys. J. C* **76** (2016) 499, doi:10.1140/epjc/s10052-016-4354-8, arXiv:1608.01880.

[92] H. Bahl, S. Heinemeyer, W. Hollik, and G. Weiglein, "Reconciling EFT and hybrid calculations of the light MSSM Higgs-boson mass", *Eur. Phys. J. C* **78** (2018) 57, doi:10.1140/epjc/s10052-018-5544-3, arXiv:1706.00346.

[93] H. Bahl et al., "Precision calculations in the MSSM Higgs-boson sector with FeynHiggs 2.14", *Comput. Phys. Commun.* **249** (2020) 107099, doi:10.1016/j.cpc.2019.107099, arXiv:1811.09073.

[94] A. Djouadi, J. Kalinowski, and M. Spira, "HDECAY: A program for Higgs boson decays in the standard model and its supersymmetric extension", *Comput. Phys. Commun.* **108** (1998) 56, doi:10.1016/S0010-4655(97)00123-9, arXiv:hep-ph/9704448.

[95] A. Djouadi, J. Kalinowski, M. Mühlleitner, and M. Spira, "HDECAY: Twenty++ years after", *Comput. Phys. Commun.* **238** (2019) 214, doi:10.1016/j.cpc.2018.12.010, arXiv:1801.09506.

[96] R. V. Harlander, S. Liebler, and H. Mantler, "SusHi: A program for the calculation of Higgs production in gluon fusion and bottom-quark annihilation in the standard model and the MSSM", *Comput. Phys. Commun.* **184** (2013) 1605, doi:10.1016/j.cpc.2013.02.006, arXiv:1212.3249.

[97] R. V. Harlander, S. Liebler, and H. Mantler, "SusHi bento: Beyond NNLO and the heavy-top limit", *Comput. Phys. Commun.* **212** (2017) 239, doi:10.1016/j.cpc.2016.10.015, arXiv:1605.03190.

[98] D. Eriksson, J. Rathsman, and O. Stål, "2HDMC: Two-Higgs-doublet model calculator physics and manual", *Comput. Phys. Commun.* **181** (2010) 189, doi:10.1016/j.cpc.2009.09.011, arXiv:0902.0851.

[99] A. Buckley et al., "LHAPDF6: parton density access in the LHC precision era", *Eur. Phys. J. C* **75** (2015) 132, doi:10.1140/epjc/s10052-015-3318-8, arXiv:1412.7420.

A The CMS Collaboration

Yerevan Physics Institute, Yerevan, Armenia
V. Chekhovsky, A. Hayrapetyan, V. Makarenko, A. Tumasyan[1]

Institut für Hochenergiephysik, Vienna, Austria
W. Adam, J.W. Andrejkovic, L. Benato, T. Bergauer, S. Chatterjee, K. Damanakis, M. Dragicevic, P.S. Hussain, M. Jeitler[2], N. Krammer, A. Li, D. Liko, I. Mikulec, J. Schieck[2], R. Schöfbeck[2], D. Schwarz, M. Sonawane, W. Waltenberger, C.-E. Wulz[2]

Universiteit Antwerpen, Antwerpen, Belgium
T. Janssen, T. Van Laer, P. Van Mechelen

Vrije Universiteit Brussel, Brussel, Belgium
N. Breugelmans, J. D'Hondt, S. Dansana, A. De Moor, M. Delcourt, F. Heyen, Y. Hong, S. Lowette, I. Makarenko, D. Müller, S. Tavernier, M. Tytgat[3], G.P. Van Onsem, S. Van Putte, D. Vannerom

Université Libre de Bruxelles, Bruxelles, Belgium
B. Bilin, B. Clerbaux, A.K. Das, I. De Bruyn, G. De Lentdecker, H. Evard, L. Favart, P. Gianneios, A. Khalilzadeh, F.A. Khan, K. Lee, A. Malara, M.A. Shahzad, L. Thomas, M. Vanden Bemden, C. Vander Velde, P. Vanlaer

Ghent University, Ghent, Belgium
M. De Coen, D. Dobur, G. Gokbulut, J. Knolle, L. Lambrecht, D. Marckx, K. Mota Amarilo, K. Skovpen, N. Van Den Bossche, J. van der Linden, L. Wezenbeek

Université Catholique de Louvain, Louvain-la-Neuve, Belgium
S. Bein, A. Benecke, A. Bethani, G. Bruno, C. Caputo, J. De Favereau De Jeneret, C. Delaere, I.S. Donertas, A. Giammanco, A.O. Guzel, Sa. Jain, V. Lemaitre, J. Lidrych, P. Mastrapasqua, T.T. Tran, S. Turkcapar

Centro Brasileiro de Pesquisas Fisicas, Rio de Janeiro, Brazil
G.A. Alves, E. Coelho, G. Correia Silva, C. Hensel, T. Menezes De Oliveira, C. Mora Herrera[4], P. Rebello Teles, M. Soeiro, E.J. Tonelli Manganote[5], A. Vilela Pereira[4]

Universidade do Estado do Rio de Janeiro, Rio de Janeiro, Brazil
W.L. Aldá Júnior, M. Barroso Ferreira Filho, H. Brandao Malbouisson, W. Carvalho, J. Chinellato[6], E.M. Da Costa, G.G. Da Silveira[7], D. De Jesus Damiao, S. Fonseca De Souza, R. Gomes De Souza, T. Laux Kuhn[7], M. Macedo, J. Martins, L. Mundim, H. Nogima, J.P. Pinheiro, A. Santoro, A. Sznajder, M. Thiel

Universidade Estadual Paulista, Universidade Federal do ABC, São Paulo, Brazil
C.A. Bernardes[7], L. Calligaris, T.R. Fernandez Perez Tomei, E.M. Gregores, I. Maietto Silverio, P.G. Mercadante, S.F. Novaes, B. Orzari, Sandra S. Padula

Institute for Nuclear Research and Nuclear Energy, Bulgarian Academy of Sciences, Sofia, Bulgaria
A. Aleksandrov, G. Antchev, R. Hadjiiska, P. Iaydjiev, M. Misheva, M. Shopova, G. Sultanov

University of Sofia, Sofia, Bulgaria

A. Dimitrov, L. Litov, B. Pavlov, P. Petkov, A. Petrov, E. Shumka

Instituto De Alta Investigación, Universidad de Tarapacá, Casilla 7 D, Arica, Chile
S. Keshri, D. Laroze, S. Thakur

Beihang University, Beijing, China
T. Cheng, T. Javaid, L. Yuan

Department of Physics, Tsinghua University, Beijing, China
Z. Hu, Z. Liang, J. Liu

Institute of High Energy Physics, Beijing, China
G.M. Chen[8], H.S. Chen[8], M. Chen[8], F. Iemmi, C.H. Jiang, A. Kapoor[9], H. Liao, Z.-A. Liu[10], R. Sharma[11], J.N. Song[10], J. Tao, C. Wang[8], J. Wang, Z. Wang[8], H. Zhang, J. Zhao

State Key Laboratory of Nuclear Physics and Technology, Peking University, Beijing, China
A. Agapitos, Y. Ban, A. Carvalho Antunes De Oliveira, S. Deng, B. Guo, C. Jiang, A. Levin, C. Li, Q. Li, Y. Mao, S. Qian, S.J. Qian, X. Qin, X. Sun, D. Wang, H. Yang, Y. Zhao, C. Zhou

Guangdong Provincial Key Laboratory of Nuclear Science and Guangdong-Hong Kong Joint Laboratory of Quantum Matter, South China Normal University, Guangzhou, China
S. Yang

Sun Yat-Sen University, Guangzhou, China
Z. You

University of Science and Technology of China, Hefei, China
K. Jaffel, N. Lu

Nanjing Normal University, Nanjing, China
G. Bauer[12], B. Li[13], H. Wang, K. Yi[14], J. Zhang

Institute of Modern Physics and Key Laboratory of Nuclear Physics and Ion-beam Application (MOE) - Fudan University, Shanghai, China
Y. Li

Zhejiang University, Hangzhou, Zhejiang, China
Z. Lin, C. Lu, M. Xiao

Universidad de Los Andes, Bogota, Colombia
C. Avila, D.A. Barbosa Trujillo, A. Cabrera, C. Florez, J. Fraga, J.A. Reyes Vega

Universidad de Antioquia, Medellin, Colombia
J. Jaramillo, C. Rendón, M. Rodriguez, A.A. Ruales Barbosa, J.D. Ruiz Alvarez

University of Split, Faculty of Electrical Engineering, Mechanical Engineering and Naval Architecture, Split, Croatia
D. Giljanovic, N. Godinovic, D. Lelas, A. Sculac

University of Split, Faculty of Science, Split, Croatia
M. Kovac, A. Petkovic, T. Sculac

Institute Rudjer Boskovic, Zagreb, Croatia
P. Bargassa, V. Brigljevic, B.K. Chitroda, D. Ferencek, K. Jakovcic, A. Starodumov[15], T. Susa

University of Cyprus, Nicosia, Cyprus
A. Attikis, K. Christoforou, A. Hadjiagapiou, C. Leonidou, J. Mousa, C. Nicolaou, L. Paizanos, F. Ptochos, P.A. Razis, H. Rykaczewski, H. Saka, A. Stepennov

Charles University, Prague, Czech Republic
M. Finger, M. Finger Jr., A. Kveton

Escuela Politecnica Nacional, Quito, Ecuador
E. Ayala

Universidad San Francisco de Quito, Quito, Ecuador
E. Carrera Jarrin

Academy of Scientific Research and Technology of the Arab Republic of Egypt, Egyptian Network of High Energy Physics, Cairo, Egypt
A.A. Abdelalim[16,17], S. Elgammal[18], A. Ellithi Kamel[19]

Center for High Energy Physics (CHEP-FU), Fayoum University, El-Fayoum, Egypt
M. Abdullah Al-Mashad, M.A. Mahmoud

National Institute of Chemical Physics and Biophysics, Tallinn, Estonia
K. Ehataht, M. Kadastik, T. Lange, C. Nielsen, J. Pata, M. Raidal, L. Tani, C. Veelken

Department of Physics, University of Helsinki, Helsinki, Finland
H. Kirschenmann, K. Osterberg, M. Voutilainen

Helsinki Institute of Physics, Helsinki, Finland
N. Bin Norjoharuddeen, E. Brücken, F. Garcia, P. Inkaew, K.T.S. Kallonen, T. Lampén, K. Lassila-Perini, S. Lehti, T. Lindén, M. Myllymäki, M.m. Rantanen, J. Tuominiemi

Lappeenranta-Lahti University of Technology, Lappeenranta, Finland
P. Luukka, H. Petrow

IRFU, CEA, Université Paris-Saclay, Gif-sur-Yvette, France
M. Besancon, F. Couderc, M. Dejardin, D. Denegri, J.L. Faure, F. Ferri, S. Ganjour, P. Gras, G. Hamel de Monchenault, M. Kumar, V. Lohezic, J. Malcles, F. Orlandi, L. Portales, A. Rosowsky, M.Ö. Sahin, A. Savoy-Navarro[20], P. Simkina, M. Titov, M. Tornago

Laboratoire Leprince-Ringuet, CNRS/IN2P3, Ecole Polytechnique, Institut Polytechnique de Paris, Palaiseau, France
F. Beaudette, G. Boldrini, P. Busson, A. Cappati, C. Charlot, M. Chiusi, T.D. Cuisset, F. Damas, O. Davignon, A. De Wit, I.T. Ehle, B.A. Fontana Santos Alves, S. Ghosh, A. Gilbert, R. Granier de Cassagnac, A. Hakimi, B. Harikrishnan, L. Kalipoliti, G. Liu, M. Nguyen, C. Ochando, R. Salerno, J.B. Sauvan, Y. Sirois, G. Sokmen, L. Urda Gómez, E. Vernazza, A. Zabi, A. Zghiche

Université de Strasbourg, CNRS, IPHC UMR 7178, Strasbourg, France
J.-L. Agram[21], J. Andrea, D. Apparu, D. Bloch, J.-M. Brom, E.C. Chabert, C. Collard, S. Falke, U. Goerlach, R. Haeberle, A.-C. Le Bihan, M. Meena, O. Poncet, G. Saha, M.A. Sessini, P. Van Hove, P. Vaucelle

Centre de Calcul de l'Institut National de Physique Nucleaire et de Physique des Particules, CNRS/IN2P3, Villeurbanne, France

A. Di Florio

Institut de Physique des 2 Infinis de Lyon (IP2I), Villeurbanne, France
D. Amram, S. Beauceron, B. Blancon, G. Boudoul, N. Chanon, D. Contardo, P. Depasse, C. Dozen[22], H. El Mamouni, J. Fay, S. Gascon, M. Gouzevitch, C. Greenberg, G. Grenier, B. Ille, E. Jourd'huy, I.B. Laktineh, M. Lethuillier, L. Mirabito, S. Perries, A. Purohit, M. Vander Donckt, P. Verdier, J. Xiao

Georgian Technical University, Tbilisi, Georgia
G. Adamov, I. Lomidze, Z. Tsamalaidze[23]

RWTH Aachen University, I. Physikalisches Institut, Aachen, Germany
V. Botta, S. Consuegra Rodríguez, L. Feld, K. Klein, M. Lipinski, D. Meuser, A. Pauls, D. Pérez Adán, N. Röwert, M. Teroerde

RWTH Aachen University, III. Physikalisches Institut A, Aachen, Germany
S. Diekmann, A. Dodonova, N. Eich, D. Eliseev, F. Engelke, J. Erdmann, M. Erdmann, P. Fackeldey, B. Fischer, T. Hebbeker, K. Hoepfner, F. Ivone, A. Jung, M.y. Lee, F. Mausolf, M. Merschmeyer, A. Meyer, S. Mukherjee, D. Noll, F. Nowotny, A. Pozdnyakov, Y. Rath, W. Redjeb, F. Rehm, H. Reithler, V. Sarkisovi, A. Schmidt, C. Seth, A. Sharma, J.L. Spah, F. Torres Da Silva De Araujo[24], S. Wiedenbeck, S. Zaleski

RWTH Aachen University, III. Physikalisches Institut B, Aachen, Germany
C. Dziwok, G. Flügge, T. Kress, A. Nowack, O. Pooth, A. Stahl, T. Ziemons, A. Zotz

Deutsches Elektronen-Synchrotron, Hamburg, Germany
H. Aarup Petersen, M. Aldaya Martin, J. Alimena, S. Amoroso, Y. An, P. Asmuss, J. Bach, S. Baxter, M. Bayatmakou, H. Becerril Gonzalez, O. Behnke, A. Belvedere, F. Blekman[25], K. Borras[26], A. Campbell, A. Cardini, F. Colombina, M. De Silva, G. Eckerlin, D. Eckstein, L.I. Estevez Banos, E. Gallo[25], A. Geiser, V. Guglielmi, M. Guthoff, A. Hinzmann, L. Jeppe, B. Kaech, M. Kasemann, C. Kleinwort, R. Kogler, M. Komm, D. Krücker, W. Lange, D. Leyva Pernia, K. Lipka[27], W. Lohmann[28], F. Lorkowski, R. Mankel, I.-A. Melzer-Pellmann, M. Mendizabal Morentin, A.B. Meyer, G. Milella, K. Moral Figueroa, A. Mussgiller, L.P. Nair, J. Niedziela, A. Nürnberg, J. Park, E. Ranken, A. Raspereza, D. Rastorguev, J. Rübenach, L. Rygaard, M. Scham[29,26], S. Schnake[26], P. Schütze, C. Schwanenberger[25], D. Selivanova, K. Sharko, M. Shchedrolosiev, R. Shevchenko, D. Stafford, F. Vazzoler, A. Ventura Barroso, R. Walsh, D. Wang, Q. Wang, K. Wichmann, L. Wiens[26], C. Wissing, Y. Yang, S. Zakharov, A. Zimermmane Castro Santos

University of Hamburg, Hamburg, Germany
A. Albrecht, S. Albrecht, M. Antonello, S. Bollweg, M. Bonanomi, P. Connor, K. El Morabit, Y. Fischer, E. Garutti, A. Grohsjean, J. Haller, D. Hundhausen, H.R. Jabusch, G. Kasieczka, P. Keicher, R. Klanner, W. Korcari, T. Kramer, C.c. Kuo, V. Kutzner, F. Labe, J. Lange, A. Lobanov, C. Matthies, L. Moureaux, M. Mrowietz, A. Nigamova, Y. Nissan, A. Paasch, K.J. Pena Rodriguez, T. Quadfasel, B. Raciti, M. Rieger, D. Savoiu, J. Schindler, P. Schleper, M. Schröder, J. Schwandt, M. Sommerhalder, H. Stadie, G. Steinbrück, A. Tews, B. Wiederspan, M. Wolf

Karlsruher Institut fuer Technologie, Karlsruhe, Germany
S. Brommer, E. Butz, T. Chwalek, A. Dierlamm, U. Elicabuk, N. Faltermann, M. Giffels, A. Gottmann, F. Hartmann[30], R. Hofsaess, M. Horzela, U. Husemann, J. Kieseler, M. Klute, O. Lavoryk, J.M. Lawhorn, M. Link, A. Lintuluoto, S. Maier, S. Mitra, M. Mormile, Th. Müller, M. Neukum, M. Oh, E. Pfeffer, M. Presilla, G. Quast, K. Rabbertz, B. Regnery, N. Shadskiy, I. Shvetsov, H.J. Simonis, L. Sowa, L. Stockmeier, K. Tauqeer, M. Toms, B. Topko, N. Trevisani, R.F. Von Cube, M. Wassmer, S. Wieland, F. Wittig, R. Wolf, X. Zuo

Institute of Nuclear and Particle Physics (INPP), NCSR Demokritos, Aghia Paraskevi, Greece
G. Anagnostou, G. Daskalakis, A. Kyriakis, A. Papadopoulos[30], A. Stakia

National and Kapodistrian University of Athens, Athens, Greece
G. Melachroinos, Z. Painesis, I. Paraskevas, N. Saoulidou, K. Theofilatos, E. Tziaferi, K. Vellidis, I. Zisopoulos

National Technical University of Athens, Athens, Greece
G. Bakas, T. Chatzistavrou, G. Karapostoli, K. Kousouris, I. Papakrivopoulos, E. Siamarkou, G. Tsipolitis, A. Zacharopoulou

University of Ioánnina, Ioánnina, Greece
I. Bestintzanos, I. Evangelou, C. Foudas, C. Kamtsikis, P. Katsoulis, P. Kokkas, P.G. Kosmoglou Kioseoglou, N. Manthos, I. Papadopoulos, J. Strologas

HUN-REN Wigner Research Centre for Physics, Budapest, Hungary
C. Hajdu, D. Horvath[31,32], K. Márton, A.J. Rádl[33], F. Sikler, V. Veszpremi

MTA-ELTE Lendület CMS Particle and Nuclear Physics Group, Eötvös Loránd University, Budapest, Hungary
M. Csanád, K. Farkas, A. Fehérkuti[34], M.M.A. Gadallah[35], Á. Kadlecsik, P. Major, G. Pásztor, G.I. Veres

Faculty of Informatics, University of Debrecen, Debrecen, Hungary
B. Ujvari, G. Zilizi

HUN-REN ATOMKI - Institute of Nuclear Research, Debrecen, Hungary
G. Bencze, S. Czellar, J. Molnar, Z. Szillasi

Karoly Robert Campus, MATE Institute of Technology, Gyongyos, Hungary
T. Csorgo[34], F. Nemes[34], T. Novak

Panjab University, Chandigarh, India
S. Bansal, S.B. Beri, V. Bhatnagar, G. Chaudhary, S. Chauhan, N. Dhingra[36], A. Kaur, A. Kaur, H. Kaur, M. Kaur, S. Kumar, T. Sheokand, J.B. Singh, A. Singla

University of Delhi, Delhi, India
A. Bhardwaj, A. Chhetri, B.C. Choudhary, A. Kumar, A. Kumar, M. Naimuddin, K. Ranjan, M.K. Saini, S. Saumya

Saha Institute of Nuclear Physics, HBNI, Kolkata, India
S. Baradia, S. Barman[37], S. Bhattacharya, S. Das Gupta, S. Dutta, S. Dutta, S. Sarkar

Indian Institute of Technology Madras, Madras, India
M.M. Ameen, P.K. Behera, S.C. Behera, S. Chatterjee, G. Dash, P. Jana,

P. Kalbhor, S. Kamble, J.R. Komaragiri[38], D. Kumar[38], T. Mishra, B. Parida[39], P.R. Pujahari, N.R. Saha, A. Sharma, A.K. Sikdar, R.K. Singh, P. Verma, S. Verma, A. Vijay

Tata Institute of Fundamental Research-A, Mumbai, India
S. Dugad, G.B. Mohanty, M. Shelake, P. Suryadevara

Tata Institute of Fundamental Research-B, Mumbai, India
A. Bala, S. Banerjee, S. Bhowmik, R.M. Chatterjee, M. Guchait, Sh. Jain, A. Jaiswal, B.M. Joshi, S. Kumar, G. Majumder, K. Mazumdar, S. Parolia, A. Thachayath

National Institute of Science Education and Research, An OCC of Homi Bhabha National Institute, Bhubaneswar, Odisha, India
S. Bahinipati[40], C. Kar, D. Maity[41], P. Mal, K. Naskar[41], A. Nayak[41], S. Nayak, K. Pal, P. Sadangi, S.K. Swain, S. Varghese[41], D. Vats[41]

Indian Institute of Science Education and Research (IISER), Pune, India
S. Acharya[42], A. Alpana, S. Dube, B. Gomber[42], P. Hazarika, B. Kansal, A. Laha, B. Sahu[42], S. Sharma, K.Y. Vaish

Isfahan University of Technology, Isfahan, Iran
H. Bakhshiansohi[43], A. Jafari[44], M. Zeinali[45]

Institute for Research in Fundamental Sciences (IPM), Tehran, Iran
S. Bashiri, S. Chenarani[46], S.M. Etesami, Y. Hosseini, M. Khakzad, E. Khazaie, M. Mohammadi Najafabadi, S. Tizchang[47]

University College Dublin, Dublin, Ireland
M. Felcini, M. Grunewald

INFN Sezione di Bari[a], Università di Bari[b], Politecnico di Bari[c], Bari, Italy
M. Abbrescia[a,b], A. Colaleo[a,b], D. Creanza[a,c], B. D'Anzi[a,b], N. De Filippis[a,c], M. De Palma[a,b], W. Elmetenawee[a,b,16], N. Ferrara[a,b], L. Fiore[a], G. Iaselli[a,c], L. Longo[a], M. Louka[a,b], G. Maggi[a,c], M. Maggi[a], I. Margjeka[a], V. Mastrapasqua[a,b], S. My[a,b], S. Nuzzo[a,b], A. Pellecchia[a,b], A. Pompili[a,b], G. Pugliese[a,c], R. Radogna[a,b], D. Ramos[a], A. Ranieri[a], L. Silvestris[a], F.M. Simone[a,c], Ü. Sözbilir[a], A. Stamerra[a,b], D. Troiano[a,b], R. Venditti[a,b], P. Verwilligen[a], A. Zaza[a,b]

INFN Sezione di Bologna[a], Università di Bologna[b], Bologna, Italy
G. Abbiendi[a], C. Battilana[a,b], D. Bonacorsi[a,b], P. Capiluppi[a,b], A. Castro[†a,b], F.R. Cavallo[a], M. Cuffiani[a,b], G.M. Dallavalle[a], T. Diotalevi[a,b], F. Fabbri[a], A. Fanfani[a,b], D. Fasanella[a], P. Giacomelli[a], L. Giommi[a,b], C. Grandi[a], L. Guiducci[a,b], S. Lo Meo[a,48], M. Lorusso[a,b], L. Lunerti[a], S. Marcellini[a], G. Masetti[a], F.L. Navarria[a,b], G. Paggi[a,b], A. Perrotta[a], F. Primavera[a,b], A.M. Rossi[a,b], S. Rossi Tisbeni[a,b], T. Rovelli[a,b], G.P. Siroli[a,b]

INFN Sezione di Catania[a], Università di Catania[b], Catania, Italy
S. Costa[a,b,49], A. Di Mattia[a], A. Lapertosa[a], R. Potenza[a,b], A. Tricomi[a,b,49], C. Tuve[a,b]

INFN Sezione di Firenze[a], Università di Firenze[b], Firenze, Italy
P. Assiouras[a], G. Barbagli[a], G. Bardelli[a,b], B. Camaiani[a,b], A. Cassese[a], R. Ceccarelli[a], V. Ciulli[a,b], C. Civinini[a], R. D'Alessandro[a,b], E. Focardi[a,b], T. Kello[a], G. Latino[a,b], P. Lenzi[a,b], M. Lizzo[a], M. Meschini[a], S. Paoletti[a],

A. Papanastassiou[a,b], G. Sguazzoni[a], L. Viliani[a]

INFN Laboratori Nazionali di Frascati, Frascati, Italy
L. Benussi, S. Bianco, S. Meola[50], D. Piccolo

INFN Sezione di Genova[a], Università di Genova[b], Genova, Italy
M. Alves Gallo Pereira[a], F. Ferro[a], E. Robutti[a], S. Tosi[a,b]

INFN Sezione di Milano-Bicocca[a], Università di Milano-Bicocca[b], Milano, Italy
A. Benaglia[a], F. Brivio[a], F. Cetorelli[a,b], F. De Guio[a,b], M.E. Dinardo[a,b], P. Dini[a], S. Gennai[a], R. Gerosa[a,b], A. Ghezzi[a,b], P. Govoni[a,b], L. Guzzi[a], M.T. Lucchini[a,b], M. Malberti[a], S. Malvezzi[a], A. Massironi[a], D. Menasce[a], L. Moroni[a], M. Paganoni[a,b], S. Palluotto[a,b], D. Pedrini[a], A. Perego[a,b], B.S. Pinolini[a], G. Pizzati[a,b], S. Ragazzi[a,b], T. Tabarelli de Fatis[a,b]

INFN Sezione di Napoli[a], Università di Napoli 'Federico II'[b], Napoli, Italy; Università della Basilicata[c], Potenza, Italy; Scuola Superiore Meridionale (SSM)[d], Napoli, Italy
S. Buontempo[a], A. Cagnotta[a,b], F. Carnevali[a,b], N. Cavallo[a,c], F. Fabozzi[a,c], A.O.M. Iorio[a,b], L. Lista[a,b,51], P. Paolucci[a,30], B. Rossi[a]

INFN Sezione di Padova[a], Università di Padova[b], Padova, Italy; Università di Trento[c], Trento, Italy
R. Ardino[a], P. Azzi[a], N. Bacchetta[a,52], P. Bortignon[a], G. Bortolato[a,b], A. Bragagnolo[a,b], A.C.M. Bulla[a], R. Carlin[a,b], P. Checchia[a], T. Dorigo[a], U. Gasparini[a,b], S. Giorgetti[a], M. Gulmini[a,53], E. Lusiani[a], M. Margoni[a,b], G. Maron[a,53], A.T. Meneguzzo[a,b], M. Migliorini[a,b], J. Pazzini[a,b], P. Ronchese[a,b], R. Rossin[a,b], F. Simonetto[a,b], M. Tosi[a,b], A. Triossi[a,b], S. Ventura[a], M. Zanetti[a,b], P. Zotto[a,b], A. Zucchetta[a,b], G. Zumerle[a,b]

INFN Sezione di Pavia[a], Università di Pavia[b], Pavia, Italy
A. Braghieri[a], S. Calzaferri[a], D. Fiorina[a], P. Montagna[a,b], V. Re[a], C. Riccardi[a,b], P. Salvini[a], I. Vai[a,b], P. Vitulo[a,b]

INFN Sezione di Perugia[a], Università di Perugia[b], Perugia, Italy
S. Ajmal[a,b], M.E. Ascioti[a,b], G.M. Bilei[a], C. Carrivale[a,b], D. Ciangottini[a,b], L. Fanò[a,b], V. Mariani[a,b], M. Menichelli[a], F. Moscatelli[a,54], A. Rossi[a,b], A. Santocchia[a,b], D. Spiga[a], T. Tedeschi[a,b]

INFN Sezione di Pisa[a], Università di Pisa[b], Scuola Normale Superiore di Pisa[c], Pisa, Italy; Università di Siena[d], Siena, Italy
C. Aimè[a], C.A. Alexe[a,c], P. Asenov[a,b], P. Azzurri[a], G. Bagliesi[a], R. Bhattacharya[a], L. Bianchini[a,b], T. Boccali[a], E. Bossini[a], D. Bruschini[a,c], R. Castaldi[a], M.A. Ciocci[a,b], M. Cipriani[a,b], V. D'Amante[a,d], R. Dell'Orso[a], S. Donato[a], A. Giassi[a], F. Ligabue[a,c], A.C. Marini[a], D. Matos Figueiredo[a], A. Messineo[a,b], S. Mishra[a], V.K. Muraleedharan Nair Bindhu[a,b,41], M. Musich[a,b], S. Nandan[a], F. Palla[a], A. Rizzi[a,b], G. Rolandi[a,c], S. Roy Chowdhury[a], T. Sarkar[a], A. Scribano[a], P. Spagnolo[a], R. Tenchini[a], G. Tonelli[a,b], N. Turini[a,d], F. Vaselli[a,c], A. Venturi[a], P.G. Verdini[a]

INFN Sezione di Roma[a], Sapienza Università di Roma[b], Roma, Italy
C. Baldenegro Barrera[a,b], P. Barria[a], C. Basile[a,b], F. Cavallari[a], L. Cunqueiro Mendez[a,b], D. Del Re[a,b], E. Di Marco[a,b], M. Diemoz[a], F. Errico[a,b], R. Gargiulo[a,b], E. Longo[a,b], L. Martikainen[a,b], J. Mijuskovic[a,b], G. Organtini[a,b], F. Pandolfi[a], R. Paramatti[a,b], C. Quaranta[a,b], S. Rahatlou[a,b], C. Rovelli[a],

F. Santanastasio[a,b], L. Soffi[a], V. Vladimirov[a,b]

INFN Sezione di Torino[a], Università di Torino[b], Torino, Italy; Università del Piemonte Orientale[c], Novara, Italy
N. Amapane[a,b], R. Arcidiacono[a,c], S. Argiro[a,b], M. Arneodo[a,c], N. Bartosik[a], R. Bellan[a,b], A. Bellora[a,b], C. Biino[a], C. Borca[a,b], N. Cartiglia[a], M. Costa[a,b], R. Covarelli[a,b], N. Demaria[a], L. Finco[a], M. Grippo[a,b], B. Kiani[a,b], F. Legger[a], F. Luongo[a,b], C. Mariotti[a], L. Markovic[a,b], S. Maselli[a], A. Mecca[a,b], L. Menzio[a,b], P. Meridiani[a], E. Migliore[a,b], M. Monteno[a], R. Mulargia[a], M.M. Obertino[a,b], G. Ortona[a], L. Pacher[a,b], N. Pastrone[a], M. Pelliccioni[a], M. Ruspa[a,c], F. Siviero[a,b], V. Sola[a,b], A. Solano[a,b], A. Staiano[a], C. Tarricone[a,b], D. Trocino[a], G. Umoret[a,b], R. White[a,b]

INFN Sezione di Trieste[a], Università di Trieste[b], Trieste, Italy
J. Babbar[a,b], S. Belforte[a], V. Candelise[a,b], M. Casarsa[a], F. Cossutti[a], K. De Leo[a], G. Della Ricca[a,b]

Kyungpook National University, Daegu, Korea
S. Dogra, J. Hong, B. Kim, J. Kim, D. Lee, H. Lee, S.W. Lee, C.S. Moon, Y.D. Oh, M.S. Ryu, S. Sekmen, B. Tae, Y.C. Yang

Department of Mathematics and Physics - GWNU, Gangneung, Korea
M.S. Kim

Chonnam National University, Institute for Universe and Elementary Particles, Kwangju, Korea
G. Bak, P. Gwak, H. Kim, D.H. Moon

Hanyang University, Seoul, Korea
E. Asilar, J. Choi[55], D. Kim, T.J. Kim, J.A. Merlin, Y. Ryou

Korea University, Seoul, Korea
S. Choi, S. Han, B. Hong, K. Lee, K.S. Lee, S. Lee, J. Yoo

Kyung Hee University, Department of Physics, Seoul, Korea
J. Goh, S. Yang

Sejong University, Seoul, Korea
H. S. Kim, Y. Kim, S. Lee

Seoul National University, Seoul, Korea
J. Almond, J.H. Bhyun, J. Choi, J. Choi, W. Jun, J. Kim, Y.W. Kim, S. Ko, H. Kwon, H. Lee, J. Lee, J. Lee, B.H. Oh, S.B. Oh, H. Seo, U.K. Yang, I. Yoon

University of Seoul, Seoul, Korea
W. Jang, D.Y. Kang, Y. Kang, S. Kim, B. Ko, J.S.H. Lee, Y. Lee, I.C. Park, Y. Roh, I.J. Watson

Yonsei University, Department of Physics, Seoul, Korea
S. Ha, K. Hwang, H.D. Yoo

Sungkyunkwan University, Suwon, Korea
M. Choi, M.R. Kim, H. Lee, Y. Lee, I. Yu

College of Engineering and Technology, American University of the Middle East (AUM), Dasman, Kuwait

T. Beyrouthy, Y. Gharbia

Kuwait University - College of Science - Department of Physics, Safat, Kuwait
F. Alazemi

Riga Technical University, Riga, Latvia
K. Dreimanis, A. Gaile, C. Munoz Diaz, D. Osite, G. Pikurs, A. Potrebko, M. Seidel, D. Sidiropoulos Kontos

University of Latvia (LU), Riga, Latvia
N.R. Strautnieks

Vilnius University, Vilnius, Lithuania
M. Ambrozas, A. Juodagalvis, A. Rinkevicius, G. Tamulaitis

National Centre for Particle Physics, Universiti Malaya, Kuala Lumpur, Malaysia
I. Yusuff[56], Z. Zolkapli

Universidad de Sonora (UNISON), Hermosillo, Mexico
J.F. Benitez, A. Castaneda Hernandez, H.A. Encinas Acosta, L.G. Gallegos Maríñez, M. León Coello, J.A. Murillo Quijada, A. Sehrawat, L. Valencia Palomo

Centro de Investigacion y de Estudios Avanzados del IPN, Mexico City, Mexico
G. Ayala, H. Castilla-Valdez, H. Crotte Ledesma, E. De La Cruz-Burelo, I. Heredia-De La Cruz[57], R. Lopez-Fernandez, J. Mejia Guisao, C.A. Mondragon Herrera, A. Sánchez Hernández

Universidad Iberoamericana, Mexico City, Mexico
C. Oropeza Barrera, D.L. Ramirez Guadarrama, M. Ramírez García

Benemerita Universidad Autonoma de Puebla, Puebla, Mexico
I. Bautista, F.E. Neri Huerta, I. Pedraza, H.A. Salazar Ibarguen, C. Uribe Estrada

University of Montenegro, Podgorica, Montenegro
I. Bubanja, N. Raicevic

University of Canterbury, Christchurch, New Zealand
P.H. Butler

National Centre for Physics, Quaid-I-Azam University, Islamabad, Pakistan
A. Ahmad, M.I. Asghar, A. Awais, M.I.M. Awan, H.R. Hoorani, W.A. Khan

AGH University of Krakow, Krakow, Poland
V. Avati, L. Forthomme, L. Grzanka, M. Malawski, K. Piotrzkowski

National Centre for Nuclear Research, Swierk, Poland
H. Bialkowska, M. Bluj, M. Górski, M. Kazana, M. Szleper, P. Zalewski

Institute of Experimental Physics, Faculty of Physics, University of Warsaw, Warsaw, Poland
K. Bunkowski, K. Doroba, A. Kalinowski, M. Konecki, J. Krolikowski, A. Muhammad

Warsaw University of Technology, Warsaw, Poland
P. Fokow, K. Pozniak, W. Zabolotny

Laboratório de Instrumentação e Física Experimental de Partículas, Lisboa, Portugal
M. Araujo, D. Bastos, C. Beirão Da Cruz E Silva, A. Boletti, M. Bozzo, T. Camporesi, G. Da Molin, P. Faccioli, M. Gallinaro, J. Hollar, N. Leonardo,

G.B. Marozzo, A. Petrilli, M. Pisano, J. Seixas, J. Varela, J.W. Wulff

Faculty of Physics, University of Belgrade, Belgrade, Serbia
P. Adzic, P. Milenovic

VINCA Institute of Nuclear Sciences, University of Belgrade, Belgrade, Serbia
D. Devetak, M. Dordevic, J. Milosevic, L. Nadderd, V. Rekovic, M. Stojanovic

Centro de Investigaciones Energéticas Medioambientales y Tecnológicas (CIEMAT), Madrid, Spain
J. Alcaraz Maestre, Cristina F. Bedoya, J.A. Brochero Cifuentes, Oliver M. Carretero, M. Cepeda, M. Cerrada, N. Colino, B. De La Cruz, A. Delgado Peris, A. Escalante Del Valle, D. Fernández Del Val, J.P. Fernández Ramos, J. Flix, M.C. Fouz, O. Gonzalez Lopez, S. Goy Lopez, J.M. Hernandez, M.I. Josa, J. Llorente Merino, C. Martin Perez, E. Martin Viscasillas, D. Moran, C. M. Morcillo Perez, Á. Navarro Tobar, C. Perez Dengra, A. Pérez-Calero Yzquierdo, J. Puerta Pelayo, I. Redondo, J. Sastre, J. Vazquez Escobar

Universidad Autónoma de Madrid, Madrid, Spain
J.F. de Trocóniz

Universidad de Oviedo, Instituto Universitario de Ciencias y Tecnologías Espaciales de Asturias (ICTEA), Oviedo, Spain
B. Alvarez Gonzalez, J. Cuevas, J. Fernandez Menendez, S. Folgueras, I. Gonzalez Caballero, P. Leguina, E. Palencia Cortezon, J. Prado Pico, V. Rodríguez Bouza, A. Soto Rodríguez, A. Trapote, C. Vico Villalba, P. Vischia

Instituto de Física de Cantabria (IFCA), CSIC-Universidad de Cantabria, Santander, Spain
S. Blanco Fernández, I.J. Cabrillo, A. Calderon, J. Duarte Campderros, M. Fernandez, G. Gomez, C. Lasaosa García, R. Lopez Ruiz, C. Martinez Rivero, P. Martinez Ruiz del Arbol, F. Matorras, P. Matorras Cuevas, E. Navarrete Ramos, J. Piedra Gomez, L. Scodellaro, I. Vila, J.M. Vizan Garcia

University of Colombo, Colombo, Sri Lanka
B. Kailasapathy[58], D.D.C. Wickramarathna

University of Ruhuna, Department of Physics, Matara, Sri Lanka
W.G.D. Dharmaratna[59], K. Liyanage, N. Perera

CERN, European Organization for Nuclear Research, Geneva, Switzerland
D. Abbaneo, C. Amendola, E. Auffray, G. Auzinger, J. Baechler, D. Barney, A. Bermúdez Martínez, M. Bianco, A.A. Bin Anuar, A. Bocci, L. Borgonovi, C. Botta, E. Brondolin, C.E. Brown, C. Caillol, G. Cerminara, N. Chernyavskaya, D. d'Enterria, A. Dabrowski, A. David, A. De Roeck, M.M. Defranchis, M. Deile, M. Dobson, G. Franzoni, W. Funk, S. Giani, D. Gigi, K. Gill, F. Glege, J. Hegeman, J.K. Heikkilä, B. Huber, V. Innocente, T. James, P. Janot, O. Kaluzinska, O. Karacheban[28], G. Karathanasis, S. Laurila, P. Lecoq, E. Leutgeb, C. Lourenço, M. Magherini, L. Malgeri, M. Mannelli, M. Matthewman, A. Mehta, F. Meijers, S. Mersi, E. Meschi, V. Milosevic, F. Monti, F. Moortgat, M. Mulders, I. Neutelings, S. Orfanelli, F. Pantaleo, G. Petrucciani, A. Pfeiffer, M. Pierini, H. Qu, D. Rabady, B. Ribeiro Lopes, F. Riti, M. Rovere, H. Sakulin, R. Salvatico, S. Sanchez Cruz, S. Scarfi, C. Schwick, M. Selvaggi, A. Sharma, K. Shchelina, P. Silva, P. Sphicas[60], A.G. Stahl Leiton, A. Steen, S. Summers, D. Treille, P. Tropea, D. Walter, J. Wanczyk[61], J. Wang, S. Wuchterl, P. Zehetner,

P. Zejdl, W.D. Zeuner

PSI Center for Neutron and Muon Sciences, Villigen, Switzerland
T. Bevilacqua[62], L. Caminada[62], A. Ebrahimi, W. Erdmann, R. Horisberger, Q. Ingram, H.C. Kaestli, D. Kotlinski, C. Lange, M. Missiroli[62], L. Noehte[62], T. Rohe, A. Samalan

ETH Zurich - Institute for Particle Physics and Astrophysics (IPA), Zurich, Switzerland
T.K. Aarrestad, M. Backhaus, G. Bonomelli, A. Calandri, C. Cazzaniga, K. Datta, P. De Bryas Dexmiers D'archiac[61], A. De Cosa, G. Dissertori, M. Dittmar, M. Donegà, F. Eble, M. Galli, K. Gedia, F. Glessgen, C. Grab, N. Härringer, T.G. Harte, D. Hits, W. Lustermann, A.-M. Lyon, R.A. Manzoni, M. Marchegiani, L. Marchese, A. Mascellani[61], F. Nessi-Tedaldi, F. Pauss, V. Perovic, S. Pigazzini, B. Ristic, R. Seidita, J. Steggemann[61], A. Tarabini, D. Valsecchi, R. Wallny

Universität Zürich, Zurich, Switzerland
C. Amsler[63], P. Bärtschi, M.F. Canelli, K. Cormier, M. Huwiler, W. Jin, A. Jofrehei, B. Kilminster, S. Leontsinis, S.P. Liechti, A. Macchiolo, P. Meiring, F. Meng, J. Motta, A. Reimers, P. Robmann, M. Senger, E. Shokr, F. Stäger, R. Tramontano

National Central University, Chung-Li, Taiwan
C. Adloff[64], D. Bhowmik, C.M. Kuo, W. Lin, P.K. Rout, P.C. Tiwari[38]

National Taiwan University (NTU), Taipei, Taiwan
L. Ceard, K.F. Chen, Z.g. Chen, A. De Iorio, W.-S. Hou, T.h. Hsu, Y.w. Kao, S. Karmakar, G. Kole, Y.y. Li, R.-S. Lu, E. Paganis, X.f. Su, J. Thomas-Wilsker, L.s. Tsai, D. Tsionou, H.y. Wu, E. Yazgan

High Energy Physics Research Unit, Department of Physics, Faculty of Science, Chulalongkorn University, Bangkok, Thailand
C. Asawatangtrakuldee, P. Chokeprasert, N. Srimanobhas, V. Wachirapusitanand

Tunis El Manar University, Tunis, Tunisia
Y. Maghrbi

Çukurova University, Physics Department, Science and Art Faculty, Adana, Turkey
D. Agyel, F. Boran, F. Dolek, I. Dumanoglu[65], E. Eskut, Y. Guler[66], E. Gurpinar Guler[66], C. Isik, O. Kara, A. Kayis Topaksu, Y. Komurcu, G. Onengut, K. Ozdemir[67], A. Polatoz, B. Tali[68], U.G. Tok, E. Uslan, I.S. Zorbakir

Middle East Technical University, Physics Department, Ankara, Turkey
M. Yalvac[69]

Bogazici University, Istanbul, Turkey
B. Akgun, I.O. Atakisi, E. Gülmez, M. Kaya[70], O. Kaya[71], S. Tekten[72]

Istanbul Technical University, Istanbul, Turkey
A. Cakir, K. Cankocak[65,73], G.G. Dincer[65], S. Sen[74]

Istanbul University, Istanbul, Turkey
O. Aydilek[75], B. Hacisahinoglu, I. Hos[76], B. Kaynak, S. Ozkorucuklu, O. Potok, H. Sert, C. Simsek, C. Zorbilmez

Yildiz Technical University, Istanbul, Turkey
S. Cerci, B. Isildak[77], D. Sunar Cerci, T. Yetkin

Institute for Scintillation Materials of National Academy of Science of Ukraine, Kharkiv, Ukraine
A. Boyaryntsev, B. Grynyov

National Science Centre, Kharkiv Institute of Physics and Technology, Kharkiv, Ukraine
L. Levchuk

University of Bristol, Bristol, United Kingdom
D. Anthony, J.J. Brooke, A. Bundock, F. Bury, E. Clement, D. Cussans, H. Flacher, M. Glowacki, J. Goldstein, H.F. Heath, M.-L. Holmberg, L. Kreczko, S. Paramesvaran, L. Robertshaw, V.J. Smith, K. Walkingshaw Pass

Rutherford Appleton Laboratory, Didcot, United Kingdom
A.H. Ball, K.W. Bell, A. Belyaev[78], C. Brew, R.M. Brown, D.J.A. Cockerill, C. Cooke, A. Elliot, K.V. Ellis, K. Harder, S. Harper, J. Linacre, K. Manolopoulos, D.M. Newbold, E. Olaiya, D. Petyt, T. Reis, A.R. Sahasransu, G. Salvi, T. Schuh, C.H. Shepherd-Themistocleous, I.R. Tomalin, K.C. Whalen, T. Williams

Imperial College, London, United Kingdom
I. Andreou, R. Bainbridge, P. Bloch, O. Buchmuller, C.A. Carrillo Montoya, G.S. Chahal[79], D. Colling, J.S. Dancu, I. Das, P. Dauncey, G. Davies, M. Della Negra, S. Fayer, G. Fedi, G. Hall, A. Howard, G. Iles, C.R. Knight, P. Krueper, J. Langford, K.H. Law, J. León Holgado, L. Lyons, A.-M. Magnan, B. Maier, S. Mallios, M. Mieskolainen, J. Nash[80], M. Pesaresi, P.B. Pradeep, B.C. Radburn-Smith, A. Richards, A. Rose, K. Savva, C. Seez, R. Shukla, A. Tapper, K. Uchida, G.P. Uttley, T. Virdee[30], M. Vojinovic, N. Wardle, D. Winterbottom

Brunel University, Uxbridge, United Kingdom
J.E. Cole, A. Khan, P. Kyberd, I.D. Reid

Baylor University, Waco, Texas, USA
S. Abdullin, A. Brinkerhoff, E. Collins, M.R. Darwish, J. Dittmann, K. Hatakeyama, V. Hegde, J. Hiltbrand, B. McMaster, J. Samudio, S. Sawant, C. Sutantawibul, J. Wilson

Catholic University of America, Washington, DC, USA
R. Bartek, A. Dominguez, A.E. Simsek, S.S. Yu

The University of Alabama, Tuscaloosa, Alabama, USA
B. Bam, A. Buchot Perraguin, R. Chudasama, S.I. Cooper, C. Crovella, S.V. Gleyzer, E. Pearson, C.U. Perez, P. Rumerio[81], E. Usai, R. Yi

Boston University, Boston, Massachusetts, USA
A. Akpinar, C. Cosby, G. De Castro, Z. Demiragli, C. Erice, C. Fangmeier, C. Fernandez Madrazo, E. Fontanesi, D. Gastler, F. Golf, S. Jeon, J. O'cain, I. Reed, J. Rohlf, K. Salyer, D. Sperka, D. Spitzbart, I. Suarez, A. Tsatsos, A.G. Zecchinelli

Brown University, Providence, Rhode Island, USA
G. Barone, G. Benelli, D. Cutts, L. Gouskos, M. Hadley, U. Heintz, K.W. Ho, J.M. Hogan[82], T. Kwon, G. Landsberg, K.T. Lau, J. Luo, S. Mondal, T. Russell, S. Sagir[83], X. Shen, F. Simpson, M. Stamenkovic, N. Venkatasubramanian

University of California, Davis, Davis, California, USA

S. Abbott, B. Barton, C. Brainerd, R. Breedon, H. Cai, M. Calderon De La Barca Sanchez, M. Chertok, M. Citron, J. Conway, P.T. Cox, R. Erbacher, F. Jensen, O. Kukral, G. Mocellin, M. Mulhearn, S. Ostrom, W. Wei, S. Yoo, F. Zhang

University of California, Los Angeles, California, USA
K. Adamidis, M. Bachtis, D. Campos, R. Cousins, A. Datta, G. Flores Avila, J. Hauser, M. Ignatenko, M.A. Iqbal, T. Lam, Y.f. Lo, E. Manca, A. Nunez Del Prado, D. Saltzberg, V. Valuev

University of California, Riverside, Riverside, California, USA
R. Clare, J.W. Gary, G. Hanson

University of California, San Diego, La Jolla, California, USA
A. Aportela, A. Arora, J.G. Branson, S. Cittolin, S. Cooperstein, D. Diaz, J. Duarte, L. Giannini, Y. Gu, J. Guiang, R. Kansal, V. Krutelyov, R. Lee, J. Letts, M. Masciovecchio, F. Mokhtar, S. Mukherjee, M. Pieri, D. Primosch, M. Quinnan, V. Sharma, M. Tadel, E. Vourliotis, F. Würthwein, Y. Xiang, A. Yagil

University of California, Santa Barbara - Department of Physics, Santa Barbara, California, USA
A. Barzdukas, L. Brennan, C. Campagnari, K. Downham, C. Grieco, M.M. Hussain, J. Incandela, J. Kim, A.J. Li, P. Masterson, H. Mei, J. Richman, S.N. Santpur, U. Sarica, R. Schmitz, F. Setti, J. Sheplock, D. Stuart, T.Á. Vámi, X. Yan, D. Zhang

California Institute of Technology, Pasadena, California, USA
S. Bhattacharya, A. Bornheim, O. Cerri, J. Mao, H.B. Newman, G. Reales Gutiérrez, M. Spiropulu, J.R. Vlimant, C. Wang, S. Xie, R.Y. Zhu

Carnegie Mellon University, Pittsburgh, Pennsylvania, USA
J. Alison, S. An, P. Bryant, M. Cremonesi, V. Dutta, T. Ferguson, T.A. Gómez Espinosa, A. Harilal, A. Kallil Tharayil, C. Liu, T. Mudholkar, S. Murthy, P. Palit, K. Park, M. Paulini, A. Roberts, A. Sanchez, W. Terrill

University of Colorado Boulder, Boulder, Colorado, USA
J.P. Cumalat, W.T. Ford, A. Hart, A. Hassani, N. Manganelli, J. Pearkes, C. Savard, N. Schonbeck, K. Stenson, K.A. Ulmer, S.R. Wagner, N. Zipper, D. Zuolo

Cornell University, Ithaca, New York, USA
J. Alexander, X. Chen, D.J. Cranshaw, J. Dickinson, J. Fan, X. Fan, S. Hogan, P. Kotamnives, J. Monroy, M. Oshiro, J.R. Patterson, M. Reid, A. Ryd, J. Thom, P. Wittich, R. Zou

Fermi National Accelerator Laboratory, Batavia, Illinois, USA
M. Albrow, M. Alyari, O. Amram, G. Apollinari, A. Apresyan, L.A.T. Bauerdick, D. Berry, J. Berryhill, P.C. Bhat, K. Burkett, J.N. Butler, A. Canepa, G.B. Cerati, H.W.K. Cheung, F. Chlebana, G. Cummings, I. Dutta, V.D. Elvira, Y. Feng, J. Freeman, A. Gandrakota, Z. Gecse, L. Gray, D. Green, A. Grummer, S. Grünendahl, D. Guerrero, O. Gutsche, R.M. Harris, T.C. Herwig, J. Hirschauer, B. Jayatilaka, S. Jindariani, M. Johnson, U. Joshi, T. Klijnsma, B. Klima, K.H.M. Kwok, S. Lammel, C. Lee, D. Lincoln, R. Lipton, T. Liu,

C. Madrid, K. Maeshima, D. Mason, P. McBride, P. Merkel, S. Mrenna, S. Nahn, J. Ngadiuba, D. Noonan, S. Norberg, V. Papadimitriou, N. Pastika, K. Pedro, C. Pena[84], F. Ravera, A. Reinsvold Hall[85], L. Ristori, M. Safdari, E. Sexton-Kennedy, N. Smith, A. Soha, L. Spiegel, S. Stoynev, J. Strait, L. Taylor, S. Tkaczyk, N.V. Tran, L. Uplegger, E.W. Vaandering, I. Zoi

University of Florida, Gainesville, Florida, USA
C. Aruta, P. Avery, D. Bourilkov, P. Chang, V. Cherepanov, R.D. Field, C. Huh, E. Koenig, M. Kolosova, J. Konigsberg, A. Korytov, K. Matchev, N. Menendez, G. Mitselmakher, K. Mohrman, A. Muthirakalayil Madhu, N. Rawal, S. Rosenzweig, Y. Takahashi, J. Wang

Florida State University, Tallahassee, Florida, USA
T. Adams, A. Al Kadhim, A. Askew, S. Bower, R. Hashmi, R.S. Kim, S. Kim, T. Kolberg, G. Martinez, H. Prosper, P.R. Prova, M. Wulansatiti, R. Yohay, J. Zhang

Florida Institute of Technology, Melbourne, Florida, USA
B. Alsufyani, S. Butalla, S. Das, T. Elkafrawy[86], M. Hohlmann, E. Yanes

University of Illinois Chicago, Chicago, Illinois, USA
M.R. Adams, A. Baty, C. Bennett, R. Cavanaugh, R. Escobar Franco, O. Evdokimov, C.E. Gerber, M. Hawksworth, A. Hingrajiya, D.J. Hofman, J.h. Lee, D. S. Lemos, C. Mills, S. Nanda, G. Oh, B. Ozek, D. Pilipovic, R. Pradhan, E. Prifti, T. Roy, S. Rudrabhatla, N. Singh, M.B. Tonjes, N. Varelas, M.A. Wadud, Z. Ye, J. Yoo

The University of Iowa, Iowa City, Iowa, USA
M. Alhusseini, D. Blend, K. Dilsiz[87], L. Emediato, G. Karaman, O.K. Köseyan, J.-P. Merlo, A. Mestvirishvili[88], O. Neogi, H. Ogul[89], Y. Onel, A. Penzo, C. Snyder, E. Tiras[90]

Johns Hopkins University, Baltimore, Maryland, USA
B. Blumenfeld, L. Corcodilos, J. Davis, A.V. Gritsan, L. Kang, S. Kyriacou, P. Maksimovic, M. Roguljic, J. Roskes, S. Sekhar, M. Swartz

The University of Kansas, Lawrence, Kansas, USA
A. Abreu, L.F. Alcerro Alcerro, J. Anguiano, S. Arteaga Escatel, P. Baringer, A. Bean, Z. Flowers, D. Grove, J. King, G. Krintiras, M. Lazarovits, C. Le Mahieu, J. Marquez, M. Murray, M. Nickel, M. Pitt, S. Popescu[91], C. Rogan, C. Royon, S. Sanders, C. Smith, G. Wilson

Kansas State University, Manhattan, Kansas, USA
B. Allmond, R. Gujju Gurunadha, A. Ivanov, K. Kaadze, Y. Maravin, J. Natoli, D. Roy, G. Sorrentino

University of Maryland, College Park, Maryland, USA
A. Baden, A. Belloni, J. Bistany-riebman, Y.M. Chen, S.C. Eno, N.J. Hadley, S. Jabeen, R.G. Kellogg, T. Koeth, B. Kronheim, Y. Lai, S. Lascio, A.C. Mignerey, S. Nabili, C. Palmer, C. Papageorgakis, M.M. Paranjpe, E. Popova[92], A. Shevelev, L. Wang, L. Zhang

Massachusetts Institute of Technology, Cambridge, Massachusetts, USA
J. Bendavid, S. Bright-Thonney, I.A. Cali, P.c. Chou, M. D'Alfonso, J. Eysermans, C. Freer, G. Gomez-Ceballos, M. Goncharov, G. Grosso, P. Harris, D. Hoang,

D. Kovalskyi, J. Krupa, L. Lavezzo, Y.-J. Lee, K. Long, C. Mcginn, A. Novak, M.I. Park, C. Paus, C. Reissel, C. Roland, G. Roland, S. Rothman, G.S.F. Stephans, Z. Wang, B. Wyslouch, T. J. Yang

University of Minnesota, Minneapolis, Minnesota, USA
B. Crossman, C. Kapsiak, M. Krohn, D. Mahon, J. Mans, B. Marzocchi, M. Revering, R. Rusack, R. Saradhy, N. Strobbe

University of Nebraska-Lincoln, Lincoln, Nebraska, USA
K. Bloom, D.R. Claes, G. Haza, J. Hossain, C. Joo, I. Kravchenko, A. Rohilla, J.E. Siado, W. Tabb, A. Vagnerini, A. Wightman, F. Yan, D. Yu

State University of New York at Buffalo, Buffalo, New York, USA
H. Bandyopadhyay, L. Hay, H.w. Hsia, I. Iashvili, A. Kalogeropoulos, A. Kharchilava, M. Morris, D. Nguyen, S. Rappoccio, H. Rejeb Sfar, A. Williams, P. Young

Northeastern University, Boston, Massachusetts, USA
G. Alverson, E. Barberis, J. Bonilla, B. Bylsma, M. Campana, J. Dervan, Y. Haddad, Y. Han, I. Israr, A. Krishna, J. Li, M. Lu, R. Mccarthy, D.M. Morse, V. Nguyen, T. Orimoto, A. Parker, L. Skinnari, E. Tsai, D. Wood

Northwestern University, Evanston, Illinois, USA
S. Dittmer, K.A. Hahn, D. Li, Y. Liu, M. Mcginnis, Y. Miao, D.G. Monk, M.H. Schmitt, A. Taliercio, M. Velasco

University of Notre Dame, Notre Dame, Indiana, USA
G. Agarwal, R. Band, R. Bucci, S. Castells, A. Das, R. Goldouzian, M. Hildreth, K. Hurtado Anampa, T. Ivanov, C. Jessop, K. Lannon, J. Lawrence, N. Loukas, L. Lutton, J. Mariano, N. Marinelli, I. Mcalister, T. McCauley, C. Mcgrady, C. Moore, Y. Musienko[23], H. Nelson, M. Osherson, A. Piccinelli, R. Ruchti, A. Townsend, Y. Wan, M. Wayne, H. Yockey, M. Zarucki, L. Zygala

The Ohio State University, Columbus, Ohio, USA
A. Basnet, M. Carrigan, L.S. Durkin, C. Hill, M. Joyce, M. Nunez Ornelas, K. Wei, D.A. Wenzl, B.L. Winer, B. R. Yates

Princeton University, Princeton, New Jersey, USA
H. Bouchamaoui, K. Coldham, P. Das, G. Dezoort, P. Elmer, A. Frankenthal, B. Greenberg, N. Haubrich, K. Kennedy, G. Kopp, S. Kwan, D. Lange, A. Loeliger, D. Marlow, I. Ojalvo, J. Olsen, D. Stickland, C. Tully, L.H. Vage

University of Puerto Rico, Mayaguez, Puerto Rico, USA
S. Malik, R. Sharma

Purdue University, West Lafayette, Indiana, USA
A.S. Bakshi, S. Chandra, R. Chawla, A. Gu, L. Gutay, M. Jones, A.W. Jung, A.M. Koshy, M. Liu, G. Negro, N. Neumeister, G. Paspalaki, S. Piperov, V. Scheurer, J.F. Schulte, A. K. Virdi, F. Wang, A. Wildridge, W. Xie, Y. Yao

Purdue University Northwest, Hammond, Indiana, USA
J. Dolen, N. Parashar, A. Pathak

Rice University, Houston, Texas, USA
D. Acosta, A. Agrawal, T. Carnahan, K.M. Ecklund, P.J. Fernández Manteca,

S. Freed, P. Gardner, F.J.M. Geurts, I. Krommydas, W. Li, J. Lin, O. Miguel Colin, B.P. Padley, R. Redjimi, J. Rotter, E. Yigitbasi, Y. Zhang

University of Rochester, Rochester, New York, USA
A. Bodek, P. de Barbaro, R. Demina, J.L. Dulemba, A. Garcia-Bellido, O. Hindrichs, A. Khukhunaishvili, N. Parmar, P. Parygin[92], R. Taus

Rutgers, The State University of New Jersey, Piscataway, New Jersey, USA
B. Chiarito, J.P. Chou, S.V. Clark, D. Gadkari, Y. Gershtein, E. Halkiadakis, M. Heindl, C. Houghton, D. Jaroslawski, S. Konstantinou, I. Laflotte, A. Lath, R. Montalvo, K. Nash, J. Reichert, P. Saha, S. Salur, S. Schnetzer, S. Somalwar, R. Stone, S.A. Thayil, S. Thomas, J. Vora

University of Tennessee, Knoxville, Tennessee, USA
D. Ally, A.G. Delannoy, S. Fiorendi, S. Higginbotham, T. Holmes, A.R. Kanuganti, N. Karunarathna, L. Lee, E. Nibigira, S. Spanier

Texas A&M University, College Station, Texas, USA
D. Aebi, M. Ahmad, T. Akhter, K. Androsov[61], O. Bouhali[93], R. Eusebi, J. Gilmore, T. Huang, T. Kamon[94], H. Kim, S. Luo, R. Mueller, D. Overton, A. Safonov

Texas Tech University, Lubbock, Texas, USA
N. Akchurin, J. Damgov, N. Gogate, Y. Kazhykarim, K. Lamichhane, S.W. Lee, A. Mankel, T. Peltola, I. Volobouev

Vanderbilt University, Nashville, Tennessee, USA
E. Appelt, Y. Chen, S. Greene, A. Gurrola, W. Johns, R. Kunnawalkam Elayavalli, A. Melo, D. Rathjens, F. Romeo, P. Sheldon, S. Tuo, J. Velkovska, J. Viinikainen

University of Virginia, Charlottesville, Virginia, USA
B. Cardwell, H. Chung, B. Cox, J. Hakala, R. Hirosky, A. Ledovskoy, C. Mantilla, C. Neu, C. Ramón Álvarez

Wayne State University, Detroit, Michigan, USA
S. Bhattacharya, P.E. Karchin

University of Wisconsin - Madison, Madison, Wisconsin, USA
A. Aravind, S. Banerjee, K. Black, T. Bose, E. Chavez, S. Dasu, P. Everaerts, C. Galloni, H. He, M. Herndon, A. Herve, C.K. Koraka, A. Lanaro, R. Loveless, J. Madhusudanan Sreekala, A. Mallampalli, A. Mohammadi, S. Mondal, G. Parida, L. Pétré, D. Pinna, A. Savin, V. Shang, V. Sharma, W.H. Smith, D. Teague, H.F. Tsoi, W. Vetens, A. Warden

Authors affiliated with an international laboratory covered by a cooperation agreement with CERN
S. Afanasiev, V. Alexakhin, D. Budkouski, I. Golutvin[†], I. Gorbunov, V. Karjavine, O. Kodolova[95], V. Korenkov, A. Lanev, A. Malakhov, V. Matveev[96], A. Nikitenko[97,95], V. Palichik, V. Perelygin, M. Savina, V. Shalaev, S. Shmatov, S. Shulha, V. Smirnov, O. Teryaev, N. Voytishin, B.S. Yuldashev[98], A. Zarubin, I. Zhizhin, Yu. Andreev, A. Dermenev, S. Gninenko, N. Golubev, A. Karneyeu, D. Kirpichnikov, M. Kirsanov, N. Krasnikov, I. Tlisova, A. Toropin

Authors affiliated with an institute formerly covered by a cooperation agreement with CERN
G. Gavrilov, V. Golovtcov, Y. Ivanov, V. Kim[99], P. Levchenko[100], V. Murzin,

V. Oreshkin, D. Sosnov, V. Sulimov, L. Uvarov, A. Vorobyev†, T. Aushev, K. Ivanov, V. Gavrilov, N. Lychkovskaya, V. Popov, A. Zhokin, R. Chistov[99], M. Danilov[99], S. Polikarpov[99], V. Andreev, M. Azarkin, M. Kirakosyan, A. Terkulov, E. Boos, V. Bunichev, M. Dubinin[84], L. Dudko, A. Ershov, A. Gribushin, V. Klyukhin, S. Obraztsov, S. Petrushanko, V. Savrin, A. Snigirev, V. Blinov[99], T. Dimova[99], A. Kozyrev[99], O. Radchenko[99], Y. Skovpen[99], V. Kachanov, S. Slabospitskii, A. Uzunian, A. Babaev, V. Borshch, D. Druzhkin

†: Deceased
[1]Also at Yerevan State University, Yerevan, Armenia
[2]Also at TU Wien, Vienna, Austria
[3]Also at Ghent University, Ghent, Belgium
[4]Also at Universidade do Estado do Rio de Janeiro, Rio de Janeiro, Brazil
[5]Also at FACAMP - Faculdades de Campinas, Sao Paulo, Brazil
[6]Also at Universidade Estadual de Campinas, Campinas, Brazil
[7]Also at Federal University of Rio Grande do Sul, Porto Alegre, Brazil
[8]Also at University of Chinese Academy of Sciences, Beijing, China
[9]Also at China Center of Advanced Science and Technology, Beijing, China
[10]Also at University of Chinese Academy of Sciences, Beijing, China
[11]Also at China Spallation Neutron Source, Guangdong, China
[12]Now at Henan Normal University, Xinxiang, China
[13]Also at University of Shanghai for Science and Technology, Shanghai, China
[14]Now at The University of Iowa, Iowa City, Iowa, USA
[15]Also at an institute formerly covered by a cooperation agreement with CERN
[16]Also at Helwan University, Cairo, Egypt
[17]Now at Zewail City of Science and Technology, Zewail, Egypt
[18]Now at British University in Egypt, Cairo, Egypt
[19]Now at Cairo University, Cairo, Egypt
[20]Also at Purdue University, West Lafayette, Indiana, USA
[21]Also at Université de Haute Alsace, Mulhouse, France
[22]Also at Istinye University, Istanbul, Turkey
[23]Also at an international laboratory covered by a cooperation agreement with CERN
[24]Also at The University of the State of Amazonas, Manaus, Brazil
[25]Also at University of Hamburg, Hamburg, Germany
[26]Also at RWTH Aachen University, III. Physikalisches Institut A, Aachen, Germany
[27]Also at Bergische University Wuppertal (BUW), Wuppertal, Germany
[28]Also at Brandenburg University of Technology, Cottbus, Germany
[29]Also at Forschungszentrum Jülich, Juelich, Germany
[30]Also at CERN, European Organization for Nuclear Research, Geneva, Switzerland
[31]Also at HUN-REN ATOMKI - Institute of Nuclear Research, Debrecen, Hungary
[32]Now at Universitatea Babes-Bolyai - Facultatea de Fizica, Cluj-Napoca, Romania
[33]Also at MTA-ELTE Lendület CMS Particle and Nuclear Physics Group, Eötvös Loránd University, Budapest, Hungary
[34]Also at HUN-REN Wigner Research Centre for Physics, Budapest, Hungary
[35]Also at Physics Department, Faculty of Science, Assiut University, Assiut, Egypt
[36]Also at Punjab Agricultural University, Ludhiana, India
[37]Also at University of Visva-Bharati, Santiniketan, India
[38]Also at Indian Institute of Science (IISc), Bangalore, India
[39]Also at Amity University Uttar Pradesh, Noida, India
[40]Also at IIT Bhubaneswar, Bhubaneswar, India

[41]Also at Institute of Physics, Bhubaneswar, India
[42]Also at University of Hyderabad, Hyderabad, India
[43]Also at Deutsches Elektronen-Synchrotron, Hamburg, Germany
[44]Also at Isfahan University of Technology, Isfahan, Iran
[45]Also at Sharif University of Technology, Tehran, Iran
[46]Also at Department of Physics, University of Science and Technology of Mazandaran, Behshahr, Iran
[47]Also at Department of Physics, Faculty of Science, Arak University, ARAK, Iran
[48]Also at Italian National Agency for New Technologies, Energy and Sustainable Economic Development, Bologna, Italy
[49]Also at Centro Siciliano di Fisica Nucleare e di Struttura Della Materia, Catania, Italy
[50]Also at Università degli Studi Guglielmo Marconi, Roma, Italy
[51]Also at Scuola Superiore Meridionale, Università di Napoli 'Federico II', Napoli, Italy
[52]Also at Fermi National Accelerator Laboratory, Batavia, Illinois, USA
[53]Also at Laboratori Nazionali di Legnaro dell'INFN, Legnaro, Italy
[54]Also at Consiglio Nazionale delle Ricerche - Istituto Officina dei Materiali, Perugia, Italy
[55]Also at Institut de Physique des 2 Infinis de Lyon (IP2I), Villeurbanne, France
[56]Also at Department of Applied Physics, Faculty of Science and Technology, Universiti Kebangsaan Malaysia, Bangi, Malaysia
[57]Also at Consejo Nacional de Ciencia y Tecnología, Mexico City, Mexico
[58]Also at Trincomalee Campus, Eastern University, Sri Lanka, Nilaveli, Sri Lanka
[59]Also at Saegis Campus, Nugegoda, Sri Lanka
[60]Also at National and Kapodistrian University of Athens, Athens, Greece
[61]Also at Ecole Polytechnique Fédérale Lausanne, Lausanne, Switzerland
[62]Also at Universität Zürich, Zurich, Switzerland
[63]Also at Stefan Meyer Institute for Subatomic Physics, Vienna, Austria
[64]Also at Laboratoire d'Annecy-le-Vieux de Physique des Particules, IN2P3-CNRS, Annecy-le-Vieux, France
[65]Also at Near East University, Research Center of Experimental Health Science, Mersin, Turkey
[66]Also at Konya Technical University, Konya, Turkey
[67]Also at Izmir Bakircay University, Izmir, Turkey
[68]Also at Adiyaman University, Adiyaman, Turkey
[69]Also at Bozok Universitetesi Rektörlügü, Yozgat, Turkey
[70]Also at Marmara University, Istanbul, Turkey
[71]Also at Milli Savunma University, Istanbul, Turkey
[72]Also at Kafkas University, Kars, Turkey
[73]Now at Istanbul Okan University, Istanbul, Turkey
[74]Also at Hacettepe University, Ankara, Turkey
[75]Also at Erzincan Binali Yildirim University, Erzincan, Turkey
[76]Also at Istanbul University - Cerrahpasa, Faculty of Engineering, Istanbul, Turkey
[77]Also at Yildiz Technical University, Istanbul, Turkey
[78]Also at School of Physics and Astronomy, University of Southampton, Southampton, United Kingdom
[79]Also at IPPP Durham University, Durham, United Kingdom
[80]Also at Monash University, Faculty of Science, Clayton, Australia
[81]Also at Università di Torino, Torino, Italy
[82]Also at Bethel University, St. Paul, Minnesota, USA
[83]Also at Karamanoğlu Mehmetbey University, Karaman, Turkey

[84]Also at California Institute of Technology, Pasadena, California, USA
[85]Also at United States Naval Academy, Annapolis, Maryland, USA
[86]Also at Ain Shams University, Cairo, Egypt
[87]Also at Bingol University, Bingol, Turkey
[88]Also at Georgian Technical University, Tbilisi, Georgia
[89]Also at Sinop University, Sinop, Turkey
[90]Also at Erciyes University, Kayseri, Turkey
[91]Also at Horia Hulubei National Institute of Physics and Nuclear Engineering (IFIN-HH), Bucharest, Romania
[92]Now at another institute formerly covered by a cooperation agreement with CERN
[93]Also at Texas A&M University at Qatar, Doha, Qatar
[94]Also at Kyungpook National University, Daegu, Korea
[95]Also at Yerevan Physics Institute, Yerevan, Armenia
[96]Also at another international laboratory covered by a cooperation agreement with CERN
[97]Also at Imperial College, London, United Kingdom
[98]Also at Institute of Nuclear Physics of the Uzbekistan Academy of Sciences, Tashkent, Uzbekistan
[99]Also at another institute formerly covered by a cooperation agreement with CERN
[100]Also at Northeastern University, Boston, Massachusetts, USA